Dissertation zur Erlangung des Doktorgrades
der Fakultät für Chemie und Pharmazie
der Ludwig-Maximilians-Universität München

A Systems Approach to Analyze Mitochondrial Calcium Signaling

Jennifer Wettmarshausen
aus
Hildesheim, Deutschland

2021

Erklärung

Diese Dissertation wurde im Sinne von § 7 der Promotionsordnung vom 28. November 2011 von Frau Dr. Fabiana Perocchi betreut.

Eidesstattliche Versicherung

Diese Dissertation wurde eigenständig und ohne unerlaubte Hilfe erarbeitet.

München, den 27.10.2021

Jennifer Wettmarshausen

Dissertation eingereicht am	03.11.2021
1. Gutachter	Prof. Dr. Fabiana Perocchi
2. Gutachter	Prof. Dr. Klaus Förstemann
Mündliche Prüfung am	22.11.2021

List of Publications

Publication I

Wettmarshausen J*, Goh V*, Huang KT, Arduino DM, Tripathi U, Leimpek A, Cheng Y, Pittis AA, Gabaldón T, Mokranjac D, Hajnóczky G, Perocchi F.

MICU1 Confers Protection from MCU-Dependent Manganese Toxicity.

Cell Reports 2018; 25(6):1425-35.e7

*equal author contributions

Abstract

The mitochondrial calcium uniporter is a highly selective ion channel composed of species and tissue-specific subunits. However, the functional role of each component still remains unclear. Here, we establish a synthetic biology approach to dissect the interdependence between the pore-forming subunit MCU and the calcium-sensing regulator MICU1. Correlated evolutionary patterns across 247 eukaryotes indicate that their co-occurrence may have conferred a positive fitness advantage. We find that, while the heterologous reconstitution of MCU and EMRE in vivo in yeast enhances manganese stress, this is prevented by coexpression of MICU1. Accordingly, MICU1 deletion sensitizes human cells to manganese dependent cell death by disinhibiting MCU-mediated manganese uptake. As a result, manganese overload increases oxidative stress, which can be effectively prevented by NAC treatment. Our study identifies a critical contribution of MICU1 to the uniporter selectivity, with important implications for patients with MICU1 deficiency, as well as neurological disorders arising upon chronic manganese exposure.

Publication II

Arduino DM, Wettmarshausen J, Vais H, Navas-Navarro P, Cheng Y, Leimpek A, Ma Z, Delrio-Lorenzo A, Giordano A, Garcia-Perez C, Médard G, Kuster B, García-Sancho J, Mokranjac D, Foskett JK, Alonso MT, Perocchi F. et al.

Systematic Identification of MCU Modulators by Orthogonal Interspecies Chemical Screening.

Molecular Cell. 2017; 67(4):711-23.e7

Abstract

The mitochondrial calcium uniporter complex is essential for calcium (Ca^{2+}) uptake into mitochondria of all mammalian tissues, where it regulates bioenergetics, cell death, and Ca^{2+} signal transduction. Despite its involvement in several human diseases, we currently lack pharmacological agents for targeting uniporter activity. Here we introduce a high-throughput assay that selects for human MCU-specific small-molecule modulators in primary drug screens. Using isolated yeast mitochondria, reconstituted with human MCU, its essential regulator EMRE, and aequorin, and exploiting a D-lactate- and mannitol/sucrose-based bioenergetic shunt that greatly minimizes false-positive hits, we identify mitoxantrone out of more than 600 clinically approved drugs as a direct selective inhibitor of human MCU. We validate mitoxantrone in orthogonal mammalian cell-based assays, demonstrating that our screening approach is an effective and robust tool for MCU-specific drug discovery and, more generally, for the identification of compounds that target mitochondrial functions.

Summary

Calcium (Ca^{2+}) acts as one of the most versatile signalling molecules and is involved in a diversity of physiological function, including muscle contraction, neuronal excitability, cell migration, growth and apoptosis. By shaping cellular Ca^{2+} currents, mitochondria serve as important modulator of Ca^{2+} signalling. The mitochondria calcium uniporter complex (MCUC) is a macromolecular protein channel located in the mitochondrial inner membrane that mediates mitochondrial Ca^{2+} (mt-Ca^{2+}) uptake, thereby playing an essential role in mitochondria physiology and pathophysiology.

In this thesis, phylogenetic analyses, *in vitro* and *in vivo* cross-functional synthetic biology approaches using the yeast *S. cerevisiae* as a test system have been combined to

1) develop a flexible cost-effective screening solution to discover drug molecules directly targeting MCUC and effectively minimize false discovery rate, and
2) dissect the functional interconnections between MCUC components and identify an essential role for MICU1 in preventing manganese (Mn^{2+})-induced cell death.

Limited pharmacological agents targeting MCUC activity exist, despite its involvement in several human diseases. Here a primary, high-throughput drug screen was developed to identify specific small-molecule modulators of the pore-forming subunit of the human uniporter, MCU (Mitochondrial Calcium Uniporter). Isolated mitochondria from the yeast *S. cerevisiae*, which lacks MCU-activity, were deployed, providing a null-background. Mt-Ca^{2+} uptake was reconstituted by expressing human MCU and the essential structural subunit EMRE (Essential MCU Regulator) and quantitatively measured with the Ca^{2+}-sensitive photoprotein aequorin stably expressed in the mitochondrial matrix. Key to this drug screen was the exploitation of a D-lactate and mannitol/sucrose-based bioenergetic shunt, unique to mitochondria from *S. cerevisiae*, that enables mitochondrial membrane potential (mt-$\Delta\psi$) to be maintained even in the absence of a functional electron transport chain or in the presence of mt-$\Delta\psi$ uncouplers. This property drastically reduced false discovery rate. In a primary screen of ~700 small-molecules, mitoxantrone was identified as a selective and specific inhibitor of MCU. This orthogonal, interspecies drug-screening strategy lays the foundation for accelerating discovery of small-molecule pharmacological agents directed against MCU.

Other components of MCUC also constitute key drug targets as they directly regulate biophysical properties of the channel such as Ca^{2+} sensitivity, gating, and cooperative activation. The mitochondrial calcium uniporter protein 1 (MICU1) is a Ca^{2+} binding and ubiquitously expressed regulatory subunit of MCUC, which has been proposed to act as a gatekeeper. Here, a correlated evolutionary patterns across 247 eukaryotes indicated that the co-occurrence between MCU and MICU1 may have also conferred a positive fitness advantage. A synthetic biology approach was established to dissect the interdependence between these two components by heterologous expression of human MCU and EMRE either in presence or in absence of MICU1 in mitochondria from the yeast *S. cerevisiae*. So doing, Ca^{2+} entry in mitochondria was successfully reconstituted *in vivo* in the yeast cells. All strains were then screened for a selective fitness advantage in presence of different environmental stress conditions. Enhanced Mn^{2+}-dependent growth defect in yeast strains expressing MCU and EMRE was found to be prevented by co-expression of MICU1.

Similarly, MICU1 deletion sensitized human embryonic kidney (HEK-293) cells to Mn^{2+}-dependent cell death by enabling MCU-mediated Mn^{2+} uptake. As a result, manganese overload increased oxidative stress, which could be effectively prevented by NAC treatment. These results identify a critical contribution of MICU1 to the uniporter selectivity, with important implications for patients with MICU1 deficiency as well as neurological disorders arising upon chronic manganese exposure.

Zusammenfassung

Calcium (Ca^{2+}) fungiert als eines der vielseitigsten Signalmoleküle und ist an einer Vielzahl physiologischer Funktionen beteiligt, darunter Muskelkontraktion, neuronaler Erregbarkeit, Zellmigration, Wachstum und Apoptose. Durch die Formung zellulärer Ca^{2+} -Ströme dienen Mitochondrien als wichtiger Modulator der Ca^{2+} -Signalübertragung. Der Mitochondrien-Calcium-Uniporter-Komplex (MCUC) ist ein makromolekularer Proteinkanal der mitochondrialen Innenmembran, der die mitchochondriale Ca^{2+} (mt-Ca^{2+})-Aufnahme vermittelt und somit eine wesentliche Rolle in der Physiologie und Pathophysiologie der Mitochondrien spielt.

In dieser Arbeit wurden phylogenetische Analysen, *in vitro* und *in vivo* funktionsübergreifende Ansätze der synthetischen Biologie unter Verwendung der Hefe *S. cerevisiae* als Testsystem kombiniert, um

1. eine flexible und kostengünstige Screening-Lösung mit minimierter *false-dicovery* Rate zu entwickeln, um Wirkstoffmoleküle zu entdecken, die als MCUC-Modulatoren agieren und
2. die funktionelle Verbindung zwischen MCUC-Komponenten zu analysieren und eine wesentliche Rolle von MICU1 bei der Verhinderung des Mangan (Mn^{2+}) -induzierten Zelltods zu identifizieren.

Trotz seiner Beteiligung an mehreren Erkrankungen des Menschen gibt es nur begrenzte pharmakologische Wirkstoffe, die die MCUC-Aktivität beeinflussen. Hier wurde ein primäres Hochdurchsatz-Wirkstoff-Screening entwickelt, um spezifische niedermolekulare Modulatoren der porenbildenden Untereinheit des menschlichen Uniporters MCU (Mitochondrial Calcium Uniporter) zu identifizieren. Isolierte Mitochondrien aus der Hefe *S. cerevisiae*, die keine MCU-Aktivität aufweisen, wurden verwendet und lieferten einen Nullhintergrund. Die Aufnahme von mt-Ca^{2+} wurde durch Expression von humanen MCU und der strukturell essentiellen Untereinheit EMRE (Essential MCU Regulator) rekonstruiert und mit dem Ca^{2+} -sensitiven Photoprotein Aequorin, das stabil in der mitochondrialen Matrix exprimiert wurde, quantitativ gemessen. Maßgebend zur Funktion dieses Wirkstoff-Screenings war die Nutzung eines bioenergetischen Shunts auf der Basis von D-Lactat- und Mannit / Saccharose, der einzigartig für Mitochondrien von *S. cerevisiae* ist und es ermöglicht, das mitchondriale Membranpotentials (mt-$\Delta\psi$) auch in Abwesenheit einer funktionellen Elektronentransportkette oder Gegenwart mt-$\Delta\psi$ Entkoppler aufzubauen. Diese Eigenschaft reduzierte die *false-dicovery* Rate drastisch. In einem primären Screening von ~ 700 kleinen Molekülen wurde Mitoxantron als selektiver und spezifischer Inhibitor von MCU identifiziert. Diese orthogonale Interspezies-Wirkstoff-Screening Strategie legt die Grundlage für eine beschleunigte Entdeckung von niedermolekularen pharmakologischen Wirkstoffen, die gegen MCU gerichtet sind.

Andere Komponenten von MCUC stellen ebenfalls wichtige Wirkstoffziele dar, weil sie biophysikalische Eigenschaften des Kanals wie Ca^{2+} -Empfindlichkeit, Gating und kooperative Aktivierung direkt regulieren. Das mitochondriale Calcium-Uniporter-Protein 1 (MICU1) ist eine Ca^{2+}-bindende und ubiquitär exprimierte regulatorische Untereinheit von MCUC, die als Gatekeeper fungieren soll. Hier deutete ein korreliertes evolutionäres Muster bei 247 Eukaryoten darauf hin, dass das gemeinsame Auftreten von MCU und MICU1 auch einen positiven Fitnessvorteil verliehen haben könnte. Es wurde ein synthetischer biologischer Ansatz etabliert, um die gegenseitige Abhängigkeit zwischen diesen beiden Komponenten

durch heterologische Expression von humanem MCU und EMRE entweder in Gegenwart oder in Abwesenheit von MICU1 in Mitochondrien aus der Hefe *S. cerevisiae* zu untersuchen. Dabei wurde der Ca^{2+} -Eintritt in Mitochondrien in den Hefe-Zellen *in vivo* erfolgreich rekonstruiert. Alle Hefestämme wurden dann auf einen selektiven Fitnessvorteil bei Vorliegen verschiedener Umweltstressbedingungen untersucht. Es wurde festgestellt, dass ein verstärkter Mn^{2+} abhängiger Wachstumsdefekt in Hefestämmen, die MCU und EMRE exprimieren, durch die Co-Expression von MICU1 verhindert wird. In ähnlicher Weise sensibilisiert die Delation von MICU1 in menschlichen embryonalen Nierenzellen (HEK-293) für Mn^{2+} -abhängigen Zelltod, indem sie die MCU-vermittelte Mn^{2+} -Aufnahme ermöglicht. Infolgedessen erhöhte eine Manganüberladung den oxidativen Stress, der durch eine NAC-Behandlung effektiv verhindert werden konnte. Diese Ergebnisse identifizieren einen entscheidenden Beitrag von MICU1 zur Uniporter-Selektivität, mit wichtigen Implikationen für Patienten mit MICU1-Fehlexpression sowie für neurologische Störungen, die bei chronischer Manganexposition auftreten.

Table of contents

List of Publications ..... **I**

Summary ..... **III**

Zusammenfassung ..... **V**

Table of contents ..... **VII**

1 Introduction **8**

1.1 Mitochondria - the Signaling Hub of the Eukaryotic Cell and its Metabolic Fate **8**

1.2 Mitochondria shape Calcium Signalling via the Mitochondrial Calcium Uniporter **10**

1.3 MCU Complex Regulates diverse Physiological Processes **14**

1.4 Research Aims **17**

2 Publications **19**

2.1 Systematic Identification of MCU Modulators by Orthogonal Interspecies Chemical Screening **19**

Declaration of contribution **19**

2.2 MICU1 Confers Protection from MCU-Dependent Manganese Toxicity **68**

Declaration of contribution **68**

3 Discussion **92**

4 Appendix **94**

4.1 Index of abbreviations **94**

4.2 Index of figures **95**

4.3 References **95**

5 Acknowledgement **99**

1 Introduction

1.1 Mitochondria - the Signaling Hub of the Eukaryotic Cell and its Metabolic Fate

Mitochondria are essential organelles of the eukaryotic cell and play a central role in cellular metabolism and signalling.

Mitochondria are highly dynamic semiautonomous organelles present in virtually all eukaryotic cells and are vital for the cellular production of energy and support of biosynthesis. Thus, mitochondrial function is coupled to diverse biological processes demanding a communication and coordination between mitochondria and other cellular compartments.

Mitochondria are endosymbionts, likely originated from an α-proteobacteria ancestor that was incorporated into eukaryotes over billion years ago[1]. During evolution, mitochondria underwent wide adaptation with most of their genes being transferred into the nucleus. The remaining mitochondrial DNA (mt-DNA) is a circular 16.5 bp molecule, which resides in the mitochondrial matrix in multi-copies, reflecting their relation to the bacterial ancestor. It harbours 37 genes, encoding for 13 peptides, 22 tRNAs and 2 rRNAs. In addition, mitochondria underwent also a functional recombination by which they participate in various cellular processes. Considered as a milestone in evolution it enormously promoted the development of eukaryotes to multicellular life, but also required the development of mechanism to communicate [2, 3].

A further evidence of their endosymbiotic origin is the presence of a double membrane. The mitochondrial outer membrane (OMM) harbours large channels, called porins, that allow passive exchange of solutes up to ~5 kDa [4]. Consequently, the milieu of the mitochondrial inner membrane space (IMS) is rather similar to the cellular cytosol. On the contrary, the permeability of the inner mitochondrial membrane (IMM) is highly selective: Its lipid bilayer contains the highest proportion of cardiolipin compared to other cellular membranes, which confers a low permeability. Exchange of small molecules, like metabolites and ions, between the mitochondrial matrix and the cytosol is ensured by a great variety of specific transporters, carriers and channels. The import of proteins is regulated by a specialised protein machinery in the outer (TOM complex) and inner (TIM complex) mitochondrial membranes. The area of the IMM is greatly increased by series of infoldings, called cristae, that project into the matrix, ensuring sufficient surface and forming small, specialised milieus for chemical reactions.

One of this reactions has been the foundation for the scientific meme of mitochondria as the "power house of the cell", which refers to the most commonly known bioenergetic function – the generation of adenosine triphosphate (ATP)[5].

Mitochondria generate ATP through a much more efficient process than the cytosolic glycolysis. Its synthesis by mitochondria is fuelled by carbohydrate, proteins and fatty acids, which are catabolised by a

series of chemical, mainly exotherm reactions via the tricarboxylic acid (TCA) cycle (also called citric acid cylcle, or the Krebs cycle) or fatty acid ß-oxidation to the crucial metabolic intermediate acetyl-coenzyme A (acetyl-CoA). These processes generate high-energy electrons, carried by the activated carrier molecules NADH and $FADH_2$, which are transferred to the electron-transport chain (ETC), a series of mostly integral carriers of the IMM.

The ETC, also called respiratory chain, transfers the electrons from NADH and $FADH_2$ to O_2, forming H_2O, a process called respiration.

$$NADH + H^+ + \frac{1}{2} O_2 \rightarrow NAD^+ + H_2O$$

$$FADH_2 + \frac{1}{2} O_2 \rightarrow FAD + H_2O$$

The energy of this exothermic reaction is used by the ETC, which consists of the multi subunit complexes I, II; III and IV, to produce ATP along with the ATP-synthase (also named Complex V)[6].

The entry point of the ETC is the NADH-CoQ reductase complex, a ~980 kDa complex (RCCI) that carries the electrons from NADH through a series of redox centers to coenzyme Q (CoQ), also called ubiquinone [7]. RCCI is composed of 45 subunits, of which seven are encoded by mt-DNA[8]. Mammalian RCCI exhibits an active/de-active transition, which is modulated by bivalent cations and other cofactors in the mitochondrial matrix and can be inhibited by rotenone [9].

RCCII, also called succinate-CoQ reductase complex, harbors the TCA enzyme succinate dehydrogenase, which oxidizes succinate to fumarate, using FAD as a cofactor. The mammalian RCCII is the only peripheral ETC complex, consists of 4 nuclear-encoded subunits and exhibits a molecular weight of 140 kDa [10]. Finally, it guides the transport of the electron from FAD to CoQ. Consequently, reduced CoQ ($CoQH_2$) is generated by RCCI and RCCII. The electron carrier $CoQH_2$ is not bound to a protein and is soluble in phospholipids, diffusing freely in the IMM. One $CoQH_2$ donates two electrons to the $CoQH_2$-Cytochrome c reductase complex (RCCIII) of the ETC, regenerating oxidized CoQ. Mammalian RCCIII consists of 11 nuclear-encoded subunits, it has a molecular weight of 490 kDa [11] and is inhibited by antimycin A (AA). Next, RCCIII passes electrons to two cytochrome *c*, water-soluble IMS proteins, that transports one electron at the time to the Cytochrome *c* Oxidase Complex (RCCIV) of the ETC. This enzyme contains 13 different subunits, from which three are mt-DNA encoded [12]. RCCIV transfers the electron to its final acceptor, O_2, yielding H_2O and can by inhibited by cyanide (CN^-). The energy by the step-to-step electron transport of the ETC is used by complex RCCI, RCCIII and RCCIV to pump protons of the mitochondrial matrix across the IMM, building up a proton gradient.

The protons can freely pass through the OMM, resulting in a pH difference between cytosol (~pH 7.2) and mitochondrial matrix (pH 7.7 to 8.2) that is used to generate an electrochemical gradient (mt-$\Delta\Psi$) of about – 150/- 200 mV. The mt-$\Delta\Psi$ functions as an energy storage in the form of proton-motive force. The Complex V of the ETC (F_0F_1 complex) guides the backflow of protons into the mitochondrial matrix and

couples the proton driving force to the synthesis of ATP from ADP and P_i. RCCV consists of 16 subunits in mammals, of which two are encoded from the mt-DNA. The 597 kDa complex can be inhibited by oligomycin A [13]. The synthesis of ATP driven by the transfer of electrons from NADH and $FADH_2$, is called oxidative phosphorylation (OXPHOS).

While this system is mainly preserved in all eukaryotes, some differences among species exist. For instance, mitochondria of the yeast *S. cerevisiae* exhibit a simplified OXPHOS system, which lacks RCCI but contains a D-lactate dehydrogenase (DLD) that transfers electrons directly to cytochrome *c* upon oxidation of D-lactate into pyruvate. Thus, in experiments with isolated mitochondria, D-lactate can be used as a substrate, providing a bioenergetic shunt, bypassing the citric acid cycle and the ETC upstream of RCCIV while still generating sufficient mt-$\Delta\Psi$ [14].

The mt-$\Delta\Psi$ is used for several other mitochondrial functions besides ATP production, e.g. transport of proteins, metabolites and ions into the mitochondrial matrix, as well as mitochondrial quality control. Indeed, mitochondria play a crucial role in the biosynthesis of macromolecules such as heme-, iron-sulfur clusters, steroid and lipids.

The production of energy and the support of cell metabolism, couple mitochondrial function to diverse biological outcomes including proliferation, differentiation, and adaptation to stress. This and the bi-genomic nature of mitochondria demands its tight coordination with other organelles, such as the nucleus. The signalling mechanisms that ensure such communication are classified into anterograde and retrograde signalling. The former mechanism coordinates mitochondrial function in response to endogenous and environmental homeostatic alterations, the latter is a diversity of signals from the mitochondria to allow monitoring of the functional state (e.g. level of energy production or the organelle's biosynthesis capacity) by other cellular compartments. A variety of substances can act as signalling molecule, e.g. nucleotides[15], biosynthetic intermediates[16], mitochondrial derived free reactive oxygen species (ROS)[17], proteins[18], cytochrome *c*[19], or ions including calcium (Ca^{2+})[20-22].

1.2 Mitochondria shape Calcium Signalling via the Mitochondrial Calcium Uniporter

Ca^{2+} signalling is fundamental to many physiological processes, including contraction in skeletal, cardiac and smooth muscles, secretion, learning and memory, cell migration, fertilisation as well as cellular control of metabolism and death via apoptosis, necrosis and autophagy.

Intracellular Ca^{2+} signals can originate from Ca^{2+} influx through the plasma membrane (PM) (extracellular, ${}_e[Ca^{2+}] \sim 1$ mM) or from intracellular sources like golgi (${}_{Golgi}[Ca^{2+}] \sim 300$ μM) and endoplasmic reticulum (ER, ${}_{ER}[Ca^{2+}] \sim 200$-$650$ μM). To maintain a cytosolic resting Ca^{2+} concentration (${}_{cyt}[Ca^{2+}] \sim 100$ nM), Ca^{2+} is constantly removed from the cytosol by Ca^{2+} ATPase (PMCA) pumps of the plasma membrane or by sarco/endoplasmic reticulum Ca^{2+}-ATPase (SERCA) pumps of the ER[23, 24]. Mitochondria can be viewed as efficient Ca^{2+} sinks that shape the dynamic and complex patterning of Ca^{2+} signalling.

The OMM is highly permeable to cytosolic Ca^{2+}, mainly through the large voltage-dependent anion channel (VDAC) [25, 26]. Therefore, the homeostasis of mitochondrial Ca^{2+} is mediated by complexes in the IMM: The mitochondrial calcium uniporter complex enables passive but highly selective mitochondrial Ca^{2+} (mt-Ca^{2+}; $_{mt}$[Ca^{2+}]) uptake with a capacity driven by the negative mt-$\Delta\psi$, whereas release of mt-Ca^{2+} occurs via an electroneutral and stoichiometric antiport mechanism[27]. In excitable tissues, such as e.g. the heart and brain, the mitochondrial Na^+/Ca^{2+} exchanger (mNCLX) mediates the extrusion of Ca^{2+} from the matrix powered by the electrochemical gradient for Na^+ entry into the matrix [20, 21, 28, 29] (**Figure 1**). Here, mNCLX-mediated mt-Ca^{2+} export depends on the relative concentration of Na^+ in both cytosol and matrix, on the mt-$\Delta\psi$, and the stoichiometry of mNCLX. mNCLX exchanges 3 or 4 Na^+ for each Ca^{2+} ion and is therefore electrogenic, with a net import of one or two positive charges into the matrix. mNCLX has been shown to be inhibited by CGP-37157. In addition to the Na^+-dependent export of mt-Ca^{2+}, mitochondria of non-excitable cells also are capable of mt-Ca^{2+} efflux through a H^+/Ca^{2+} exchanger with a so far unclear molecular identity [30].

Although mt-Ca^{2+} uptake is a known property of mitochondria since 1960s [20-22], the molecular identity of the MCU complex remained unclear until 2010 and 2011[31, 32].

Despite the use of Ca^{2+} as a signaling molecule is ubiquitous in all eukaryotes, several functional modules of mammalian Ca^{2+} signaling systems are not conserved across all eukaryotic organisms. As mitochondria of both, higher and unicellular eukaryotes but not of fungi, were able to uptake Ca^{2+} [22, 33-36], it was hypothesized that human genes encoding for MCU complex should exhibit a "phylogenetic signature", that matched the physiological profile across taxa, namely "present in mouse and in kinetoplastids, but absent in yeast".

Progress in sequencing and annotation of whole genomes has allowed the comprehensive comparison of gene sets among different phylogenetic groups. This approach named "phylogenetic profiling" aims to identify functional related components on the assumption that proteins belonging to the same complex or pathway will show similar phyletic patterns. Phylogenetic profiles have been generated for several known pathways and successfully used to predict the function of uncharacterized proteins. The predictive power of this approach was employed to discover the molecular identity of the MCU complex [31, 32, 37]. By combining evolutionary genomics, organelle proteomics, and RNAi screening, in 2010 the first component of the mitochondrial Ca^{2+} unipoter channel, MICU1, were identified [31]. One year later, searching for proteins that either co-evolved with MICU1 or are conserved in kinetoplastids, but absent in yeast, and have at least two predicted transmembrane domains, have led to the discovery of the pore-forming subunit of MCU complex, MCU [32, 37]. BN-PAGE demonstrated that MCU exists in a large protein complex (~480 kDa) [14], with possible, at that time unknown, additional proteins. Indeed, up to now several other members of the MCU complex have been described, namely MICU2, MICU3, MCUb, EMRE, and MCUR1 supporting a macromolecular nature of the complex[38-41].

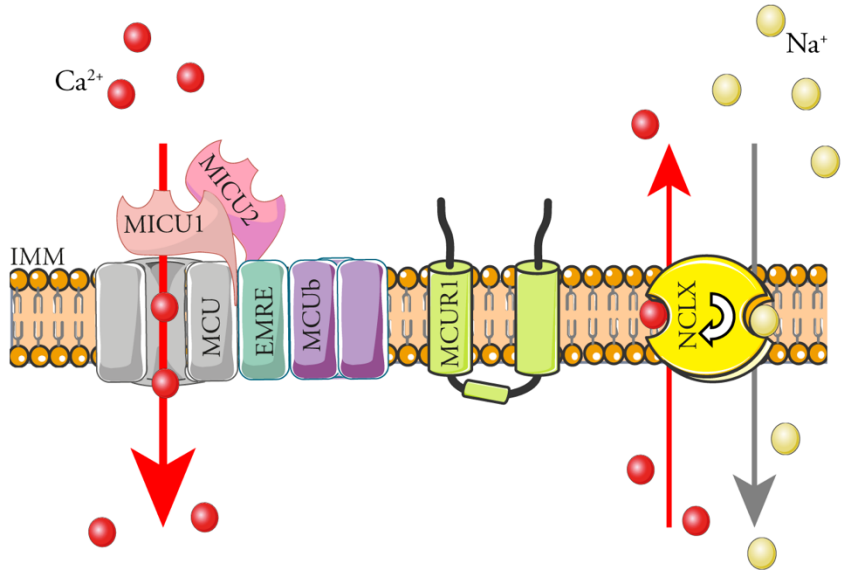

Figure 1: Mitochondrial Calcium Transporters

Schematic illustration of the mitochondrial calcium uniporter complex, (mitochondrial calcium uniporter (MCU), MCU paralog MCUb, mitochondrial calcium uptake protein 1 and 2 (MICU1 and MICU2), essential MCU regulator (EMRE); MCU regulator 1 (MCUR1) and Na^+/Ca^{2+} exchanger (NCLX) in the mitochondrial inner membrane (IMM)

Mitochondrial Calcium uniporter (MCU)

MCU is a 40 kDa protein consistent of two transmembrane domains (TMH) that are linked by a short hydrophilic loop enriched in acidic residues, called DXXE motif. Single-point mutation within the acidic residues of this motif (E257A, D261A and E264A) abrogate the ability of MCU to conduct mt-Ca^{2+} currents, indicating that they are required for its function as a selectivity filter [32, 37, 42]. Both N-terminal and C-terminal domains are facing the matrix. Loss of MCU results into an abrogation of mt-Ca^{2+} uptake, whereas overexpression leads to an upregulation of ruthenium red (RuRed)-sensitive mt-Ca^{2+} uptake in both intact and permeabilized cells [32, 37]. Point mutation in the residue A259A of the DXXE motive of MCU, conferred resistance to an analog of RuRed, Ru360 [32]. MCU knockout mice are viable only on a mixed genetic background exhibiting a not even Mendelian ratio, while deletion of MCU on the inbred C57BL/6 background is embryonically lethal [43].

Recent crystal structure results of the N-terminal domain of MCU indicate similarity to a β-grasp-like fold, which can be regulated by Ca^{2+} and Mg^{2+} cations [44]. The binding of cations on this domain destabilizes the assembly of the MCU complex resulting in a block of its activity [45]. In addition, the region is important for post-translational modifications since it harbors a putative phosphorylation site for CaMKII (S92), previously reported to regulate channel activity [46]. A conserved cysteine residue can undergo S-glutathionylation and connects MCU activity with reactive oxygen species (ROS) signaling [47].

Mitochondrial Calcium uniporter b (MCUb)

Genomic analysis identified a MCU paralog, namely MCUb, which exhibits similar topology and 50 % similarity in amino acid sequence. It functions as dominant negative regulator of MCU complex driven mt-Ca^{2+} uptake [40]. MCU/MCUb ratio differs within different tissues, indicating a spatiotemporal control of mt-Ca^{2+} uptake.

Mitochondrial Calcium Uptake protein (MICU)-family

Indeed, MCU complex is a highly regulated and Ca^{2+} activated complex: It is closed at resting cellular Ca^{2+} concentrations (100 nM) and is activated about a threshold above 0.5-1 μM Ca^{2+} concentration [48]. This specific activation features of MCU complex are mediated by the two proteins of the MICU family, namely MICU1 (Mitochondrial Ca^{2+} Uniporter 1) and MICU2. Similar to other Ca^{2+} sensors, MICU1/2 proteins harbour a pair of functional active helix-loop-helix motifs with a Ca^{2+} binding property, termed EF-hand [49]. Up to now 242 EF-hand proteins have been detected in the human genome fulfilling important functions as Ca^{2+} buffers and sensors [50]. MICU1 and MICU2 hetero-dimerize via a disulphide bond and MICU2 protein stability depends on MICU1 presence. They both operate together to keep MCU complex closed at low cytosolic Ca^{2+} concentrations to prevent a Ca^{2+} overload in the mitochondria due to a high MCU complex capacity, coupled to the constant presence of huge driving force for cation accumulation into the matrix [39, 48, 51]. On the other hand, their cooperative high-affinity binding to Ca^{2+} allows MCU complex to directly respond to increasing cytosolic Ca^{2+}concentrations, resulting in the sigmoid activation curve of MCU complex [52, 53]. MICU3 is another paralog of MICU1 and its expression is thought to be restricted to nervous system and, at low levels, to muscle [39]. A recent study shows that MCIU3, similar to MICU2, forms a dimer with MICU1 and acts as an enhancer of MCU-dependent mt-Ca^{2+} uptake. Its silencing in primary cortical neurons resulted in an impaired Ca^{2+} signal elicited by synaptic activity, further indicating a specific role in regulation of neuronal Ca^{2+} signaling and function [54].

Essential MCU Regulator (EMRE)

The interaction of the MICU1/2 hetero-dimer and MCU is bridged by EMRE (Essential MCU Regulator) and MCU binding through their TMH and to MICU1 via its C-terminal poly-aspartate tail [55]. The small ~10 kDa protein EMRE resides with one TMH in the IMM and is essential for mt-Ca^{2+} uptake in human. Previous reconstitution experiments of mt-Ca^{2+} uptake in *S. cerevisiae* show, that both human MCU and EMRE are required, but *Dictyostelium discoideum* MCU is sufficient alone to enable Ca^{2+} uptake in yeast mitochondria,[38, 56]. Therefore, the precise contribution of EMRE to the MCU holocomplex remains unclear. EMRE stability is highly regulated by its interaction with MCU [38]: Without MCU interaction EMRE is degraded by the m-AAA proteases SPG7 and AFG3L, explaining why a 30-fold increase of EMRE mRNA does not alter EMRE protein level [57]. This demonstrates the tight co-regulation of MCU complex subunits. Interestingly, the m-AAA interacting protein 1 (MIAP1) binds newly imported EMRE precursor proteins in the matrix and protects them against degradation by m-AAA proteases, and ensures their maturation by MPP. Maturation of EMRE occurs after the aminoacid in position 53 and is essential for MICU1 interaction [58].

Mitochondrial Calcium Uniporter Regulator 1 (MCUR1)

The role of MCUR1 (Mitochondrial Calcium Uniporter Regulator 1), also called CCDC90a (coiled-coil domain containing 90a), in mt-Ca^{2+} uptake has been object of several studies; however, its function is still

debated. MCUR1 is a 40 kDa protein containing two TMH domains, one on the C-terminal and the other towards the N-terminal end of the protein [41]. As for MCU and MICU1, MCUR1 itself has a paralogue, CCDC90b. Its function is not clear, but it seems to have no impact on MCU complex activity [59].

MCUR1 was initially identified in a genetic screen performed in HEK293T cells as an integral membrane protein required for MCU-dependent mt-Ca^{2+} uptake. Also, HeLa cells with knockdown of MCUR1, despite normal mt-$\Delta\psi$ and localization of MCU, showed a decreased mt-Ca^{2+} uptake, whereas overexpression of MCUR1 increases mt-Ca^{2+} uptake [41]. Measurements of MCU activity by patch clamp electrophysiology of mitoplasts isolated from HEK cells with MCUR1 knocked down showed decreased mitochondrial calcium current [60].

These conclusions were then challenged by Paupe et al., who proposed that MCUR1 is a cytochrome c oxidase (COX) assembly factor and that the mt-Ca^{2+} uptake phenotype was a secondary effect due to a reduced membrane potential as a consequence of defective COX assembly [61]. In addition, a possible regulatory function for MCUR1 in the Ca^{2+} threshold of the putative mitochondrial permeability transition pore and in proline metabolism were described recently [62] [101].

1.3 MCU Complex Regulates diverse Physiological Processes

Mt-Ca^{2+} is involved in a diversity of physiological processes such as cellular energy metabolism, tissue growth and development, neurotransmitter release, muscle cell contraction, autophagy and cell death. The discovery of the molecular identity of MCU complex enabled loss of function experiment to gain a better understanding of the MCU complex function in these pathways.

Based on the various impacts of mt-Ca^{2+} in mitochondria physiology, it is no surprise that disruption of Ca^{2+} homeostasis is found in multiple disorders and an imbalance of mt-Ca^{2+} is linked to several diseases, such as hyperglycaemia, insulin resistance, cardiomyopathy, muscle atrophy, cerebral ischemic stroke, Alzheimer's disease (AD), Parkinson's disease (PD) and amyotrophic lateral sclerosis (ALS, **Figure 2** [63-67].

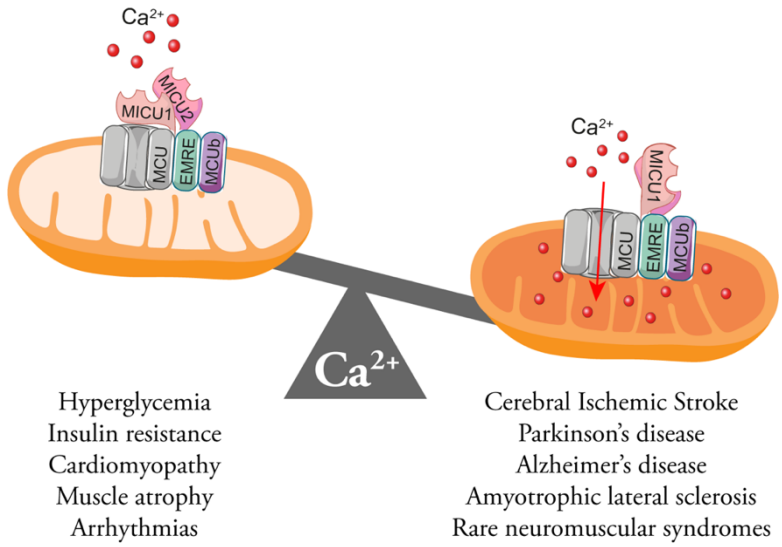

Figure 2: Pathophysiology of imbalanced mt-Ca^{2+} homeostasis

Dysregulation of mt-Ca^{2+} levels are linked to variety of neurological, muscular, cardio and metabolic diseases.

The discovery of the molecular identity of the uniporter has improved the understanding of the link between an altered mt-Ca^{2+} homeostasis and human pathophysiology and has accelerated its research.

Functional consequences of an altered mt-Ca^{2+} homeostasis through MCU complex where first characterised by cell line and mouse models [31, 63, 66]. Loss of mt-Ca^{2+} accumulation was demonstrated in mice either carrying a MCU knockout on an outbreed CD1 background, induced MCU deletion at adulthood, or by the expression of a dominant-negative MCU mutant [64, 65, 67, 68]. Consistently these mice strains exhibit normal basal cardiac function and heart morphology but were irresponsive to an acute increase in workload via the β-adrenergic receptor stimulation due to cellular inability to activate mitochondrial dehydrogenases, decreased energy production and impaired physiological fight-or-flight heart rate acceleration [64, 67]. Skeletal muscles from MCU-knock out mice exhibit a decrease in exercise capacity and muscle strengths [63]. Furthermore, postnatal overexpression or silencing of MCU in skeletal muscles resulted in muscle hypertrophy or atrophy, respectively [69]. Furthermore, C57BL/6J mice lacking MCU are embryonic lethal, indicating a relevance of mt-Ca^{2+} uptake for vitality [43]. So far, no pathogenic human MCU mutation have been described.

Contrary, a number of paediatric patients were discovered with frame-shift mutations or homozygous deletion in the gene encoding MICU1 [70, 71]. These patients suffer from mild cognitive deficit, fatigue and lethargy, neuromuscular weakness and a progressive extrapyramidal motor disorder, as well as some other characteristics which have been previously associated with mitochondrial diseases, including ataxia, microcephaly, opthalmoplegia, aptosis, optic atrophy and peripheral axonal neuropathy. The precise mechanism of how these mutations translate into the disease phenotype remains incomplete. Assays on MICU1 patient-derived fibroblasts exhibit an altered mt-Ca^{2+} uptake but did not reveal a significant alteration in OXPHOS and membrane potential. Patients with null-mutations in MICU2 have also been identified, suffering of a neurodevelopmental disorder with severe cognitive impairment and spasticity [72].

The broad and significant impact of MCU-mediated Ca^{2+} homeostasis in human physiology and pathophysiology demonstrates the importance of a comprehensive understanding of the MCU uniporter's function, structure, and regulation and the need to develop strategies to modulate MCU activity for broad therapeutically interventions [130].

1.4 Research Aims

Research Aim 1: To develop an orthogonal interspecies chemical screening for systematic identification of MCU modulators

Publication 1: Systematic Identification of MCU Modulators by Orthogonal Interspecies Chemical Screening

Strategies to modulate MCU activity are of great biomedical interest and could have broad therapeutical applications [73]. Nevertheless, pharmacological agents that directly target MCU are not yet available. Chemical inhibitors of MCU are limited to ruthenium red (RuR) and its derivatives [74-76], which lack specificity and are generally membrane impermeable. Thus, there is a need to identify novel lead compounds that directly target MCU.

Drug discovery depends on the availability of robust, affordable and highly selective assays for high-throughput screening (HTS) [77]. At present, none of the methods commonly employed to quantify MCU-mediated Ca^{2+} dynamics, for example Ca^{2+} imaging in cell-based assays and patch-clamp electrophysiology of mitoplasts have been optimized for HTS. The biophysical properties of uniporter-mediated Ca^{2+} uptake pose a major challenge: The entry of Ca^{2+} in mitochondria is driven by the same steep membrane potential (mt-$\Delta\psi$) used to produce ATP [78]. Moreover, MCU is an intracellular target and its activity depends on increases of cytoplasmic Ca^{2+} concentrations by signalling events upstream of mitochondria. Accordingly, there is the potential in cell-based assays for false positive hits, that only apparently modulate MCU-mediated Ca^{2+} uptake, including those that affect the electron transport chain (ETC), tricarboxylic acid (TCA) cycle, mt-$\Delta\psi$, mitochondrial membrane integrity, or other components of intracellular Ca^{2+} signalling networks. An effective assay to be used in a primary HTS at the early stage of drug discovery must be designed to report on specific modulation of MCU activity while minimizing false positive hits.

Therefore, the aim of this project is the development of a robust HTS assay that effectively minimizes false discovery rate, greatly facilitating the discovery of specific MCU modulators.

Research Aim 2: To investigate the functional interconnection between MCU and MICU1 and its implication in human disorders

Publication 2: MICU1 Confers Protection from MCU-Dependent Manganese Toxicity

Mitochondria from several organisms are able to regulate intracellular Ca^{2+} dynamics, due to their ability to rapidly and transiently uptake Ca^{2+}. Overall, the complex molecular nature of the mammalian uniporter highlights the physiological relevance of achieving great plasticity and selectivity in mt-Ca^{2+} uptake.

It is from great physiological relevance that the MCU complex is highly selective in Ca^{2+} uptake, by promoting Ca^{2+} entry powered by a very large driving force for cations influx into the mitochondrial matrix and preventing or limiting uptake of other divalent ions. The highly selective permeability of the uniporter for Ca^{2+} is thought to derive from the high-affinity binding of the ion to the DXXE motif at the MCU pore [32, 42, 79, 80], whereas both gating and cooperative activation of the uniporter have been attributed to its interaction with hetero-oligomers of MICU1 and MICU2 or MICU3 [41, 48, 52-54].

However, the respective functional and mechanistic roles of those subunits in regulating uniporter activity have been so far investigated in mammalian systems where the interpretation of results is hampered by differences in the degree of gene silencing, tissue-specific protein composition [81, 82], stoichiometry and compensatory remodelling [83, 84] of the channel. Instead, the budding yeast *S. cerevisiae* represents an ideal testbed for dissecting the functional contribution of each exogenous component of the human uniporter, given that it completely lacks any detectable MCU homolog [85, 86] and endogenous mt-Ca^{2+} transport activity [22, 56, 87, 88], while enabling the facile expression and targeting of human mitochondrial proteins. Moreover, mt-Ca^{2+} uptake can be readily reconstituted in isolated mitochondria from yeast, an organism devoid of mt-Ca^{2+} uptake activity, by co-expressing the human MCU and EMRE subunits [56, 87].

The aim is here to establish a yeast-based heterologous system to investigate the functional relationship between MCU and MICU1 *in vivo* by co-expressing the human MCU, EMRE and MICU1 subunits in different combination in *S. cerevisiae*. The evolutional correlation between MCU and MICU1 is analysed, followed by a screen for environmental stress conditions, whereby the reconstitution of a MICU1-regulated and MCU-dependent mt-Ca^{2+} uptake would confer a fitness advantage to yeast cells. Consistency of findings are further evaluated in HEK-293 cells lacking MICU1.

2 Publications

2.1 Systematic Identification of MCU Modulators by Orthogonal Interspecies Chemical Screening

Declaration of contribution

Daniela M. Arduino, Jennifer Wettmarshausen, Horia Vais, Paloma Navas-Navarro, Yiming Cheng, Anja Leimpek, Zhongming Ma, Alba Delrio-Lorenzo, Andrea Giordano, Cecilia Garcia-Perez, Guillaume Médard, Bernhard Kuster, Javier García-Sancho, Dejana Mokranjac, J. Kevin Foskett, M. Teresa Alonso, and Fabiana Perocchi

I contributed to the development of the MCU-specific drug screening strategy in yeast (Figure 2) and in HeLa cells (Figure 3). To this goal, I contributed to the generation of all the yeast strains for this study. I performed the heterologous reconstitution of MCU-driven Ca^{2+} uptake in yeast and established the method for measuring mt-Ca^{2+} uptake. My work provided the foundation for the entire drug screening strategy. Specifically, I generated the data shown in Figure 1C-E and Supplementary Figure 7B. In addition, I established the experimental protocols for isolating functional mitochondria in both mouse tissues and human cells, which I used to generate the data shown in figure 4E-G. Experiments were designed in collaboration with Dr. Fabiana Perocchi and Dr. Dejana Makranjac.

Published in final edited form as:
Mol Cell. 2017 August 17; 67(4): 711–723.e7. doi:10.1016/j.molcel.2017.07.019.

Systematic Identification of MCU Modulators by Orthogonal Interspecies Chemical Screening

Daniela M. Arduino[1,2], **Jennifer Wettmarshausen**[1,2], **Horia Vais**[3], **Paloma Navas-Navarro**[4], **Yiming Cheng**[1,2], **Anja Leimpek**[1,2], **Zhongming Ma**[3], **Alba Delrio-Lorenzo**[4], **Andrea Giordano**[1,2], **Cecilia Garcia-Perez**[1,2], **Guillaume Médard**[5], **Bernhard Kuster**[5,6], **Javier García-Sancho**[4], **Dejana Mokranjac**[7], **J. Kevin Foskett**[3,8], **M. Teresa Alonso**[4], and **Fabiana Perocchi**[1,2,9,*]

[1]Gene Center/Department of Biochemistry, Ludwig-Maximilians Universität München, Munich 81377, Germany

[2]Institute for Diabetes and Obesity, Helmholtz Zentrum München, Neuherberg 85764, Germany

[3]Department of Physiology, Perelman School of Medicine, University of Pennsylvania, Philadelphia, PA 19104, USA

[4]Instituto de Biología y Genética Molecular (IBGM), University of Valladolid and Consejo Superior de Investigaciones Científicas (CSIC), Valladolid 47003, Spain

[5]Chair for Proteomics and Bioanalytics, Technical University Munich, Freising 85354, Germany

[6]Center for Integrated Protein Science Munich, Freising 85354, Germany

[7]Biomedical Center, Department of Physiological Chemistry, Ludwig-Maximilians Universität München, Martinsried 81377, Germany

[8]Department of Cell and Developmental Biology, Perelman School of Medicine, University of Pennsylvania, Philadelphia, PA 19104, USA

SUMMARY

The mitochondrial calcium uniporter complex is essential for calcium (Ca^{2+}) uptake into mitochondria of all mammalian tissues, where it regulates bioenergetics, cell death, and Ca^{2+} signal transduction. Despite its involvement in several human diseases, we currently lack pharmacological agents for targeting uniporter activity. Here we introduce a high-throughput assay that selects for human MCU-specific small-molecule modulators in primary drug screens. Using isolated yeast mitochondria, reconstituted with human MCU, its essential regulator EMRE, and aequorin, and exploiting a D-lactate-and mannitol/sucrose-based bioenergetic shunt that greatly

*Correspondence: perocchi@genzentrum.lmu.de.
9Lead Contact

SUPPLEMENTAL INFORMATION

Supplemental Information includes seven figures and can be found with this article online at http://dx.doi.org/10.1016/j.molcel.2017.07.019.

AUTHOR CONTRIBUTIONS

D.M.A. and F.P. conceived the idea for this project and designed the experiments. D.M.A., J.W., H.V., P.N.-N., A.L., Z.M., A.G., C.G.-P., A.D.-L., and D.M. performed the experiments and data analysis. Y.C. developed the software for data analysis. G.M. and B.K. advised on structure-activity relationship. D.M.A. and F.P. wrote the manuscript with input from J.G.-S., D.M., M.T.A., and J.K.F.

minimizes false-positive hits, we identify mitoxantrone out of more than 600 clinically approved drugs as a direct selective inhibitor of human MCU. We validate mitoxantrone in orthogonal mammalian cell-based assays, demonstrating that our screening approach is an effective and robust tool for MCU-specific drug discovery and, more generally, for the identification of compounds that target mitochondrial functions.

In Brief

Arduino et al. develop a high-throughput drug discovery strategy to identify chemical modulators of the mitochondrial calcium uniporter. They find that mitoxantrone is a selective and direct inhibitor of the MCU channel.

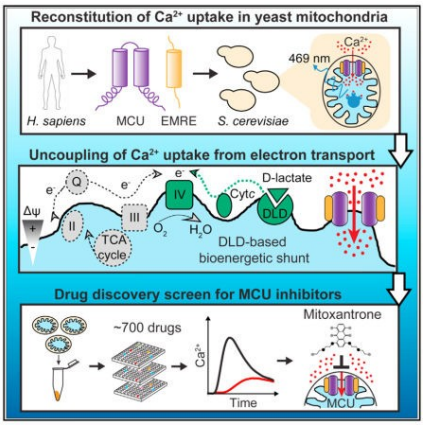

INTRODUCTION

For over half a century, it has been recognized that large amounts of Ca^{2+} can rapidly enter the matrix of mammalian mitochondria through an electrogenic mechanism driven by the large voltage generated across the inner mitochondrial membrane (IMM) during oxidative phosphorylation (OXPHOS) (Deluca and Engstrom, 1961; Vasington and Murphy, 1962). Subsequently, direct electrophysiological recordings of IMM Ca^{2+} currents demonstrated that the so-called mitochondrial calcium uniporter that mediates these fluxes was a Ca^{2+}-selective ion channel with a remarkably high capacity (Kirichok et al., 2004). During the last few years, the molecular identity and composition of the uniporter have been unraveled, including the poreforming subunit MCU (Baughman et al., 2011; Chaudhuri et al., 2013; De Stefani et al., 2011) and several positive and negative regulators (De Stefani et al., 2016; Foskett and Philipson, 2015).

Genetic loss- and gain-of-function analyses have shown that MCU-dependent regulation of mitochondrial matrix Ca^{2+} concentration (mt-Ca^{2+}) is required for numerous biological processes, including hormone secretion, neurotransmission, muscle contraction, and cell death (Marchi and Pinton, 2014). MCU dysregulation has been associated with a wide range

of human diseases, from cancer to metabolic syndrome, myopathies, and neurological diseases, whereas its ablation protects brain and heart from ischemic injury induced by mt-Ca^{2+} overload (Mammucari et al., 2016). Strategies to modulate MCU activity are of great biomedical interest and could have broad therapeutic applications (Giorgi et al., 2012). Nevertheless, pharmacological agents that directly target MCU are not yet available. Chemical inhibitors of MCU are limited to ruthenium red (RuR) and its derivatives (Moore, 1971; Nathan et al., 2017; Ying et al., 1991), which lack specificity and are generally membrane impermeable. Thus, there is a need to identify lead compounds that directly target MCU.

Drug discovery depends on the availability of robust, affordable, and highly selective assays for high-throughput screening (HTS) (Walters and Namchuk, 2003). At present, none of the methods commonly employed to quantify MCU-mediated Ca^{2+} dynamics, for example, Ca^{2+} imaging in cell-based assays and patch-clamp electrophysiology of mitoplasts, have been optimized for HTS. The biophysical properties of uniporter-mediated Ca^{2+} uptake pose a major challenge: the entry of Ca^{2+} in mitochondria is driven by the same steep membrane potential (mt-$\Delta\psi$) used to produce ATP (Gunter and Gunter, 1994). Moreover, MCU is an intracellular target, and its activity depends on increases of cytoplasmic Ca^{2+} concentrations by signaling events upstream of mitochondria. Accordingly, there is the potential in cell-based assays for false-positive hits that only apparently modulate MCU-mediated Ca^{2+} uptake, including those that affect the electron transport chain (ETC), tricarboxylic acid (TCA) cycle, mt-$\Delta\psi$, mitochondrial membrane integrity, or other components of intracellular Ca^{2+}-signaling networks. An effective assay to be used in a primary HTS at the early stage of drug discovery must be designed to report on specific modulation of MCU activity while minimizing false-positive hits.

Here we introduce a robust HTS assay that effectively minimizes false discovery rate, greatly facilitating the discovery of specific MCU modulators. We employ mitochondria from the yeast *S. cerevisiae*, which lacks MCU (Carafoli and Lehninger, 1971), providing a null background. Human MCU and its essential regulator EMRE (Kovács-Bogdán et al., 2014) are reconstituted into the yeast IMM, and MCU-mediated Ca^{2+} uptake is quantitatively measured by the Ca^{2+}-sensitive photoprotein aequorin (Bonora et al., 2013) stably expressed in the mitochondrial matrix (mt-AEQ). Key to our approach is the exploitation of a D-lactate- and mannitol/sucrose-based bionenergetic shunt unique to mitochondria from *S. cerevisiae* that enables mt-$\Delta\psi$ to be maintained in the absence of much of the ETC and in the presence of mitochondrial uncouplers. This feature greatly eliminates many false-positive hits. In a primary screen of ~700 small molecules, we identify mitoxantrone as a selective and specific inhibitor of MCU. Our orthogonal, interspecies drug-screening strategy lays the foundation for accelerating the discovery of small-molecule pharmacological agents directed against MCU.

RESULTS

A Yeast-Based Bioenergetic Shunt as a Tool to Identify Specific MCU Inhibitors

A primary challenge in developing MCU-specific drug-screening approaches consists in minimizing the false discovery rate due to compounds that compromise the driving force for

Ca^{2+} uptake, for example, inhibitors of mitochondrial bioenergetics and agents that dissipate mt-Δψ. Yeast mitochondria contain a D-lactate dehydrogenase (DLD) that transfers electrons directly to cytochrome *c* upon oxidation of D-lactate into pyruvate (Figure 1A) (Pajot and Claisse, 1974). When D-lactate is used as the respiratory substrate, it provides a bioenergetic shunt, bypassing the TCA cycle and the ETC upstream of complex IV while still generating sufficient electron transfer to develop a considerable mt-Δψ. Furthermore, the yeast IMM is only slightly affected by uncoupling agents, for example, the protonophore carbonyl cyanide m-chlorophenylhydrazone (CCCP), when the organelle is assayed in isosmotic respiratory media (e.g., mannitol/sucrose [MAS]), enabling mt-Δψ to be relatively insensitive to non-specific uncoupling.

We reconstituted and quantified human uniporter activity in the IMM of yeast mitochondria by heterologous co-expression of full-length human MCU, its essential regulator EMRE, and mt-AEQ (Figure 1B). The addition of a Ca^{2+} bolus triggered a luminescence signal that was inhibited by Ru360, confirming the functional reconstitution of uniporter-mediated Ca^{2+} uptake (Figure 1C). Ru360-dependent inhibition could be rescued by the concomitant addition of an electrogenic Ca^{2+} ionophore (ETH129), indicating that the mt-Δψ of reconstituted yeast mitochondria was intact and provided a sufficient driving force for Ca^{2+} uptake. As expected, mitochondria fueled with D-lactate were able to take up Ca^{2+}, even in the presence of specific ETC inhibitors, for example, malonate and antimycin A (Figures 1D and 1E). In contrast, mt-Ca^{2+} uptake was dramatically reduced in the presence of the same ETC inhibitors with succinate as the substrate. Likewise, mt-Ca^{2+} uptake was not affected by the addition of CCCP in a MAS buffer, whereas it was abolished in a KCl-based, intracellular-like medium (Figures 1D and 1E). Together, these results establish reconstituted yeast mitochondria energized with D-lactate in an isosmotic media as a drug-screening assay with the potential ability to discriminate against false-positive MCU modulators in early stages of drug discovery.

Drug Screening in MCU-Reconstituted Yeast Mitochondria

We optimized the yeast mitochondria-based assay for small-molecule HTS (Figure 2A). To achieve a high signal-to-noise ratio, we selected an exogenous-free [Ca^{2+}], coelenterazine analog and mitochondria density that provided a robust MCU-dependent mt-AEQ response. mt-AEQ was functionally reconstituted with native coelenterazine directly added to the purified mitochondrial pellet, which was then frozen for assaying at a later stage. For screening, reconstituted yeast mitochondria were first energized in MAS buffer supplemented with D-lactate and then transferred into a 96-well compound plate. To systematically quantify the effect of each drug on mt-Ca^{2+} uptake kinetics, the maximum amplitude of the luminescence signal (peak) and the rising phase of the bell-shaped kinetic trace (uptake rate) were extracted after automated fitting of raw light signals. Each drug was scored based on its inhibitory effect (I_{drug}) on either peak amplitude or uptake rate when compared to positive (Ru360) and negative (DMSO) controls. Compounds that exerted >50% inhibition ($I_{drug} > 0.5$) on mt-Ca^{2+} uptake kinetics were selected as hits.

As a proof of concept, we screened the NIH Clinical Collection (NCC) library in biological duplicates, which includes ~700 compounds that are not represented in other small molecule

collections and have a history of use in human clinical trials (Figure 2B). As shown in Figures 2C and 2D, the assay was highly reproducible based on a positive correlation between biological duplicates ($R_{peak(R1\ versus\ R2)}{}^2 = 0.81$), as well as between both kinetic parameters ($R_{(rate\ versus\ peak)}{}^2 = 0.99$). For statistical validation of the HTS assay, we calculated the Z′-factor, defined as the degree of separation between positive and negative controls (Zhang et al., 1999). The screen resulted in a Z′-factor of 0.69 and 0.65 for peak and uptake rate, respectively, indicating that the assay is robust and suitable for HTS applications (Figure 2E). For most drugs, I_{drug} scores were close to zero, indicating a lack of effect on MCU-mediated Ca^{2+} uptake (Figure 2F). Only two compounds scored as hits, amiodarone and mitoxantrone, which showed a strong and reproducible inhibition of mt-Ca^{2+} uptake kinetics. These lead compounds might represent specific inhibitors of the human MCU channel.

Orthogonal Yeast-Human Chemical Screening Validates Mitoxantrone as a Specific Inhibitor of MCU-Mediated Ca^{2+} Uptake

To validate the yeast assay system for identification of specific human MCU inhibitors, we compared positive hit rates in yeast and mammalian mitochondria-based drug screens (Figure 3). To this end, we re-screened the NCC library in human epitheloid cervix carcinoma (HeLa) cells (Figure 3A). The mt-Ca^{2+} uptake was measured in permeabilized HeLa cells that stably expressed mt-AEQ (Figures S1A–S1C) (Alonso et al., 2017). First, the endoplasmic reticulum (ER) was depleted of Ca^{2+} by pre-treatment with the sarco/ER Ca^{2+}-ATPase (SERCA) inhibitor thapsigargin, and the plasma membrane was selectively permeabilized with digitonin, enabling the direct delivery of an exogenous Ca^{2+} bolus to mitochondria. The mitochondria of permeabilized cells were energized in a KCl-based medium with succinate and pyruvate as respiratory substrates, resulting in the full activation of the TCA cycle and the ETC. The addition of Ca^{2+} caused a rapid enhancement of mt-AEQ luminescence that was completely abrogated by the inhibition of MCU with Ru360 (Figure 3B), as well as by uncoupling of mt-$\Delta\psi$ with CCCP (Figures S1D and S1E). Conversely, CGP37157, an inhibitor of mt-Ca^{2+} efflux by the Na^+/Ca^{2+} exchanger (Palty et al., 2010), enhanced the luminescence signal (Figure 3B). These results confirm that mt-AEQ luminescence faithfully reflects changes in the level of mt-Ca^{2+} in permeabilized HeLa cells.

Drug screening in permeabilized HeLa cells was less robust than in yeast mitochondria, with a Z′-factor of 0.47 and 0.46 for peak and uptake rate, respectively, suggesting that mammalian cell-based assays for MCU drug screening are less amenable for HTS. However, the screen was reproducible ($R_{uptake\ rate(R1\ versus\ R2)}{}^2 = 0.78$) (Figures 3C and 3D). In total, we identified 29 hits with an I_{drug} score > 0.5, indicating that these compounds likely inhibited mt-Ca^{2+} uptake (Figure 3E). Hits belonged to three main pharmacological classes (Figure 3F), anti-psychotics, antidepressants, and antihypertensives, all of which are consistently represented in small molecule libraries (Attene-Ramos et al., 2015; Gohil et al., 2010; Stavrovskaya et al., 2004). The majority of hits have been shown to uncouple mt-$\Delta\psi$ (e.g., carvedilol, triclosan, sertraline, and hexachlorophene) (Cammer and Moore, 1972; Oliveira et al., 2000; Weatherly et al., 2016), to induce mitochondrial swelling (e.g., meclomen and benzbromarone) (Tatematsu et al., 2016), and to impair ETC and OXPHOS

(e.g., miconazol, tamoxifen, trifluoperazine, and mefloquine) (Cheah and Waring, 1983; Dickinson, 1977; Gohil et al., 2010; Tuquet et al., 2000). The remaining compounds included a monoamine transporter inhibitor (indatraline), two plasma membrane voltage-gated Ca^{2+} channel blockers (amlodipine and nicardipine), and one 5-HT receptor agonist (tegaserod). Strikingly, when comparing the I_{drug} scores of each compound in the two orthogonal chemical screens (Figure 3G), we observed that all hits in the HeLa cell-based screen, except amiodarone and mitoxantrone (Figure S2), were ineffective in the yeast mitochondria-based assay. These results suggest that, whereas almost all hits from the permeabilized cell-based screen are false positives, the inhibitory activity of amiodarone and mitoxantrone on mt-Ca^{2+} uptake is not a mere consequence of a bioenergetic crisis.

Amiodarone is frequently used as a first-line therapy for arrhythmias, although its molecular mechanism remains poorly understood (Schleifer et al., 2015). Unexpectedly, amiodarone-mediated inhibition of Ca^{2+} uptake in yeast mitochondria was not concentration dependent (Figure 3H). Up to 3 μM, amiodarone inhibited both peak and uptake rate, whereas at higher concentrations it induced a dramatic increase in mt-Ca^{2+} uptake rate, which could not be prevented by pre-treatment of mitochondria with Ru360 (Figure 3I). These results suggest that amiodarone has Ca^{2+} ionophoretic properties, which is consistent with previous observations of opposite concentration-dependent effects of amiodarone on several mitochondrial functions (Varbiro et al., 2003). Accordingly, we excluded amiodarone from follow-up studies. In contrast, mitoxantrone exerted a concentration-dependent inhibition of mt-Ca^{2+} uptake in both permeabilized HeLa cells and yeast mitochondria, with half-maximal inhibition at ~10 μM (Figure 3J). Mitoxantrone has been used as an antineoplastic agent against non-Hodgkin's lymphomas and acute myeloid leukemia (Evison et al., 2016; Zee-Cheng and Cheng, 1978). It contains aromatic amines, conferring to it intrinsic optical properties (Bell, 1988; Le et al., 2006) (Figures S3A–S3C). To exclude possible interference with the mt-AEQ-based assay, we examined the effects of different concentrations of mitoxantrone on the total light signal from lysed yeast mitochondria in the presence of high [Ca^{2+}] (Figure S3D). The effects of drug and DMSO treatments were indistinguishable, indicating that mitoxantrone-dependent inhibition of mt-Ca^{2+} uptake kinetics was not an optical artifact.

Altogether, these results indicate that the DLD-based bioenergetic shunt in yeast enables the selective filtering of non-specific MCU inhibitors in drug screening.

Mitoxantrone Inhibits MCU Ca^{2+} Currents without Affecting Oxidative Phosphorylation

To confirm whether the inhibitory effects of mitoxantrone on mt-Ca^{2+} uptake were due to specific inhibition of the MCU channel, we directly recorded Ca^{2+} currents by patch-clamp electrophysiology of mitoplasts from wild-type HEK293 cells (Fieni et al., 2012; Vais et al., 2016). Typical RuR-sensitive, inwardly rectifying, Ca^{2+} concentration-dependent currents were observed in control mitoplasts (Figure 4A). Notably, 10 μM mitoxantrone reversibly and strongly reduced MCU Ca^{2+} currents by ~85% (Figures 4A–4D), with slow kinetics compared with block by RuR. In contrast, substrate-dependent oxygen consumption and response to CCCP in isolated mouse liver mitochondria were not affected by mitoxantrone (Figure 4E). Likewise, mitoxantrone was without effect on the respiratory control ratio,

which reflects the coupling between respiration and OXPHOS, in contrast to the effects of oligomycin A, a specific blocker of the mitochondrial ATP synthase (Figure 4F). Furthermore, treatment of permeabilized HeLa cells with mitoxantrone was without effect on maximal respiration rate and spare respiratory capacity (Figure 4G). These results suggest that mitoxantrone inhibits MCU-mediated Ca^{2+} uptake by specifically targeting MCU activity.

Mitoxantrone Selectively Antagonizes the MCU Channel in Intact Cells

To determine the effect of mitoxantrone on MCU-mediated Ca^{2+} uptake in intact cells, we monitored mt-Ca^{2+} kinetics during agonist-evoked intracellular Ca^{2+} signaling in HeLa cells stimulated with histamine. As shown in Figures 5A–5C, half-maximal inhibition of both mt-Ca^{2+} peak and uptake rate was reached with ~10 μM mitoxantrone and manifested after ~2 hr of drug exposure, consistent with the permeability and known intracellular pharmacokinetics of mitoxantrone (Sundman-Engberg et al., 1993). Although mitoxantrone has antineoplastic activity, effects on cell viability could not account for its inhibition of mt-Ca^{2+} uptake (Figure S4).

Next, we examined the effect of mitoxantrone on other components of the Ca^{2+}-signaling system upstream of mitochondria, including plasma membrane and intracellular ion channels. Mitoxantrone reduced mt-Ca^{2+} (Figure 5D) without altering either resting [Ca^{2+}] in the ER or amplitude of histamine-induced Ca^{2+} release in intact cells (Figure 5E) and IP_3R-mediated release of Ca^{2+} from the ER of permeabilized cells (Figure 5F). In addition, mitoxantrone was without effects on voltage-activated Ca^{2+} currents recorded in non-differentiated SH-SY5Y neuroblastoma cells (Figure 5G), store-operated Ca^{2+} channels (Figures 5H and 5I), or Ca^{2+}-activated Cl^- currents (Figures 5J and 5K) in *Xenopus* oocytes. Likewise, mitoxantrone did not affect Na^+ and K^+ currents through voltage-gated channels in mouse type II taste cells (Figures 5L–5N). Collectively, the results in per-meabilized and intact cells, isolated mitochondria, and mitoplasts demonstrate that mitoxantrone selectively inhibits the MCU channel.

The Charged Side Arms of Mitoxantrone Are Necessary for MCU Inhibition

Having established a functional link between mitoxantrone and MCU, we next sought to elucidate its pharmacophore. To establish a preliminary structure-activity relationship, we selected four anthracyclines, all chemotherapeutic drugs (daunorubicin, doxorubicin, epirubicin, and idarubicin), that share with mitoxantrone the 1,4-dihydroxyanthraquinone ring (quinizarin) (Evison et al., 2016) (Figure 6). These compounds were initially tested in duplicates at 10 μM in both yeast mitochondria and permeabilized HeLa cell-based primary screens. However, none of them had significant inhibitory effects on mt-Ca^{2+} uptake, even at high concentrations (50–100 μM) (Figure 6, top). These results indicate that the quinizarin ring is not sufficient to confer MCU inhibition by mitoxantrone and that positively charged side chains (the arms) at positions 5 and 8 may play a role. We identified four commercially available analogs (pixantrone, impurity A, disperse blue 7, and AQ4) that differ from mitoxantrone by the symmetry, length, and terminal group of their arms, and we tested them in dose-response assays (Figure 6, bottom). Compared with mitoxantrone ($k_{0.5}$ = 8.3 ± 0.9 μM), only pixantrone ($k_{0.5}$ = 15 ± 1.0 μM) (Figure S5) and impurity A ($k_{0.5}$ = 36 ± 0.2 μM)

retained inhibitory activity on Ca^{2+} uptake in yeast mitochondria. Strikingly, despite sharing the same scaffold with three planar rings and a very similar substitution pattern, disperse blue 7 and AQ4 failed to inhibit MCU activity (Figure S5). These findings suggest that the side arms of mitoxantrone, hosting both a protonated secondary amine and an extended hydroxyl-ethyl moiety, are necessary to confer its inhibitory activity on MCU. The shorter hydroxyl-ethyl arms of disperse blue 7 and the bulkier tertiary amino groups of AQ4 may weaken the affinity for MCU. Moreover, the ~4-fold decrease in the inhibitory effect of impurity A, which lacks one of the two arms, suggests that both side chains of mitoxantrone contribute to MCU inhibition.

The antitumor activities of both anthracyclines and anthracenedione-derived drugs, such as mitoxantrone and pixantrone, have been ascribed to the intercalation of the extended planar ring system into the DNA and its inhibition of topoisomerase II (Evison et al., 2016). Based on our finding that the quinizarin moiety is dispensable for MCU inhibition, we reasoned that the anti-neoplastic and anti-MCU properties of mitoxantrone should be independent. We examined the effects of the two most active inhibitors of MCU, mitoxantrone and pixantrone, as well as the inactive analog AQ4 on the viability of three cancer cell lines expressing different levels of MCU protein (Figure S6). All three anti-cancer agents were cytotoxic after 48 hr of treatment, without any change in their antiproliferative activity on control (pLKO) and MCU knockdown or overexpressing tumor cells.

Altogether, these results indicate that the MCU channel represents a previously unknown intracellular target of mitoxantrone and that the pharmacophore lies within the charged side arms.

Acidic Residues in the Selectivity Filter Mediate Mitoxantrone-Dependent Inhibition of MCU

To further characterize the mechanism of mitoxantrone-dependent MCU inhibition, we first examined its effect on MCU current densities recorded in the whole-mitoplast configuration, with either 10 μM in the pipette (matrix side) or in the bath (cytosolic side) solution. Strikingly, when mitoxantrone was present in the matrix, it was without effect on RuR-sensitive Ca^{2+} currents (Figures 7A–7D). Furthermore, matrix mitoxantrone did not prevent its inhibitory effect when added to the bath solution, on either the extent (Figure 7C) or kinetics (Figure 7D) of Ca^{2+} current inhibition. Thus, mitoxantrone likely interacts with its target on the cytosolic side of the IMM.

Because mitoxantrone inhibits mt-Ca^{2+} uptake in yeast mitochondria, which express only MCU and EMRE, its most likely target is the minimal channel complex. MCU contains two trans-membrane helices, with amino and carboxyl termini facing into the matrix, with a short hydrophilic stretch of amino acids (YSWDI) linking them at the mouth of the channel facing the mitochondrial intermembrane space (Baughman et al., 2011; De Stefani et al., 2011). This region of the channel has highly conserved acidic residues, including an aspartate in position 261 that is involved in Ca^{2+} permeation and selectivity (Cao et al., 2017; Chaudhuri and Clapham, 2014; Oxenoid et al., 2016). To predict a drug-target interaction and to identify key residues, we performed molecular docking using the YSWDI motif in the pentameric *C. elegans* MCU pore structure (Oxenoid et al., 2016) (Figure 7E). Mitoxantrone was flexibly docked into this region and a key interaction was found between

one of the positively charged secondary amines in its 2-hydroxyethylamino side chains and three of the five aspartates in the selectivity filter (Figures 7F and 7G). The electrostatic interaction enforced by these hydrogen bonds was further enhanced by two hydrogen bonds with the hydroxyl groups of two serine residues in the YSWDI motif, which have been previously shown to mediate the interaction of Ru360 and RuR with MCU (Baughman et al., 2011; Chaudhuri and Clapham, 2014).

To validate the hypothesis of a specific mitoxantrone-MCU interaction, we examined the effects of replacing the Asp261 with an alanine (D261A) on the inhibitory efficacy of mitoxantrone. We created a yeast strain expressing the human MCU D261A mutant together with human EMRE and mt-AEQ (Figure S7A). Compared with the wild-type channel, yeast mitochondria expressing the D261A mutant exhibited a ~4-fold decrease in mt-Ca^{2+} uptake (Figure S7B). Notably, this single point mutation was sufficient to confer nearly complete resistance to inhibition by RuR (Figure 7H), highlighting a previously unknown role of this highly conserved residue in mediating ruthenium-dependent MCU inhibition. As predicted by the molecular docking, mt-Ca^{2+} uptake in the D261A mutant strain was less sensitive to inhibition by both mitoxantrone ($k_{0.5}$ (D261A) = 10.7 ± 1.4 μM versus $k_{0.5}$ (WT) = 7.7 ± 0.4 μM; $p < 0.001$) and pixantrone ($k_{0.5}$ (D261A) = 31.8 ± 6.5 μM versus $k_{0.5}$ (WT) = 16.5 ± 0.8 μM; $p < 0.001$) (Figures 7I and 7J). These results provide compelling biochemical and functional evidence that mitoxantrone is a direct inhibitor of MCU.

DISCUSSION

Since the breakthrough discovery of the molecular identity of MCU (Baughman et al., 2011; De Stefani et al., 2011; Perocchi et al., 2010), numerous studies have suggested that this channel is a potential target of broad pharmacological interest (De Stefani et al., 2016). Nevertheless, the lack of specific reagents that directly regulate MCU function has greatly impeded progress in this area. Specific chemical modulators of MCU activity would be invaluable for assessing the roles of the uniporter in mitochondrial biology and cell physiological processes, and they could also provide lead compounds for the development of therapeutic candidate drugs for many human diseases.

The tight interconnection among intracellular Ca^2 signaling, energy production, mitochondrial membrane potential, and MCU-mediated Ca^{2+} uptake poses a major challenge in the design of robust and effective HTS assays for the discovery of specific modulators of this channel. Compounds that directly or indirectly affect the ETC, uncouple OXPHOS, dissipate mt-Δψ, and/or disrupt membrane integrity can significantly increase the false discovery rate in primary screens. In vitro reconstitution systems (De Stefani et al., 2011) may not offer an optimal tool for MCU drug discovery, given that the expression of MCU was shown to be not sufficient to reconstitute a functional channel (Kovács-Bogdán et al., 2014). Similarly, in silico predictions of drug-MCU interactions are limited by the lack of high-resolution structural information (Lee et al., 2015, 2016; Oxenoid et al., 2016).

Here we have developed a yeast-based drug-screening assay that robustly identifies direct modulators of human MCU to facilitate systematic assessment of clinically approved compounds for targeting uniporter activity in vivo. We exploit unique evolutionary and

biophysical properties of yeast mitochondria for MCU-targeted drug discovery. First, mitochondria from *S. cerevisiae* lack a uniporter mechanism and are unable to take up Ca^{2+} (Carafoli and Lehninger, 1971), providing an in vitro system devoid of intrinsic mt-Ca^{2+} permeability and insensitive to interference from upstream, intracellular Ca^{2+}-signaling events. Second, *S. cerevisiae* expresses a mitochondrial shunt pathway that bypasses the majority of ETC complexes and NADH-generating pathways but is sufficient for maintaining mt-$\Delta\psi$. Furthermore, when yeast mitochondria are energized in isosmotic respiratory media, mt-$\Delta\psi$ is resistant to the concentrations of the protonophore CCCP that are sufficient to dissipate the proton gradient in mammalian cells. Importantly, human MCU-mediated Ca^{2+} uptake can be reconstituted in yeast mitochondria by exogenous expression of human MCU and EMRE (Kovács-Bogdán et al., 2014). Together, these properties confer to yeast mitochondria-based Ca^{2+} uptake assays a remarkable advantage over mammalian ones, in which direct and indirect effects of drugs on MCU-dependent Ca^{2+} uptake cannot be readily deconvolved. In addition, purified yeast mitochondria can be frozen and stored without losing the ability to respond to an added bolus of Ca^{2+} with enhanced aequorin luminescence, providing an assay platform that can be used at any stage of drug discovery. Finally, only small quantities of yeast mitochondria (1 μg/compound) are required to screen even large chemical libraries, providing a drug-screening assay that is cost- and time-effective and easily scalable.

As a proof of concept, we used thawed yeast mitochondria energized with D-lactate in a mannitol/sucrose-based medium to screen the NCC library, which covers a broad range of pharmacological classes. We identify mitoxantrone, one of the oldest chemotherapeutic drugs still on the market (Zee-Cheng and Cheng, 1978), as an inhibitor of MCU. Mitoxantrone has not been previously linked to the regulation of mt-Ca^{2+} homeostasis, proving the potential and efficacy of our yeast-based assay in the discovery of MCU modulators. In subsequent assays, including permeabilized and intact human cells, isolated mitochondria, and mitoplast electrophysiology, we confirmed that mitoxantrone inhibited mt-Ca^{2+} uptake in a dose-dependent manner that was not secondary to the impairment of mitochondrial bioenergetics or to effects on other ion channels. Mitoxantrone reversibly inhibited MCU Ca^{2+} currents from the inner membrane space side in mammalian cell mitochondria, suggesting that its target was likely the MCU/EMRE complex itself. Its specificity was further confirmed by the demonstration that inhibition of MCU activity was sensitive to modifications of mitoxantrone structure, specifically its positively charged side chains, and to mutations in highly conserved aspartate residues in the selectivity filter of the MCU channel. Neutralization of these negatively charged residues conferred almost complete protection against RuR inhibition, suggesting a rather unspecific binding to the uniporter, which is based on an ionic interaction between the Asp261 residues and the protonated amines of RuR. Instead, molecular docking analysis predicted for mitoxantrone a more complex binding architecture involving both the arms and the ring system, whereby a single D261A point mutation significantly compromised the inhibitory effect of mitoxantrone on uniporter-mediated Ca^{2+} uptake but was not sufficient to completely abrogate its binding to MCU. Finally, our results suggest that the anti-neoplastic and anti-MCU activities derive from different structural moieties within mitoxantrone, providing a

foundation for medicinal chemistry efforts to develop effective lead compounds for the specific modulation of MCU.

More generally, our yeast mitochondria-based drug-screening approach should have broad utility. Of note, the orthogonal screen in permeabilized human cells suggests that, at the concentrations employed here, many clinically approved drugs impinge upon mitochondrial metabolism. This result further validates the yeast system as a more robust screening assay. Furthermore, this system is versatile, and additional MCU components and regulatory mechanisms can be reconstituted, providing a broad drug discovery strategy for the selection of lead compounds against the uniporter complex.

STAR★METHODS

KEY RESOURCES TABLE

REAGENT or RESOURCE	SOURCE	IDENTIFIER
Antibodies		
Rabbit polyclonal anti-MCU	Sigma-Aldrich	Cat. No. HPA016480; Lot No.C0114358; RRID: AB_2071893
Rabbit polyclonal anti-EMRE - C22orf32 (clone C-12)	Santa Cruz Biotechnology	Cat. No. sc-86337; Lot No.K0215; RRID: AB_2250685
Mouse monoclonal anti-Aequorin (clone 6E3.2)	Merck/Millipore	Cat. No. MAB4405; RRID: AB_94900
Mouse monoclonal anti-β-Actin (clone AC-74)	Sigma-Aldrich	Cat. No. A2228; Lot No.085M4754V; RRID: AB_476697
Mouse monoclonal anti-Phosphoglycerate Kinase (PKGA) (clone 22C5D8)	Thermo Fisher Scientific	Cat. No. 459250; RRID: AB_2532235
Anti-MCU (residues 285-351) produced in rabbit	This paper	N/A
Anti-Sc-Yme1 produced in rabbit	Schreiner et al., 2012	N/A
Biological Samples		
Human Dermal Fibroblasts, neonatal (NHDFn)	Laboratory of Holger Prokisch	N/A
Chemicals, Peptides, and Recombinant Proteins		
Coelenterazine, derivative n	Biotium	Cat. No. 10115-1; CAS: 123437-22-9
Coelenterazine, native	Abcam	Cat. No. ab145165; CAS: 55779-48-1
Ru360	Calbiochem	Cat. No. 557440
Ruthenium red	Abcam	Cat. No. ab120264; CAS: 11103-72-3
Calcium Ionophore II (ETH-129)	Sigma-Aldrich	Cat. No. 21193; CAS: 74267-27-9
Sodium-D-lactate	Sigma-Aldrich	Cat. No. 71716; CAS: 920-49-0
Sodium succinate dibasic hexahydrate	Sigma-Aldrich	Cat. No. S2378; CAS: 6106-21-4
Dimethyl malonate	Sigma-Aldrich	Cat. No. 136441; CAS: 108-59-8
Antimycin A from *Streptomyces sp.*	Sigma-Aldrich	Cat. No. A8674; CAS: 1397-94-0
Carbonyl cyanide m-chlorophenyl hydrazone (CCCP)	Sigma-Aldrich	Cat. No. C2759; CAS: 555-60-2
Potassium cyanide	Sigma-Aldrich	Cat. No. 60178; CAS: 151-50-8
Thapsigargin	Sigma-Aldrich	Cat. No. 586005; CAS: 67526-95-8

REAGENT or RESOURCE	SOURCE	IDENTIFIER
Digitonin	Sigma-Aldrich	Cat. No. D141; CAS:11024-24-1
CGP-37157	Sigma-Aldrich	Cat. No. C8874; CAS: 75450-34-9
Mitoxantrone	Sigma-Aldrich	Cat. No. M6545; CAS:70476-82-3
Amiodarone	Sigma-Aldrich	Cat. No. A8423; CAS: 19774-82-4
AQ4	Sigma-Aldrich	Cat. No. A9236; CAS: 70476-63-0
Zymolyase 20T from *Arthrobacter luteus*	Amsbio	Cat. No. 120491-1
Adenosine 5′-diphosphate sodium salt	Sigma-Aldrich	Cat. No. A2754; CAS: 20398-34-9
Oligomycin A	Sigma-Aldrich	Cat. No. 75351; CAS: 579-13-5
Rotenone	Sigma-Aldrich	Cat. No. R8875; CAS: 83-79-4
Histamine dihydrochloride	Sigma-Aldrich	Cat. No. H7250; CAS: 56-92-8
D-myo-Inositol 1,4,5-tris-phosphate trisodium salt	Sigma-Aldrich	Cat. No. I9766
2,5-ditert-butyl-benzohydroquinone (TBH)	Sigma-Aldrich	Cat. No. 419648 CAS: 2460-77-7
Pixantrone dimaleate (Pixuvri)	CTI Life Sciences	N/A
Impurity A	Sigma-Aldrich	Cat. No. M2305005; CAS: 89991-52-6
Disperse blue 7	Boc Sciences	Cat. No. 3179-90-6; CAS: 3179-90-6
Daunorubicin hydrochloride	Sigma-Aldrich	Cat. No. 30450; CAS: 23541-50-6
Doxorubicin hydrochloride	Sigma-Aldrich	Cat. No. D1515; CAS: 25316-40-9
Epirubicin hydrochloride	Sigma-Aldrich	Cat. No. E9406; CAS: 56390-09-1
Idarubicin hydrochloride	Sigma-Aldrich	Cat. No. I1656; CAS: 57852-57-0
Lipofectamine 2000 Transfection Reagent	Thermo Fisher Scientific	Cat. No. 11668019
Critical Commercial Assays		
Cell Titer-Glo Luminescent Cell Viability Assay	Promega	Cat. No. G7571
Pierce BCA Protein Assay Kit	Thermo Fisher Scientific	Cat. No. 23227
Deposited Data		
Unprocessed Image Data	This paper	http://dx.doi.org/10.17632/54jw24wvn5.1
Experimental Models: Cell Lines		
HeLa cells	ATCC	CCL-2
HEK293T cells	ATCC	CRL-11268
SH-SY5Y cells	Sigma-Aldrich	Cat. No. 94030304
HeLa cells stably expressing mt-AEQ	This paper	N/A
HeLa cells stably expressing ER-AEQ	Rodríguez-Prados et al., 2015	N/A
NHDF cells stably expressing mt-AEQ	This paper	N/A
SH-SY5Y cells stably expressing mt-AEQ	This paper	N/A
MCF-7 cells stably overexpressing full-length MCU	This paper	N/A
MCF-7 cells stably expressing sh-MCU	This paper	N/A
PLB-985 cells stably overexpressing full-length MCU	This paper	N/A
PLB-985 cells stably expressing sh-MCU	This paper	N/A

REAGENT or RESOURCE	SOURCE	IDENTIFIER
Toledo cells stably overexpressing full-length MCU	This paper	N/A
Toledo cells stably expressing sh-MCU	This paper	N/A
Experimental Models: Organisms/Strains		
S. cerevisiae: Strain background: YPH499 expressing $HsMCU^{WT}$/EMRE or $HsMCU^{D261A}$/EMRE and mt-AEQ	This paper	N/A
Mouse: Crl:NMRI(Han)	Charles River	N/A
Mouse: TRPM5-GFP *Calhm1*-KO: B6.129S - TRPM5- GFP/$Calhm1^{-/-}$	Ma et al., 2017	N/A
Xenopus laevis	*Xenopus* One	N/A
Oligonucleotides		
shRNA targeting sequence: MCU 5′-GCAAGGAGTTTCTTTCTCTTT-3′	RNAi consortium, Broad Institute	TRCN0000133861
Recombinant DNA		
MCU full length (pLX304)	This paper	N/A
p316GPD (plasmid)	This paper	N/A
p423GPD (plasmid)	Mumberg et al., 1995	N/A
p425GPD (plasmid)	Mumberg et al., 1995	N/A
Software and Algorithms		
pClamp 10	Molecular Devices	N/A
GraphPad Prism 5.0	GraphPad Software	N/A
Igor Pro	Wavemetrics	N/A
MATLAB R2014b	MathWorks	N/A

CONTACT FOR REAGENT AND RESOURCE SHARING

Further information and requests for resources and reagents should be directed to and will be fulfilled by the Lead Contact, Fabiana Perocchi (perocchi@genzentrum.lmu.de).

EXPERIMENTAL MODEL AND DETAILS

Cell lines—HeLa cells stably expressing a mitochondrial matrix-targeted GFP-aequorin (mt-AEQ) were generated as in Manjarrés et al. (2008). The mitochondrial-targeting sequence consisted of the first 31 residues of the subunit VIII of the human cytochome c oxidase fused in frame to GFP-aequorin. HeLa cells stably expressing an endoplasmic reticulum-(ER) targeted GFP-aequorin (ER-AEQ) were previously generated (Rodríguez-Prados et al., 2015). The low Ca^{2+}-affinity GFP-aequorin carrying the D119A substitution in the aequorin gene and fused at its N terminus to the Igγ2b heavy chain gene was previously described (Chamero et al., 2008). HeLa cells were grown in Dulbecco's modified Eagle's medium (DMEM) with high-glucose (Sigma-Aldrich; D6429), 10% FBS (Sigma-Aldrich; F7524) and 100 μg/ml geneticin (Thermo Fisher Scientific; 10131027). HEK293T cells were grown in DMEM with high-glucose, 10% FBS, 100 U/ml penicillin, and 100 μg/ml streptomycin. SH-SY5Y cells were grown in a 1:1 mixture of F-12 and MEM media supplemented with 10% FBS, 0.1 mM essential aminoacids, 1 mM Na^{+}-pyruvate, 100 U/ml

penicillin and 100 μg/ml streptomycin. Human breast adenocarcinoma (MCF-7) cells were grown in DMEM with high-glucose supplemented with 10% FBS. Human peripheral blood acute myeloid leukemia (PLB-985) and non-Hodgkin's B cell lymphoma (Toledo) cells were grown in 90% RPMI 1640 (Thermo Fisher Scientific, 11879020) medium supplemented with 10% h.i. dialyzed FBS (Thermo Fisher Scientific, 26400044). Normal human dermal neonatal fibroblasts (NHDF) were grown in DMEM with high-glucose, supplemented with 10% FBS and 2 mM GlutaMAX (Thermo Fisher Scientific, 35050061). All cell lines were incubated at 37°C and 5% CO_2.

MCF-7, PLB-985 and Toledo cell lines were infected with lentivirus generated from an empty vector (pLKO), a pLKO vector expressing a shRNA targeting MCU (TRCN0000133861, 5′ GCAAGGAGTTTCTTTCTCTTT-3′) or a pLEX304 vector expressing a tagged wild-type human MCU and 48 hr post-transduction cells were selected with puromycin (2 μg/ml) or blasticidin (5 μg/ml), respectively, for 5–7 days and expanded.

Animals, housing and genotyping—Mice were housed in a pathogen-free, temperature- and humidity-controlled vivarium on a 12:12-h light-dark cycle. Diet consisted of standard laboratory chow and double-distilled water. All animal procedures in NMRI mice were in accordance with the European Community Council Directive for the Care and Use of Laboratory Animals (86/609/ECC) and German Law for Protection of Animals and were approved by the local authorities. All experiments were performed with female NMRI mice that were at least 3 mo old.

All methods regarding the handling of TRPM5-GFP Calhm1-KO mice were approved by the University of Pennsylvania's Animal Care and Use Committee and in accordance with the National Institutes of Health "Guidelines for the Care and Use of Experimental Animals." Only transgenic mice expressing GFP were used in experiments. All experiments were performed with Calhm1-KO knockout littermates of both sexes that were at least 3 mo old. Mouse genotypes were determined by real-time PCR (Transnetyx, Cordova, TN).

Yeast Strains—The yeast mt-AEQ construct was made by cloning the aequorin-coding sequence into the p316GPD expression plasmid. To ensure mitochondrial localization, the aequorin-coding sequence was preceded by the sequence coding for the first 69 residues, encompassing the matrix targeting sequence, of subunit 9 of *Neurospora crassa* F_oF_1-ATPase. DNA sequences coding for intron-less versions of human wild-type MCU or D261A mutant and EMRE were cloned into yeast expression plasmids p423GPD and p425GPD, respectively (Mumberg et al., 1995). The three plasmids were simultaneously transformed into the wild-type yeast strain YPH499 (Sikorski and Hieter, 1989). Transformants were selected on selective glucose medium lacking uracil, histidine and leucine. To test expression and subcellular localization of heterologous proteins, yeast were grown in selective lactate medium containing 8.5 g/L yeast nitrogen base, 25 g/L ammonium sulfate, 2% (v/v) lactic acid (90%) and 0.1% glucose, supplemented with adenine, lysine and tryptophan as selection markers. At an OD ~0.8 cells were harvested at 1000 *g* for 5 min at room temperature. The cell pellet was re-suspended in SHK buffer (0.6 M sorbitol, 20 mM HEPES/KOH pH 7.2, 80 mM KCl, and 1mM PMSF) and vortexed with glass beads 5 times for 30 s with cooling down in between. This mix was centrifuged at 1000 *g* for 5 min at 4°C

and the collected supernatant was further centrifuged at 20,000 *g* for 10 min at 4°C. The resulting supernatant (cytosolic fraction) was precipitated with trichloroacetic acid and re-suspended in Laemmli buffer. The pellet (mitochondrial fraction) was also directly re-suspended in Laemmli buffer. Mitochondrial and cytosolic fractions were separated under reducing conditions on 14% SDS-PAGE gels. Immunoblotting was performed according to standard procedures using affinity-purified home-made antibodies raised in rabbits against the C-terminal segment of human MCU (residues 285-351) fused to maltose binding protein, and commercially available antibodies: MCU (Sigma-Aldrich, HPA016480), EMRE (Santa Cruz Biotechnology, sc-86337) and Aequorin (clone 6E3.2, Merck/Millipore; MAB4405). Antibodies against YME1 and PKGa (Thermofisher/Novex, 459250) were used as markers for mitochondrial and cytosolic fractions, respectively.

METHOD DETAILS

Isolation of Yeast Mitochondria for Drug Screening—Yeast were grown at 30°C in selective lactate medium to an OD ~1, harvested by centrifugation at 5,000 *g* for 5 min at room temperature and washed twice with milliQ water. The yeast pellet was re-suspended in pre-warmed DTT buffer (10 mM DTT, 100 mM Tris) and incubated for 10 min at 30°C on an orbital shaker. The suspension was then centrifuged at 3,000 *g* for 5 min and the pellet was washed twice with 1.2 M sorbitol. The pellet was collected by centrifugation at 4,000 *g,* resuspended in zymolyase buffer (1.2 M sorbitol, 20 mM KH_2PO4, 3 mg zymolyase/g yeast pellet) and shaken gently at 30°C for 45 min to obtain spheroplasts. Afterward, spheroplasts were harvested by centrifugation at 3,000 *g* for 5 min and re-suspended in ice-cold homogenization buffer (10 mM Tris pH 7.4, 0.6 M sorbitol, 1 mM EDTA, 0.2% BSA, 1 mM PMSF). Homogenization was performed with 15 strokes in a glass homogenizer. The homogenate was then centrifuged twice at 4,000 *g* for 5 min and the supernatant was further centrifuged at 10,000 *g* for 10 min. The pellet was re-suspended in 30 mL of SEM-buffer (0.25 M sucrose, 1 mM EDTA, 10 mM MOPS-KOH, pH 7.2) and crude mitochondria were isolated by centrifugation at 12,000 *g* for 12 min. The final mitochondrial pellet was gently re-suspended in SEM-buffer and protein concentration was determined with the Pierce BCA Protein Assay Kit using BSA as a standard. The photoprotein aequorin was reconstituted with 3 μM native coelenterazine directly added to the mitochondrial pellet which was incubated on ice, in darkness for 2 hr. Aliquots of 10 μg/μL were flash-frozen in liquid nitrogen and stored at −80°C for further use.

Yeast Mitochondria-Based Drug Discovery Screen—Frozen aliquots of reconstituted yeast mitochondria were thawed on ice and diluted into MAS buffer (70 mM sucrose, 220 mM mannitol, 10 mM KH_2PO_4, 5 mM $MgCl_2$, 2 mM HEPES, 50 μM EGTA, 0.2% essentially fatty acid-free BSA, pH 7.2/KOH) supplemented with 10 mM D-lactate as respiratory substrate. Yeast mitochondria were seeded into white 96-well compound plates (PerkinElmer) at 1 μg/90 μL using a MultiDrop Combi (Thermo Fisher Scientific). The NIH Clinical Collection library, consisting of 686 compounds (10 μM, in 0.1% DMSO) was screened in biological duplicates. The first and last column of each plate contained 10 μL of 1% DMSO (negative control) and 100 μM Ru360 (positive control), respectively. Mitochondria were incubated in the presence of compounds for 5 min at room temperature

and Ca^{2+}-stimulated light signal was recorded at 469 nm every 0.1 s with a luminescence counter (MicroBeta^2 LumiJET Microplate Counter, PerkinElmer).

Permeabilized HeLa Cell-Based Drug Discovery Screen— HeLa cells stably expressing mt-AEQ were harvested at a density of 500,000 cells/mL in growth medium supplemented with 20 mM HEPES (pH 7.4/NaOH), and the photoprotein aequorin was reconstituted by incubation with 3 μM coelenterazine derivative n for 3 hr at room temperature. Cells were centrifuged at 300 *g* for 3 min and the pellet was re-suspended in an extracellular-like buffer containing 145 mM NaCl, 5 mM KCl, 1 mM $MgCl_2$, 10 mM glucose, 10 mM HEPES and 500 μM EGTA (pH 7.4/NaOH), supplemented with 200 nM thapsigargin. After 20 min at room temperature, cells were collected by centrifugation at 300 *g* for 3 min and the pellet was resuspended in an intracellular-like buffer containing 140 mM KCl, 1 mM KH_2PO_4/K_2HPO_4, 1 mM $MgCl_2$, 20 mM HEPES, 100 μM EGTA (pH 7.2/KOH), supplemented with 1 mM Na^+-pyruvate, 1 mM ATP/$MgCl_2$ and 2 mM Na^+-succinate. Cells were permeabilized with 60 μM digitonin for 5 min, collected by centrifugation at 300 *g* for 3 min, resuspended in intracellular-like buffer at a density of ~800 cells/μL, and 90 μL were then dispensed in a white 96-well compound plate (PerkinElmer) using a MultiDrop Combi (Thermo Fisher Scientific). The first and last column of each plate contained 10 μL of 1% DMSO (negative control) and 100 μM Ru360 (positive control), respectively. Cells were incubated for 5 min at room temperature and Ca^{2+}-stimulated light signal was recorded at 469 nm every 0.1 s with a luminescence counter (MicroBeta^2 LumiJET Microplate Counter, PerkinElmer).

Mitoplast Patch-Clamp Recording— Mitoplast isolation and electrophysiology were performed as described (Fieni et al., 2012; Vais et al., 2016). Patch pipettes had resistances of 20 – 60 MΩ when filled with (in mM): 130 TMA-OH, 100 HEPES, 10 glutathione, 2 $MgCl_2$, 1.5 EGTA, pH 7.0/D-gluconic acid, osmolarity 330–350 mOsm/kg. Mitoplasts were initially bathed in (in mM): 150 KCl, 10 HEPES, pH 7.2, osmolarity 300 mOsm/Kg ("KCl-DVF" solution). Voltage pulses of 350 – 500 mV amplitude and 15 – 50 ms duration, delivered by the PClamp-10 (Molecular Devices) program, were used to obtain the "whole-mitoplast" configuration. Access resistance (30 – 90 MΩ) and mitoplast capacitance C_m (0.2 – 1 pF) were determined using the membrane test protocol of the PClamp-10 software. After the whole-mitoplast configuration was obtained, the KCl-DVF bath solution was exchanged with HEPES-EGTA (150 mM HEPES, 1.5 mM EGTA, pH 7.0/Tris-base) for baseline (control) measurements, followed by HEPES (no EGTA) solutions with 0.1 and 1 mM $CaCl_2$ (with or without 10 μM mitoxantrone), successively. Finally, a HEPES-based solution with 1 mM $CaCl_2$ and 200 nM ruthenium red (RuR) was perfused to record the baseline (I_{RuR}) after complete block of MCU Ca^{2+} currents. Osmolarities of all bath solutions were 297–305 mOsm/Kg, adjusted with sucrose. The voltage protocol, delivered by the PClamp-10 software with a DigiData-1550 interface (Molecular Devices), consisted in stepping from V_m = 0 mV to −160 mV for 20 ms, followed by ramping to 80 mV for 860 ms, dwelling at 80 mV for 20 ms and return to 0 mV. Currents were recorded using an Axopatch 200-B amplifier (Molecular Devices). Data were acquired at room temperature with a sampling rate of 50 kHz and anti-aliasing filtered at 1 kHz. Data analysis was

performed with the PClamp-10 software. For quantitative comparisons, current densities were calculated with the formula:

$$\frac{I_{MCU}}{C_m}=\frac{I_{Ca}-I_{RuR}}{C_m},$$

I_{Ca} and I_{RuR} being measured at $V_m = -160$ mV, with 1 mM Ca^{2+} in the bath.

Isolation of Mouse Liver Mitochondria— Mitochondria were isolated from freshly collected livers of female NMRI mice. After cardiac perfusion, livers were excised and minced with 20 mL isolation buffer containing (in mM): 220 mannitol, 80 sucrose, 10 HEPES, 1 EDTA, and 0.5% essentially fatty acid-free BSA supplemented with protease inhibitors (pH 7.4/KOH). The tissue was homogenized with two strokes at 300 rpm using a loose-fitting Teflon homogenizer followed by nitrogen cavitation at 800 *psi* for 10 min. The homogenate was centrifuged at 600 *g* for 10 min at 4°C and the supernatant was further centrifuged at 4,000 *g* for 10 min. The buffy-coat was removed and the pellet was re-suspended in 20 mL of ice-cold isolation buffer. The wash-and-centrifugation step was repeated twice, once in the presence of BSA and then in the absence of BSA. The final pellet was re-suspended in isolation buffer without BSA and stored on ice for further use. Mitochondrial protein concentration was determined with the Pierce BCA Protein Assay Kit (Thermo Fisher Scientific) using BSA as standard.

Mitochondrial Bioenergetics Assays— Freshly isolated mouse liver mitochondria or HeLa cells were re-suspended in MAS buffer (in mM: 70 sucrose, 220 mannitol, 10 KH_2PO4, 5 $MgCl_2$, 2 HEPES, 0.05 EGTA, supplemented with 0.2% essentially fatty acid-free BSA, pH 7.2/KOH) to a final concentration of 0.6 mg mitochondria/mL and $2x10^6$ cells/mL, respectively. HeLa cells were permeabilized with 60 μM digitonin. Oxygen consumption rate (OCR) was measured using a Clark-type oxygen electrode (Oxytherm System, Hansatech Instruments). Substrate-dependent respiration (basal) was initiated by addition of 10 mM succinate and 2 μM rotenone; ADP-dependent respiration (ADP-coupled) was stimulated by the addition of 4 mM ADP; maximal respiration (uncoupled) was reached upon addition of 3 μM and 15 μM CCCP to isolated mitochondria and permeabilized HeLa cells, respectively. Respiratory control ratio (RCR), maximal respiration, drug-stimulated respiration and spare respiratory capacity were calculated as follows: ADP-coupled/basal OCR, uncoupled-antimycin OCR, drug-coupled/ basal OCR, uncoupled-basal OCR after accounting for non-mitochondrial respiration as previously described (Brand and Nicholls, 2011; Divakaruni et al., 2014).

Mitochondrial and ER Ca^{2+} Uptake Measurements— HeLa and SH-SY5Y cells stably expressing mt-AEQ were seeded in white 96-well plates at 25,000 cells/well. NHDFn cells stably expressing mt-AEQ were seeded in white 96-well plates at 12,000 cells/well. After 24 hr, aequorin was reconstituted with 2 μM native coelenterazine for 1 hr at 37°C. Cells were treated with different concentrations of mitoxantrone or DMSO (0.2%) added to the growth media and incubated for 1 or 2 hr. Under the same conditions, cell viability was measured with the Cell Titer-Glo Luminescent Viability assay kit (Promega, G7571). Mt-

AEQ-based measurements of Ca^{2+}-dependent light kinetics were performed upon 100 μM histamine (HeLa and NHDFn cells) or 90 mM KCl (SH-SY5Y cells) stimulation. Light emission was measured in a luminescence counter (MicroBeta^2 LumiJET Microplate Counter, PerkinElmer) at 469 nm every 0.1 s. Experiments were also performed in HeLa cells transiently transfected with mt-AEQ (Manjarrés et al., 2008). Briefly, cells were seeded in 4-well plates at 4x10^4 cells/well 24 hr prior to transfection with Lipofectamine 2000 (Thermo Fisher Scientific, 11668-019). One day after transfection, cells expressing apoaequorin were incubated with 1 μM native coelenterazine and mitoxantrone (20 μM) or vehicle DMSO (0.2%) for 2 hr at 22°C in an external medium containing (in mM): 145 NaCl, 5 KCl, 1 $CaCl_2$, 1 $MgCl_2$, 10 glucose, 10 Na–HEPES, pH 7.4. Luminescence was recorded in a purpose-built luminometer (Cairn, UK) equipped with a perfusion system (~5 mL/min flow rate) at 22°C and mt-[Ca^{2+}] was quantified (Montero et al., 2000). For ER-[Ca^{2+}] measurements, cells stably-expressing ER-AEQ were reconstituted with 1 μM coelenterazine derivative n by incubation in Ca^{2+}-free external medium with 0.5 mM EGTA and 10 μM of the SERCA inhibitor 2,5-ditert-butyl-benzohydroquinone, TBH) with either mitoxantrone (20 μM) or vehicle DMSO (0.2%) for 2 hr at 22°C. The experiment was started by washing out TBH with external medium containing 1 mM $CaCl_2$ during 5 min. Then, cells were challenged with histamine (100 μM) during 30 s. In the experiments using permeabilized cells, these were incubated for 1 min with digitonin (50 μM) in an intracellular-like medium containing (in mM): 140 KCl, 1 K_2HPO_4, 1 $MgCl_2$, 1 Mg-ATP, 2 sodium succinate, 1 sodium pyruvate, 20 sodium-HEPES (pH 7.2), and 0.5 EGTA. The solution was then switched to an intracellular-like medium containing 100 nM free-Ca^{2+} (buffered with EGTA) during 5 min in order to refill the ER. Inositol trisphosphate (200 nM) was spiked in the same intracellular-like medium for 30 s. At the end of each experiment, cells were lysed by perfusion with a solution containing 0.1 mM digitonin and 10 mM $CaCl_2$ to release all the residual aequorin counts. Light emission was calibrated using the constant values previously published (Montero et al., 2000).

Electrophysiological Measurements on Taste Cells— Whole-cell currents were measured from individual type II taste cells isolated from the circumvallate papillae of TRPM5-GFP *Calhm1*-KO mice. Currents were measured with an Axopatch 200-B amplifier (Molecular Devices) controlled via an ITC-16 interface (Instrutech) by Pulse software (Heka). Currents were evoked by 100 ms voltage pulses from −80 to +65 mV in 5 mV increments, from a holding potential of −70 mV. The pipette solution contained (in mM): 140 K^+, 6 Na^+, 1 Mg^{2+}, 1 Ca^{2+}, 30 Cl^-, 11 EGTA, 3 ATP^{2-}, 0.3 Tris GTP, and 10 HEPES, pH 7.3 adjusted by methanesulfonic acid, 290 mOsm. The bath solution contained (in mM): 150 Na^+, 5.4 K^+, 1.5 Ca^{2+}, 1 Mg^{2+}, 150 Cl^-, 20 glucose, and 10 HEPES, pH 7.4 adjusted by methanesulfonate, 330 mOsm. I–V relations of peak inward Na^+ currents were determined before and after > 5 min continuous perfusion of 10 μM mitoxantrone into the recording chamber (Perfusion Fast-Step, SF-77B, Warner Instruments) and again after drug washout. Likewise, I–V relations of outward K^+ currents were obtained by measurements of steady-state currents at the end of 100-ms pulses. All currents were normalized by the whole-cell capacitance (the average capacitance of 4.5 pF; n = 3).

Electrophysiological Measurements on SH-SY5Y Cells—SH-SY5Y cells were plated onto glass coverslips and mounted in a recording chamber that was continuously perfused with either regular bath solution (in mM): 10 $BaCl_2$, 145 TEA-Cl, 10 HEPES, 10 glucose, pH 7.4/TEA-OH, osmolarity 300 mOsm/Kg; or with bath solution supplemented with 10 μM mitoxantrone. Patch pipettes were filled with (in mM): 30 CsCl, 110 CsOH, 2 TEA-OH, 1 Ca(OH),; 11 EGTA, 10 HEPES, pH 7.3/methanesulfonic acid, osmolarity 310 mOsm/Kg. Whole-cell currents were recorded upon voltage stimulation with 500 ms depolarizing step pulses, starting at −80 mV in 10 mV increments delivered every 5 s (holding potential - 100 mV). Traces were on-line corrected for leakage with the -P/5 procedure. Currents were recorded with the same patch-clamp setup used for mitochondrial electrophysiology.

Electrophysiological Measurements on Xenopus Oocytes—Oocytes were isolated from female *Xenopus laevis* (*Xenopus* One) and defolliculated with type IV collagenase (Worthington Biochemical) in OR2 medium (in mM: 85 NaCl, 2.5 KOH, 1 $MgCl_2$, 5 HEPES, pH 7.6). Defolliculated oocytes were injected with 15 ng of *Xenopus* connexin-38 antisense RNA. 48 hr after injection, oocytes were incubated in OR2 medium in the presence or absence of 2 μM thapsigargin (dissolved in DMSO; DMSO did not exceed 1% in the working solution). Recordings were done at least 3 hr after incubation in 2 μM thapsigargin. Currents were recorded using a Warner OC 725-C voltage-clamp amplifier controlled via an ITC-18 interface (Instrutech) by Pulse software (Heka). Oocytes were placed in standard bath solution containing (in mM): 100 Na^+, 100 Cl^-, 2 K^+, 1 Mg^{2+} and HEPES (pH 7.2), with either 5 Ca^{2+}/0 Mg^{2+} with or without 10 μM mitoxantrone. To record activities of store operated Ca^{2+} currents, currents were evoked by a voltage ramp protocol from −120 mV to +80 mV for 10 s, repeated every 40 s (holding potential: −60 mV). Peak inward currents at −120 mV were carried by Ca^{2+}, since Ca^{2+}-activated Cl^- channels are closed at this voltage and the currents were eliminated by removal of extracellular Ca^{2+}. To record Ca^{2+}-activated Cl^- currents, oocytes clamped at a holding potential of −60 mV were first depolarized by a pre-pulse to +60 mV for 5 s, to activate Ca^{2+}-activated Cl^- channels. The voltage was then stepped to a hyperpolarizing pulse of −120 mV for 300 ms to drive Ca^{2+} influx. After that, the transient Ca^{2+}-activated Cl^- currents were immediately recorded by a depolarizing test pulse to +60 mV for 5 s. The double pulse protocol was repeated every 40 s. The transient Ca^{2+}-activated Cl^- currents were quantified offline by measuring the peak currents at the depolarizing test pulse and subtracting the peak currents at the depolarizing pre-pulse, and normalizing the result to the peak current at the depolarizing test pulse in 5 mM Ca^{2+}. Current analysis was done using Igor software (Wavemetrics, USA).

QUANTIFICATION AND STATISTICAL ANALYSIS

Statistical Analysis of Primary Screens—Data analysis was performed using MATLAB software. The dynamics of mt-Ca^{2+} -dependent luminescence was smoothed by the cubic spline function:

$$p\sum_{1}^{n}(y_i-f(x_i))^2+(1-p)\int\left(\frac{d^2f}{dx^2}\right)^2dx,$$

where, p is a smoothing parameter, controlling the tradeoff between fidelity to the data and roughness of the function estimate, f is the estimated cubic spline function to minimize the above function, and x_i and y_i are the dynamical data points. Here, p is set at 0.5. For each compound, two parameters were directly extracted: the maximal amplitude of the luminescence signal (peak) and the left slope of the bell-shaped kinetic trace (uptake rate). Based on these parameters an inhibition score, I_{drug}, was assigned to each compound C_i as follows:

$$I_{drug}(C_i)=\frac{u_i-\overline{\mu}_{DMSO}}{\overline{\mu}_{Ru360}-\overline{\mu}_{DMSO}},$$

where, u_i is the fitted value of the compound C_i, and $\bar{\mu}$ is the trimmed average of positive and negative controls. Compounds were considered as hits when I_{drug} was higher than 0.5. For each plate, the Z′-factor was calculated as follows (Zhang et al., 1999):

$$Z'=1-\frac{3\delta_{DMSO}+3\delta_{Ru360}}{|\mu_{Ru360}-\mu_{DMSO}|},$$

where, μ and δ are the mean and standard deviation, respectively.

Quantification of mt-Ca^{2+} Concentrations—Systematic quantification of mt-Ca^{2+} concentrations was performed using the algorithm reported in Bonora et al. (2013) with the following formula:

$$\left[Ca^{2+}\right](M)=\frac{\left(\frac{L}{L_{max}}\times\lambda\right)^{\frac{1}{n}}+\left(\left(\frac{L}{L_{max}}\times\lambda\right)^{\frac{1}{n}}\times K_{TR}\right)-1}{K_R-\left(\left(\frac{L}{L_{max}}\times\lambda\right)^{\frac{1}{n}}\times K_R\right)},$$

where λ = 1, K_R = 7.23x10^6, K_{TR} = 120 and n = 2.99.

Data Analysis—All data are represented as mean ± SEM and the statistical details of experiments can be found in the figure legends. Differences between two datasets were evaluated by two tailed unpaired Student's t test. Statistical tests between multiple datasets and conditions were carried out using one-way analysis of variance (ANOVA) followed by Tukey's post hoc test. A P-value < 0.05 was considered statistically significant. Statistical analyses were performed using GraphPad Prism version 5.0 (GraphPad Software, San Diego, CA, USA).

DATA AND SOFTWARE AVAILABILITY

The unprocessed image files used to prepare the figures in this manuscript have been deposited to Mendeley Data and are available at http://dx.doi.org/10.17632/54jw24wvn5.1.

Supplementary Material

Refer to Web version on PubMed Central for supplementary material.

Acknowledgments

We thank M. Jastroch and T. Misgeld for helpful discussions, U. Uhrig for assistance on molecular docking studies, and J. Lewis and B. Jehle for assistance on drug screening. This work was supported by the German Research Foundation (DFG) under the Emmy Noether Programme (PE 2053/1-1) to F.P., J.W., D.M.A., and A.L.; the Bavarian Ministry of Sciences, Research and the Arts in the framework of the Bavarian Molecular Biosystems Research Network (D2-F5121.2-10c/4822) to F.P., A.G., C.G.-P., and Y.C.; the Munich Center for Systems Neurology (SyNergy; EXC 1010) to F.P.; the NIH grants GM56328 to J.K.F. and R01DC012538 to J.K.F. and Z.M.; the Spanish Ministerio de Economía y Competitividad grant BFU2014-53469P and the Instituto de Saludo Carlos III grant RD16/0011/0003 to M.T.A. and J.G.-S.; and the DFG grant MO1944/1-1 to D.M.

References

Alonso MT, Navas-Navarro P, García-Sancho J. A microplate-based bioluminescence assay of mitochondrial calcium uptake. Methods Mol Biol. 2017; 1567:245–253. [PubMed: 28276023]

Attene-Ramos MS, Huang R, Michael S, Witt KL, Richard A, Tice RR, Simeonov A, Austin CP, Xia M. Profiling of the Tox21 chemical collection for mitochondrial function to identify compounds that acutely decrease mitochondrial membrane potential. Environ Health Perspect. 2015; 123:49–56. [PubMed: 25302578]

Baughman JM, Perocchi F, Girgis HS, Plovanich M, Belcher-Timme CA, Sancak Y, Bao XR, Strittmatter L, Goldberger O, Bogorad RL, et al. Integrative genomics identifies MCU as an essential component of the mitochondrial calcium uniporter. Nature. 2011; 476:341–345. [PubMed: 21685886]

Bell DH. Characterization of the fluorescence of the antitumor agent, mitoxantrone. Biochim Biophys Acta. 1988; 949:132–137. [PubMed: 3334848]

Bonora M, Giorgi C, Bononi A, Marchi S, Patergnani S, Rimessi A, Rizzuto R, Pinton P. Subcellular calcium measurements in mammalian cells using jellyfish photoprotein aequorin-based probes. Nat Protoc. 2013; 8:2105–2118. [PubMed: 24113784]

Brand MD, Nicholls DG. Assessing mitochondrial dysfunction in cells. Biochem J. 2011; 435:297–312. [PubMed: 21726199]

Cammer W, Moore CL. The effect of hexachlorophene on the respiration of brain and liver mitochondria. Biochem Biophys Res Commun. 1972; 46:1887–1894. [PubMed: 5015232]

Cao C, Wang S, Cui T, Su XC, Chou JJ. Ion and inhibitor binding of the double-ring ion selectivity filter of the mitochondrial calcium uniporter. Proc Natl Acad Sci USA. 2017; 114:E2846–E2851. [PubMed: 28325874]

Carafoli E, Lehninger AL. A survey of the interaction of calcium ions with mitochondria from different tissues and species. Biochem J. 1971; 122:681–690. [PubMed: 5129264]

Chamero P, Manjarres IM, García-Verdugo JM, Villalobos C, Alonso MT, García-Sancho J. Nuclear calcium signaling by inositol trisphosphate in GH3 pituitary cells. Cell Calcium. 2008; 43:205–214. [PubMed: 17583789]

Chaudhuri D, Clapham DE. Outstanding questions regarding the permeation, selectivity, and regulation of the mitochondrial calcium uniporter. Biochem Biophys Res Commun. 2014; 449:367–369. [PubMed: 24792175]

Chaudhuri D, Sancak Y, Mootha VK, Clapham DE. MCU encodes the pore conducting mitochondrial calcium currents. eLife. 2013; 2:e00704. [PubMed: 23755363]

Cheah KS, Waring JC. Effect of trifluoperazine on skeletal muscle mitochondrial respiration. Biochim Biophys Acta. 1983; 723:45–51. [PubMed: 6830768]

De Stefani D, Raffaello A, Teardo E, Szabò I, Rizzuto R. A forty-kilodalton protein of the inner membrane is the mitochondrial calcium uniporter. Nature. 2011; 476:336–340. [PubMed: 21685888]

De Stefani D, Rizzuto R, Pozzan T. Enjoy the trip: calcium in mitochondria back and forth. Annu Rev Biochem. 2016; 85:161–192. [PubMed: 27145841]

Deluca HF, Engstrom GW. Calcium uptake by rat kidney mitochondria. Proc Natl Acad Sci USA. 1961; 47:1744–1750. [PubMed: 13885269]

Dickinson DP. The effects of miconazole on rat liver mitochondria. Biochem Pharmacol. 1977; 26:541–542. [PubMed: 849351]

Divakaruni AS, Paradyse A, Ferrick DA, Murphy AN, Jastroch M. Analysis and interpretation of microplate-based oxygen consumption and pH data. Methods Enzymol. 2014; 547:309–354. [PubMed: 25416364]

Evison BJ, Sleebs BE, Watson KG, Phillips DR, Cutts SM. Mitoxantrone, more than just another topoisomerase II poison. Med Res Rev. 2016; 36:248–299. [PubMed: 26286294]

Fieni F, Lee SB, Jan YN, Kirichok Y. Activity of the mitochondrial calcium uniporter varies greatly between tissues. Nat Commun. 2012; 3:1317. [PubMed: 23271651]

Foskett JK, Philipson B. The mitochondrial Ca(2+) uniporter complex. J Mol Cell Cardiol. 2015; 78:3–8. [PubMed: 25463276]

Giorgi C, Agnoletto C, Bononi A, Bonora M, De Marchi E, Marchi S, Missiroli S, Patergnani S, Poletti F, Rimessi A, et al. Mitochondrial calcium homeostasis as potential target for mitochondrial medicine. Mitochondrion. 2012; 12:77–85. [PubMed: 21798374]

Gohil VM, Sheth SA, Nilsson R, Wojtovich AP, Lee JH, Perocchi F, Chen W, Clish CB, Ayata C, Brookes PS, Mootha VK. Nutrient-sensitized screening for drugs that shift energy metabolism from mitochondrial respiration to glycolysis. Nat Biotechnol. 2010; 28:249–255. [PubMed: 20160716]

Gunter KK, Gunter TE. Transport of calcium by mitochondria. J Bioenerg Biomembr. 1994; 26:471–485. [PubMed: 7896763]

Kirichok Y, Krapivinsky G, Clapham DE. The mitochondrial calcium uniporter is a highly selective ion channel. Nature. 2004; 427:360–364. [PubMed: 14737170]

Kovács-Bogdán E, Sancak Y, Kamer KJ, Plovanich M, Jambhekar A, Huber RJ, Myre MA, Blower MD, Mootha VK. Reconstitution of the mitochondrial calcium uniporter in yeast. Proc Natl Acad Sci USA. 2014; 111:8985–8990. [PubMed: 24889638]

Le SB, Holmuhamedov EL, Narayanan VL, Sausville EA, Kaufmann SH. Adaphostin and other anticancer drugs quench the fluorescence of mitochondrial potential probes. Cell Death Differ. 2006; 13:151–159. [PubMed: 16052237]

Lee Y, Min CK, Kim TG, Song HK, Lim Y, Kim D, Shin K, Kang M, Kang JY, Youn HS, et al. Structure and function of the N-terminal domain of the human mitochondrial calcium uniporter. EMBO Rep. 2015; 16:1318–1333. [PubMed: 26341627]

Lee SK, Shanmughapriya S, Mok MCY, Dong Z, Tomar D, Carvalho E, Rajan S, Junop MS, Madesh M, Stathopulos PB. Structural insights into mitochondrial calcium uniporter regulation by divalent cations. Cell Chem Biol. 2016; 23:1157–1169. [PubMed: 27569754]

Ma Z, Saung WT, Foskett JK. Action potentials and ion conductances in wild-type and CALHM1-knockout type II taste cells. J Neurophysiol. 2017; 117:1865–1876. [PubMed: 28202574]

Mammucari C, Raffaello A, Vecellio Reane D, Rizzuto R. Molecular structure and pathophysiological roles of the mitochondrial calcium uniporter. Biochim Biophys Acta. 2016; 1863:2457–2464. [PubMed: 26968367]

Manjarrés IM, Chamero P, Domingo B, Molina F, Llopis J, Alonso MT, García-Sancho J. Red and green aequorins for simultaneous monitoring of Ca2+ signals from two different organelles. Pflugers Arch. 2008; 455:961–970. [PubMed: 17912545]

Marchi S, Pinton P. The mitochondrial calcium uniporter complex: molecular components, structure and physiopathological implications. J Physiol. 2014; 592:829–839. [PubMed: 24366263]

Montero M, Alonso MT, Carnicero E, Cuchillo-Ibáñez I, Albillos A, García AG, García-Sancho J, Alvarez J. Chromaffin-cell stimulation triggers fast millimolar mitochondrial Ca2+ transients that modulate secretion. Nat Cell Biol. 2000; 2:57–61. [PubMed: 10655583]

Moore CL. Specific inhibition of mitochondrial Ca++ transport by ruthenium red. Biochem Biophys Res Commun. 1971; 42:298–305. [PubMed: 4250976]

Mumberg D, Müller R, Funk M. Yeast vectors for the controlled expression of heterologous proteins in different genetic backgrounds. Gene. 1995; 156:119–122. [PubMed: 7737504]

Nathan SR, Pino NW, Arduino DM, Perocchi F, MacMillan SN, Wilson JJ. Synthetic methods for the preparation of a functional analogue of Ru360, a potent inhibitor of mitochondrial calcium uptake. Inorg Chem. 2017; 56:3123–3126. [PubMed: 28244741]

Oliveira PJ, Marques MP, Batista de Carvalho LA, Moreno AJ. Effects of carvedilol on isolated heart mitochondria: evidence for a protonophoretic mechanism. Biochem Biophys Res Commun. 2000; 276:82–87. [PubMed: 11006086]

Oxenoid K, Dong Y, Cao C, Cui T, Sancak Y, Markhard AL, Grabarek Z, Kong L, Liu Z, Ouyang B, et al. Architecture of the mitochondrial calcium uniporter. Nature. 2016; 533:269–273. [PubMed: 27135929]

Pajot P, Claisse ML. Utilization by yeast of D-lactate and L-lactate as sources of energy in the presence of antimycin A. Eur J Biochem. 1974; 49:275–285. [PubMed: 4376486]

Palty R, Silverman WF, Hershfinkel M, Caporale T, Sensi SL, Parnis J, Nolte C, Fishman D, Shoshan-Barmatz V, Herrmann S, et al. NCLX is an essential component of mitochondrial Na+/Ca2+ exchange. Proc Natl Acad Sci USA. 2010; 107:436–441. [PubMed: 20018762]

Perocchi F, Gohil VM, Girgis HS, Bao XR, McCombs JE, Palmer AE, Mootha VK. MICU1 encodes a mitochondrial EF hand protein required for Ca(2+) uptake. Nature. 2010; 467:291–296. [PubMed: 20693986]

Rodríguez-Prados M, Rojo-Ruiz J, Aulestia FJ, García-Sancho J, Alonso MT. A new low-Ca^{2+} affinity GAP indicator to monitor high Ca^{2+} in organelles by luminescence. Cell Calcium. 2015; 58:558–564. [PubMed: 26412347]

Schleifer JW, Sorajja D, Shen WK. Advances in the pharmacologic treatment of ventricular arrhythmias. Expert Opin Pharmacother. 2015; 16:2637–2651. [PubMed: 26513538]

Schreiner B, Westerburg H, Forné I, Imhof A, Neupert W, Mokranjac D. Role of the AAA protease Yme1 in folding of proteins in the intermembrane space of mitochondria. Mol Biol Cell. 2012; 23:4335–4346. [PubMed: 22993211]

Sikorski RS, Hieter P. A system of shuttle vectors and yeast host strains designed for efficient manipulation of DNA in Saccharomyces cerevisiae. Genetics. 1989; 122:19–27. [PubMed: 2659436]

Stavrovskaya IG, Narayanan MV, Zhang W, Krasnikov BF, Heemskerk J, Young SS, Blass JP, Brown AM, Beal MF, Friedlander RM, Kristal BS. Clinically approved heterocyclics act on a mitochondrial target and reduce stroke-induced pathology. J Exp Med. 2004; 200:211–222. [PubMed: 15263028]

Sundman-Engberg B, Tidefelt U, Gruber A, Paul C. Intracellular concentrations of mitoxantrone in leukemic cells in vitro vs in vivo. Leuk Res. 1993; 17:347–352. [PubMed: 8487583]

Tatematsu Y, Hayashi H, Taguchi R, Fujita H, Yamamoto A, Ohkura K. Effect of N-phenylanthranilic acid scaffold nonsteroidal anti-inflammatory drugs on the mitochondrial permeability transition. Biol Pharm Bull. 2016; 39:278–284. [PubMed: 26830486]

Tuquet C, Dupont J, Mesneau A, Roussaux J. Effects of tamoxifen on the electron transport chain of isolated rat liver mitochondria. Cell Biol Toxicol. 2000; 16:207–219. [PubMed: 11101003]

Vais H, Mallilankaraman K, Mak DO, Hoff H, Payne R, Tanis JE, Foskett JK. EMRE is a matrix Ca(2+) sensor that governs gatekeeping of the mitochondrial Ca(2+) uniporter. Cell Rep. 2016; 14:403–410. [PubMed: 26774479]

Varbiro G, Toth A, Tapodi A, Veres B, Sumegi B, Gallyas F Jr. Concentration dependent mitochondrial effect of amiodarone. Biochem Pharmacol. 2003; 65:1115–1128. [PubMed: 12663047]

Vasington FD, Murphy JV. Ca ion uptake by rat kidney mitochondria and its dependence on respiration and phosphorylation. J Biol Chem. 1962; 237:2670–2677. [PubMed: 13925019]

Walters WP, Namchuk M. Designing screens: how to make your hits a hit. Nat Rev Drug Discov. 2003; 2:259–266. [PubMed: 12669025]

Weatherly LM, Shim J, Hashmi HN, Kennedy RH, Hess ST, Gosse JA. Antimicrobial agent triclosan is a proton ionophore uncoupler of mitochondria in living rat and human mast cells and in primary human keratinocytes. J Appl Toxicol. 2016; 36:777–789. [PubMed: 26204821]

Ying WL, Emerson J, Clarke MJ, Sanadi DR. Inhibition of mitochondrial calcium ion transport by an oxo-bridged dinuclear ruthenium ammine complex. Biochemistry. 1991; 30:4949–4952. [PubMed: 2036363]

Zee-Cheng RK, Cheng CC. Antineoplastic agents. Structure-activity relationship study of bis(substituted aminoalkylamino)anthraquinones. J Med Chem. 1978; 21:291–294. [PubMed: 628005]

Zhang JH, Chung TD, Oldenburg KR. A simple statistical parameter for use in evaluation and validation of high throughput screening assays. J Biomol Screen. 1999; 4:67–73. [PubMed: 10838414]

Highlights

- Targeting human MCU in yeast mitochondria is an effective drug discovery strategy
- A yeast-specific bioenergetic shunt minimizes detection of false-positive hits
- An orthogonal, interspecies drug screening can identify specific MCU modulators
- Mitoxantrone is a selective and direct inhibitor of MCU

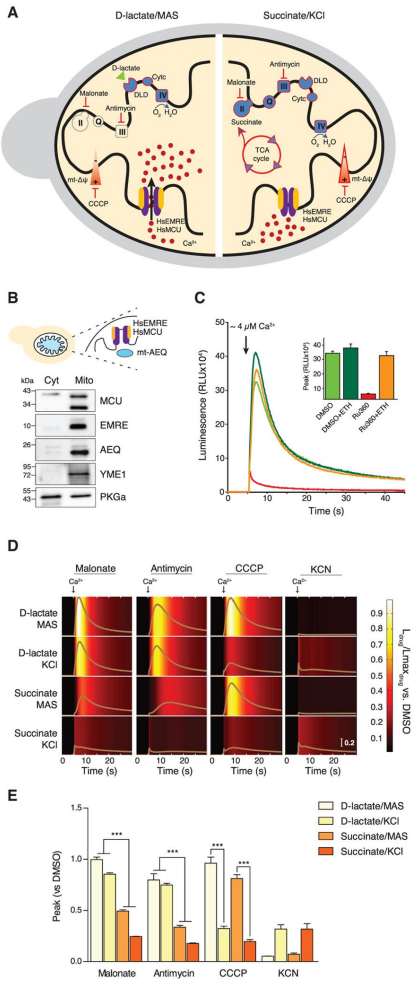

Figure 1. A Yeast Bioenergetic Shunt to Reduce False-Positive Hits in MCU-Targeted Drug Discovery Screens

(A) Schematic representation of yeast mitochondrial energy production pathways in media with either mannitol/sucrose (MAS) and D-lactate or KCl and succinate. II, succinate dehydrogenase; III, coenzyme Q:cytochrome *c*-oxidoreductase; Q, coenzyme Q; DLD, D-lactate:cytochrome *c* oxidore-ductase; Cytc, cytochrome *c*; IV, cytochrome *c* oxidase. (B)Immunoblot analysis of cytoplasmic (Cyt) and mitochondrial (Mito) fractions isolated from yeast cells expressing human MCU, EMRE, and mt-AEQ. YME1, mitochondrial i-AAA protease; PKGa, protein kinase G alpha.

(C)Representative traces of Ca^{2+}-dependent, AEQ-based light kinetics in yeast mitochondria treated with either 0.1% DMSO or 10 μM Ru360 in the presence or absence of 15 μM ETH129 (ETH). RLU, relative luminescence units. Mean ± SEM; n = 4.
(D)Effect of respiratory chain inhibitors (malonate, 10 mM; antimycin A, 1 μM; and KCN, 6 mM) and CCCP (6 μM) on Ca^{2+} uptake kinetics in yeast mitochondria energized with either succinate or D-lactate (10 mM) in MAS or KCl-based media. Averaged light kinetics (n = 3, brown) are quantified as ratio of light signal (L_{drug}) over maximal peak luminescence ($Lmax_{drug}$), normalized to DMSO (0.1%).
(E)Quantification of Ca^{2+}-dependent, AEQ-based light kinetics shown in (D). Mean ± SEM; n = 3; ***p < 0.001, one-way ANOVA.

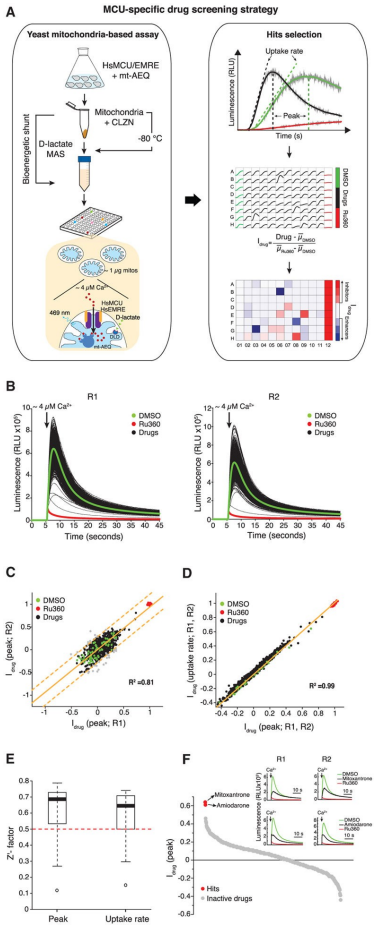

Figure 2. Drug Discovery Screen in Reconstituted Yeast Mito-chondria

(A) General workflow of the yeast mitochondria-based drug discovery screen. CLZN, native coelenterazine; I_{drug}, inhibition score.

(B)Drug screen in biological replicates (R1 and R2). Ca^{2+}-dependent, AEQ-based light kinetics from reconstituted yeast mitochondria are shown for each compound, whereas averaged light kinetics are shown for positive (Ru360, n = 160) and negative (DMSO, n = 160) controls.

(C)Reproducibility of the drug screen. Linear regression (solid orange line) is fitted to the inhibition score (I_{drug}) of each compound (dot). I_{drug} scores that deviate from the linear

regression (gray dots) by two root mean square errors (dotted orange lines) are considered outliers. The correlation coefficient (R^2) refers to data points upon the removal of outliers.
(D) Correlation of I_{drug} scores for peak and uptake rate.
(E)Performance of the screen based on Z′-factors. Highest and lowest values indicate third and first quartiles, while the thick line represents the median. Z′-factors that do not replicate between biological duplicates are shown as small circles. Median values > 0.5 indicate screening assays suitable for HTS.
(F) Ranking of compounds based on I_{drug} scores.

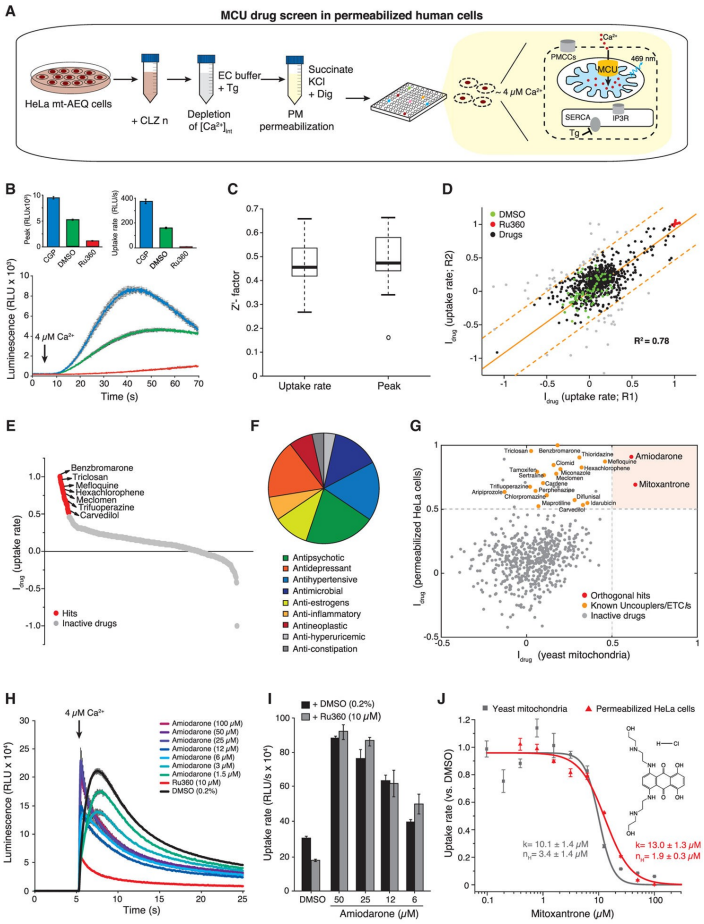

Figure 3. Orthogonal Drug Screens in Permeabilized HeLa Cells and Reconstituted Yeast Mitochondria Validate Mitoxantrone as a Specific MCU Inhibitor

(A) General workflow of the permeabilized HeLa cell-based assay. CLZ n, coelenterazine derivative n; EC, extracellular-like solution; Tg, thapsigargin; Dig, digitonin; PM, plasma membrane; PMCCs, plasma membrane Ca^{2+} channels; SERCA, sarco/endoplasmic reticulum Ca^{2+}-ATPase; IP3R, inositol trisphosphate receptor. See also Figures S1A–S1C.

(B)Ca^{2+}-dependent, AEQ-based light kinetics in digitonin-permeabilized HeLa cells upon the addition of Ca^{2+} in the presence and absence of Ru360 (5 μM), CGP-37157 (20 μM), or DMSO (0.2%). Mean ± SEM; n = 8. See also Figures S1D and S1E.

(C) Performance of the drug screen based on Z′-factors.

(D) Reproducibility of the drug screen.

(E) Ranking of compounds based on I_{drug} scores.
(F) Distribution of candidate drugs in therapeutic classes.
(G)Validation of true-positive hits by orthogonal, inter-species screens. ETCIs, electron transport chain inhibitors. See also Figure S2.
(H)Ca^{2+}-dependent, AEQ-based light kinetics in yeast mitochondria treated with amiodarone. Mean ± SEM; n = 3.
(I)Effect of amiodarone on Ca^{2+}-dependent, AEQ-based light kinetics in yeast mitochondria pre-treated with either Ru360 or DMSO. Mean ± SEM; n = 3.
(J)Dose response of mitoxantrone on Ca^{2+} uptake relative to DMSO and fitted with a Hill equation (continuous lines) to extract Michaelis constant ($k_{0.5}$) and Hill coefficient (n_H). Inset: mitoxantrone hydrochloride chemical structure. Mean ± SEM; n = 4.
See also Figure S3.

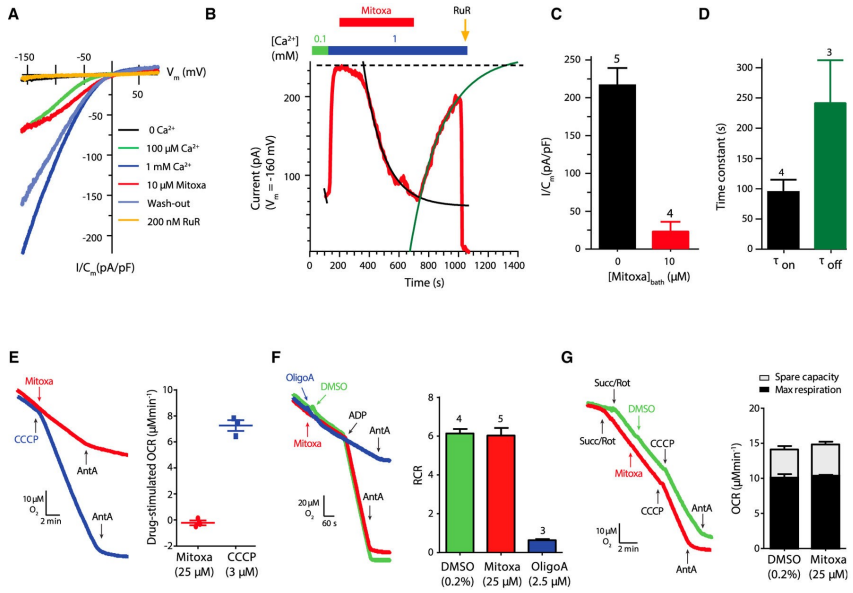

Figure 4. MCU-Mediated Ca^{2+} Currents and Mitochondrial Bioenergetics in Response to Mitoxantrone

(A) Representative recordings of MCU current densities (I/C_m) in HEK293T cell mitoplasts in various bath [Ca^{2+}].

(B)Representative time course of MCU current during exposure to and washout of 10 µM mitoxantrone in bath solution. Each point represents the amplitude of MCU current at −160 mV, sampled every 5 s. RuR, ruthenium red (200 nM).

(C)Quantification of MCU Ca^{2+} current density (pA/pF) in 1 mM bath Ca^{2+} before (n = 5) and after (n = 4) the addition of 10 µM mitoxantrone. Mean ± SEM.

(D)Quantification of time constant for inhibition (τ_{on}; n = 4) and recovery (τ_{off}; n = 3) of MCU Ca^{2+} current. Mean ± SEM.

(E)Oxygen consumption rate (OCR) upon acute treatment of crude mouse liver mitochondria with either mitoxantrone or CCCP and then antimycin A. Mean ± SEM; n = 3.

(F)Respiratory control ratio (RCR) of crude mouse liver mitochondria energized with succinate/rotenone (10 mM; 2 µM) and treated with DMSO (n = 4), mitoxantrone (n = 5), or oligomycin A (n = 3). ADP (4 mM), AntA, Antimycin A (4 µM). Mean ± SEM.

(G)Effect of mitoxantrone on maximal respiration and spare respiratory capacity of permeabilized HeLa cells. Mean ± SEM; n = 3.

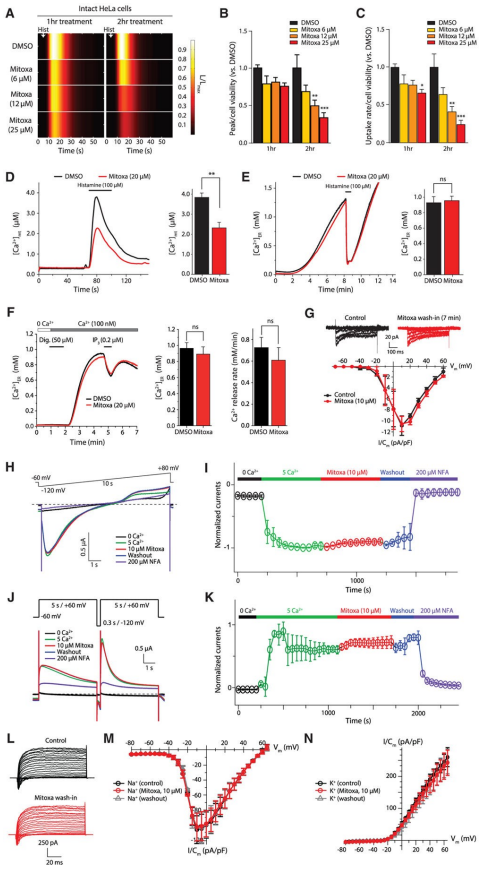

Figure 5. Effect of Mitoxantrone on Intracellular and Plasma Membrane Ion Channels

(A) Ca^{2+}-dependent, AEQ-based light kinetics upon stimulation of intact HeLa cells with 100 μM histamine and after treatment with either vehicle (DMSO 0.2%) or different concentrations of mitoxantrone for 1 or 2 hr.

(B and C) Quantification of peak luminescence (B) and rate of light emission (uptake rate) (C)for light kinetics in (A) after normalization to number of viable cells. Mean ± SEM; *p < 0.05, **p < 0.01, and ***p < 0.001, one-way ANOVA; n = 12. See also Figure S4.

(D)Representative traces and quantification of mt-Ca^{2+} concentrations in HeLa cells stimulated with histamine (100 μM) in response to mitoxantrone (20 μM) or DMSO (0.2%) treatment for 2 hr. Mean ± SEM; n = 4; **p < 0.01, t test. Light emission was calibrated using the constant values previously published (Montero et al., 2000).

(E)Representative traces and quantification of ER-Ca^{2+} concentrations in HeLa cells stimulated with histamine (100 μM) in the presence of 1 mM $CaCl_2$ and pre-treated with either 20 μM mitoxantrone (n = 4) or 0.2% DMSO (n = 3) for 2 hr. Mean ± SEM.
(F)Representative traces and quantification of the amplitude and rate of released ER-Ca^{2+} upon stimulation of digitonin-permeabilized HeLa cells with IP_3 (0.2 μM) after mitoxantrone (20 μM) or DMSO (0.2%) treatment. Mean ± SEM; n = 3.
(G)Effect of mitoxantrone on voltage-activated Ca^{2+} currents in non-differentiated SH-SY5Y cells. Mean ± SEM; n = 3.
(H)Representative traces of store-operated Ca^{2+}currents in *Xenopus* oocytes treated with mitoxantrone.
(I)Time course of peak inward Ca^{2+} currents shown in (H) at −120 mV, normalized to maximum value. Mean ± SEM; n = 3.
(J)Representative traces of Ca^{2+}-activated Cl^- currents in *Xenopus* oocytes treated with mitoxantrone.
(K)Time course of normalized peak Ca^{2+}-activated Cl^- currents shown in (J). Mean ± SEM; n = 3.
(L)Effect of mitoxantrone on voltage-activated Na^+ and K^+ currents in single mouse type II taste cells.
(M)I–V relations of inward Na^+ currents before (control), during exposure, and washout of the drug (Mitoxa, 10 μM). Mean ± SEM; n = 3.
(N)I–V relations of outward K^+ currents before (control), during (Mitoxa, 10 μM), and after exposure to mitoxantrone. Mean ± SEM; n = 3.

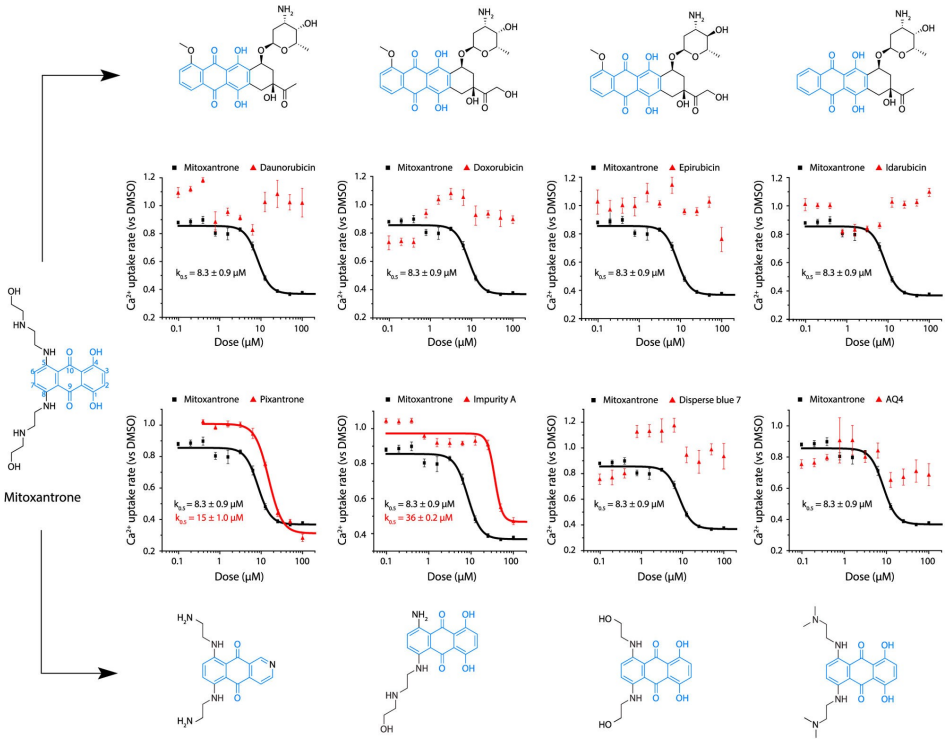

Figure 6. Structure-Activity Relationship Analysis of Mitoxantrone

Dose-response curves for anthracyclines (top) and structural analogs of mitoxantrone (bottom) in yeast mitochondria. The mt-Ca^{2+} uptake rates ($\mu M.s^{-1}$) relative to DMSO are fitted with a Hill equation (continuous lines) to extract the Michaelis constant ($k_{0.5}$). The quinizarin core is highlighted in blue. Mean ± SEM; n = 4. See also Figures S5 and S6.

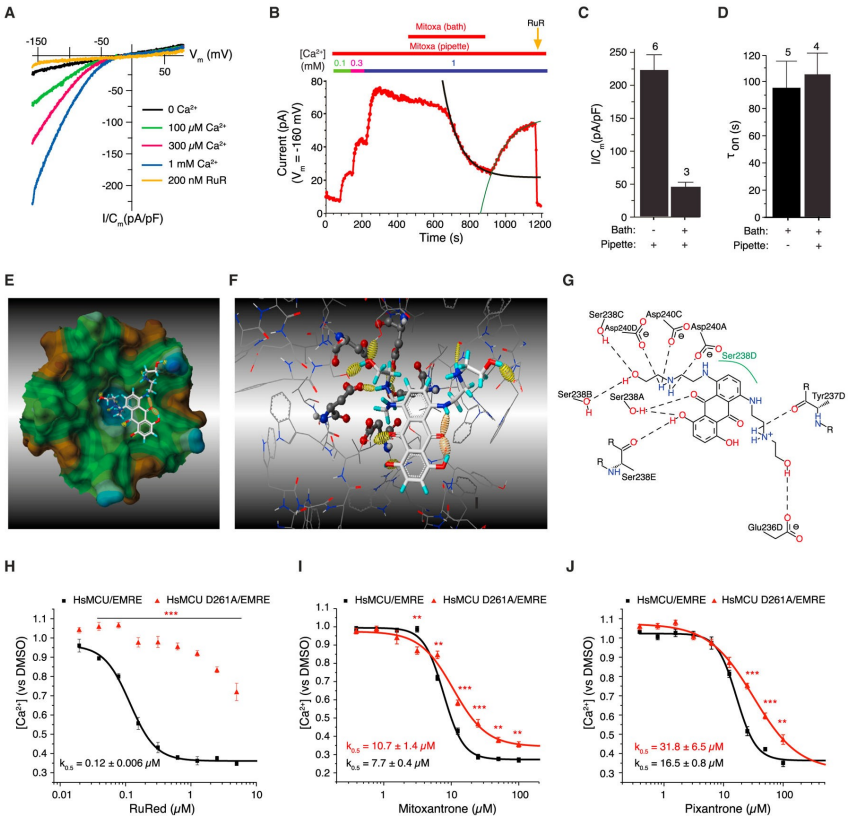

Figure 7. Validation of Mitoxantrone-MCU Direct Interaction

(A) Representative recordings of MCU Ca^{2+} current densities (I/C_m) in HEK293T cell mitoplasts treated with 10 μM mitoxantrone in the pipette (matrix) solution.

(B)Representative time course of MCU Ca^{2+} currents in the presence of mitoxantrone in the matrix and upon its addition to the bath solution.

(C)Quantification of MCU current densities (pA/pF) in 1 mM bath Ca^{2+} after the addition of 10 μM mitoxantrone to the matrix (pipette; n = 6) and to the bath solution (n = 3). Mean ± SEM.

(D)Average time constants for the inhibition (τ_{on}) of MCU current densities by the addition of mitoxantrone in the bath (n = 5) in the presence or absence of mitoxantrone in the matrix (pipette) (n = 4).

(E) Flexible molecular docking analysis of *C. elegans* MCU pore domain and mitoxantrone.

(F) Magnification of (E).

(G) Prediction of molecular interactions between mitoxantrone and the MCU selectivity filter.

(H–J) Dose-response curves for yeast mitochondria reconstituted with either wild-type human MCU or a D261A mutant and treated with RuR (H), mitoxantrone (I), or pixantrone (J). The mt-Ca^{2+} peak values (μM) relative to DMSO are fitted with a Hill equation (continuous lines) to extract the Michaelis constant ($k_{0.5}$). Mean ± SEM; n = 4.

See also Figure S7.

Molecular Cell, Volume 67

Supplemental Information

Systematic Identification of MCU Modulators by Orthogonal Interspecies Chemical Screening

Daniela M. Arduino, Jennifer Wettmarshausen, Horia Vais, Paloma Navas-Navarro, Yiming Cheng, Anja Leimpek, Zhongming Ma, Alba Delrio-Lorenzo, Andrea Giordano, Cecilia Garcia-Perez, Guillaume Médard, Bernhard Kuster, Javier García-Sancho, Dejana Mokranjac, J. Kevin Foskett, M. Teresa Alonso, and Fabiana Perocchi

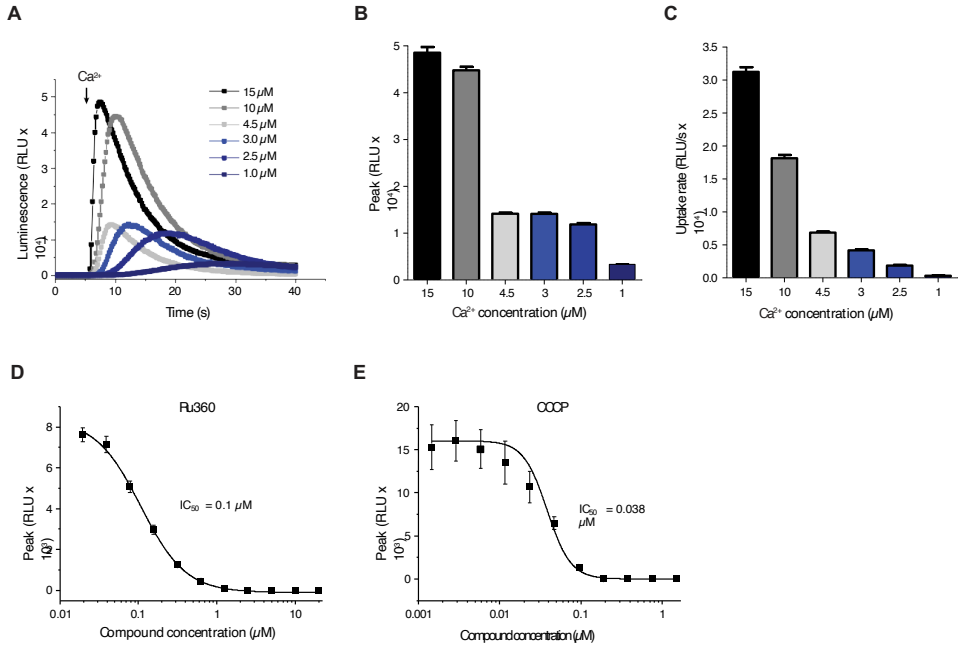

Figure S1

Figure S1, Related to Figure 3. Optimization of the permeabilized HeLa cell-based assay for drug screening

(**A**) Representative traces of AEQ-based light kinetics in mitochondria of permeabilized HeLa cells in response to different concentrations of Ca^{2+}.

(**B**) Quantification of maximal luminescence (peak) for traces in (A). Mean ± SEM; n = 6.

(**C**) Quantification of rate of light emission (uptake rate) for traces in (A). Mean ± SEM; n = 6.

(**D**) Ru360 dose-response curve derived from AEQ-based light kinetics in mitochondria of permeabilized HeLa cells. Data are fitted with a logistic function (continuous line) to determine the half maximal inhibitory concentration (IC_{50}). Mean ± SEM; n = 3.

(**E**) Carbonyl cyanide m-chlorophenyl hydrazone (CCCP) dose-response curve derived from AEQ-based light kinetics in mitochondria of permeabilized HeLa cells. Mean ± SEM; n = 3. RLU, relative luminescence units.

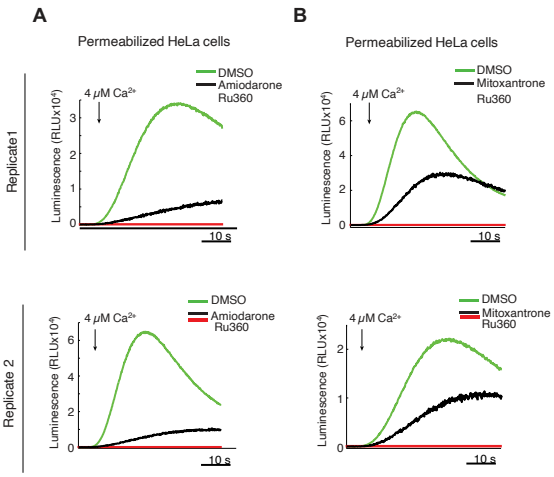

Figure S2

Figure S2, Related to Figure 3. Hits from the HeLa-permeabilized cell-based drug screen

(**A**) Biological duplicates of Ca^{2+}-dependent, AEQ-based light kinetics in mitochondria of permeabilized HeLa cells treated with 10 μM amiodarone. Averaged light kinetics are shown for DMSO (0.1%; n=8; negative control) and Ru360 (10 μM; n=8; positive control). Data represent mean ± SEM.

(**B**) Biological duplicates of Ca^{2+}-dependent, AEQ-based light kinetics in mitochondria of permeabilized HeLa cells treated with 10 μM mitoxantrone. Averaged light kinetics are shown for DMSO (0.1%; n=8; negative control) and Ru360 (10 μM; n=8; positive control). Data represent mean ± SEM.

RLU, relative luminescence units.

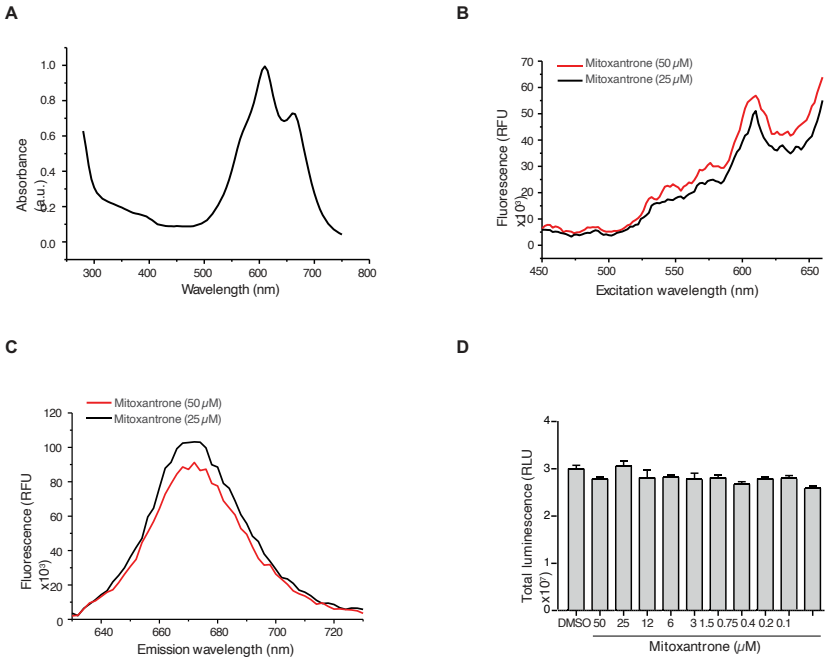

Figure S3

Figure S3, Related to Figure 3. Optical properties of mitoxantrone

(**A**) Absorbance spectrum of mitoxantrone (25 μM) in PBS (pH 7.2).

(**B**) Fluorescence excitation (Em 690 nm) spectrum of mitoxantrone in PBS (pH 7.2).

(**C**) Fluorescence emission (Ex 605 nm) spectrum of mitoxantrone in PBS (pH 7.2).

(**D**) Effect of different concentrations of mitoxantrone on the total luminescence signal (RLU, relative luminescence units) from yeast mitochondria expressing mt-AEQ, reconstituted with native coelenterazine and lysed with Triton X-100 (2%) in the presence of 50 mM $CaCl_2$.

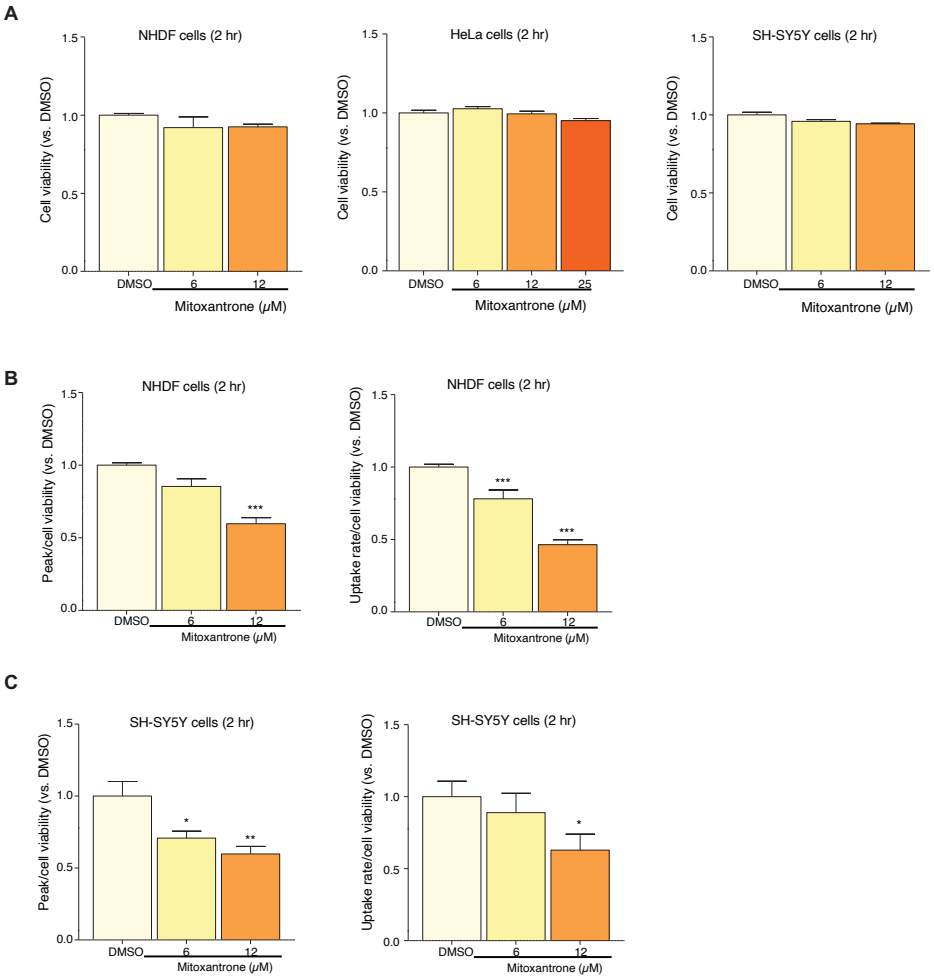
A
NHDF cells (2 hr)
HeLa cells (2 hr)
SH-SY5Y cells (2 hr)
Cell viability (vs. DMSO)
1.5
1.0
0.5
0.0
DMSO
6
12
25
Mitoxantrone (μM)
B
NHDF cells (2 hr)
Peak/cell viability (vs. DMSO)
Uptake rate/cell viability (vs. DMSO)
***
C
SH-SY5Y cells (2 hr)
*
**

Figure S4

Figure S4, Related to Figure 5. Effect of mitoxantrone on the viability of HeLa, NHDF, and SH-SY5Y cells

(**A**) Cell viability in NHDF human neonatal fibroblasts, HeLa and SH-SY5Y cells treated with mitoxantrone for 2 hours. Data are normalized to DMSO (0.2%). Mean ± SEM; n = 4.

(**B**) Ca^{2+}-dependent, AEQ-based light kinetics in mitochondria of intact NHDF cells treated with different concentrations of mitoxantrone for 2 hours. Data are normalized to the number of viable cells. Mean ± SEM; ***, P < 0.001; one-Way ANOVA; n = 12.

(**C**) Ca^{2+}-dependent, AEQ-based light kinetics in mitochondria of intact SH-SY5Y cells treated with different concentrations of mitoxantrone for 2 hours. Data are normalized to the number of viable cells. Mean ± SEM; *, P < 0.05; **, P < 0.01; n = 12.

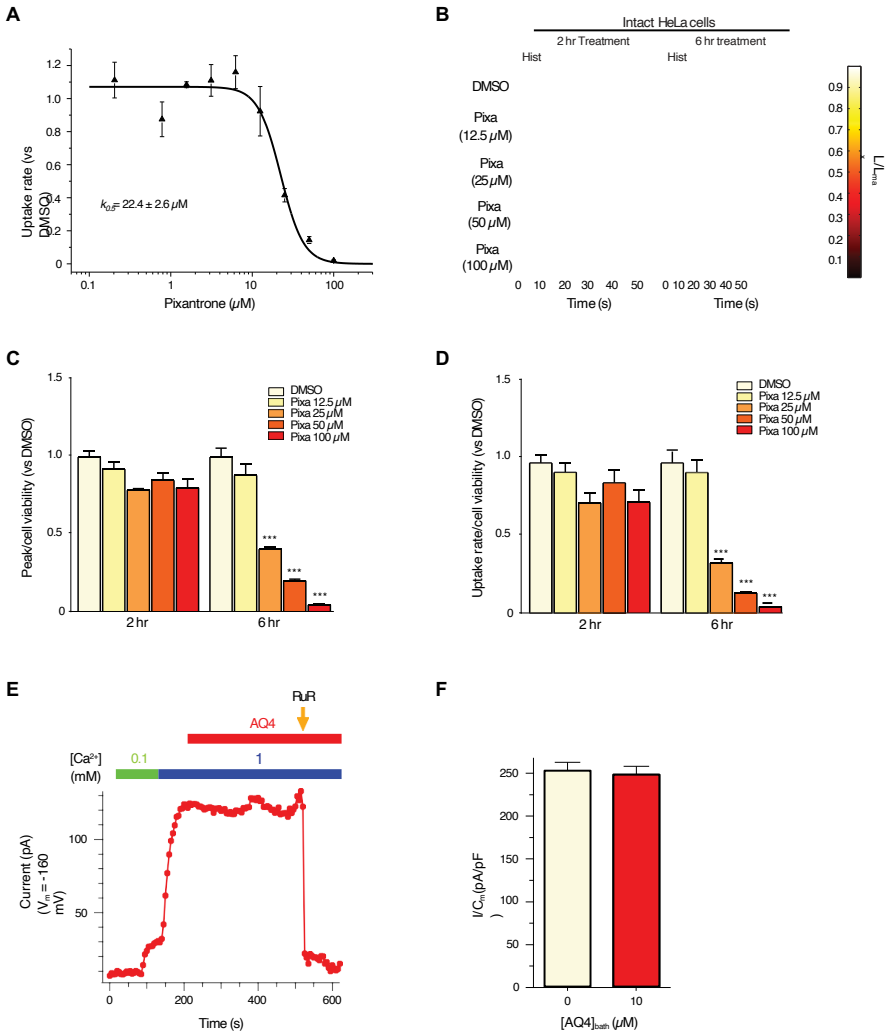
A
Uptake rate (vs DMSO)
$k_{0.5}$= 22.4 ± 2.6 μM
Pixantrone (μM)
B
Intact HeLa cells
2 hr Treatment
6 hr treatment
Hist
Hist
DMSO
Pixa (12.5 μM)
Pixa (25 μM)
Pixa (50 μM)
Pixa (100 μM)
Time (s)
Time (s)
I/I_{min}
C
Peak/cell viability (vs DMSO)
DMSO
Pixa 12.5 μM
Pixa 25 μM
Pixa 50 μM
Pixa 100 μM
2 hr
6 hr
D
Uptake rate/cell viability (vs DMSO)
E
RuR
AQ4
[Ca2+] (mM)
Current (pA) (V_m = -160 mV)
Time (s)
F
I/C_m (pA/pF)
$[AQ4]_{bath}$ (μM)

Figure S5

Figure S5, Related to Figure 6. **Effect of pixantrone and AQ4 on mitochondrial calcium uptake**

(**A**) Dose–response curve derived from AEQ-based light kinetics in mitochondria of permeabilized HeLa cells treated with pixantrone in response to 4 µM Ca^{2+}. Uptake rate values relative to DMSO (0.2%) are fitted with a Hill equation (continuous lines) to extract Michaelis constant ($k_{0.5}$). Mean ± SEM; n = 4.

(**B**) Representative AEQ-based light kinetics in mitochondria of intact HeLa cells treated with either vehicle (DMSO, 0.2%) or different concentrations of pixantrone (Pixa) for 2 or 6 hr. Intracellular Ca^{2+} signaling was stimulated with 100 µM histamine (Hist). Data represent the ratio of luminescence (L) over maximal peak luminescence (L_{max}).

(**C**) Quantification of peak luminescence normalized to the number of viable cells. Mean ± SEM; ***, P < 0.001; one-Way ANOVA; n = 12.

(**D**) Quantification of rate of light emission (uptake rate) normalized to the number of viable cells. Mean ± SEM; ***, P < 0.001; one-Way ANOVA; n = 12.

(**E**) Representative time course of MCU current densities during exposure to 10 µM AQ4 in the bath solution. Each point represents the amplitude of MCU current at - 160 mV, sampled every 5 s. Bars (Top) indicate in bath [Ca^{2+}] and period of drug exposure. Ruthenium Red (RuR, 200 nM) is added at end of each experiment.

(**F**) Quantification of MCU current densities (pA/pF) in 1 mM Ca^{2+} before and after AQ4 treatment (10 µM). Mean ± SEM; n = 3.

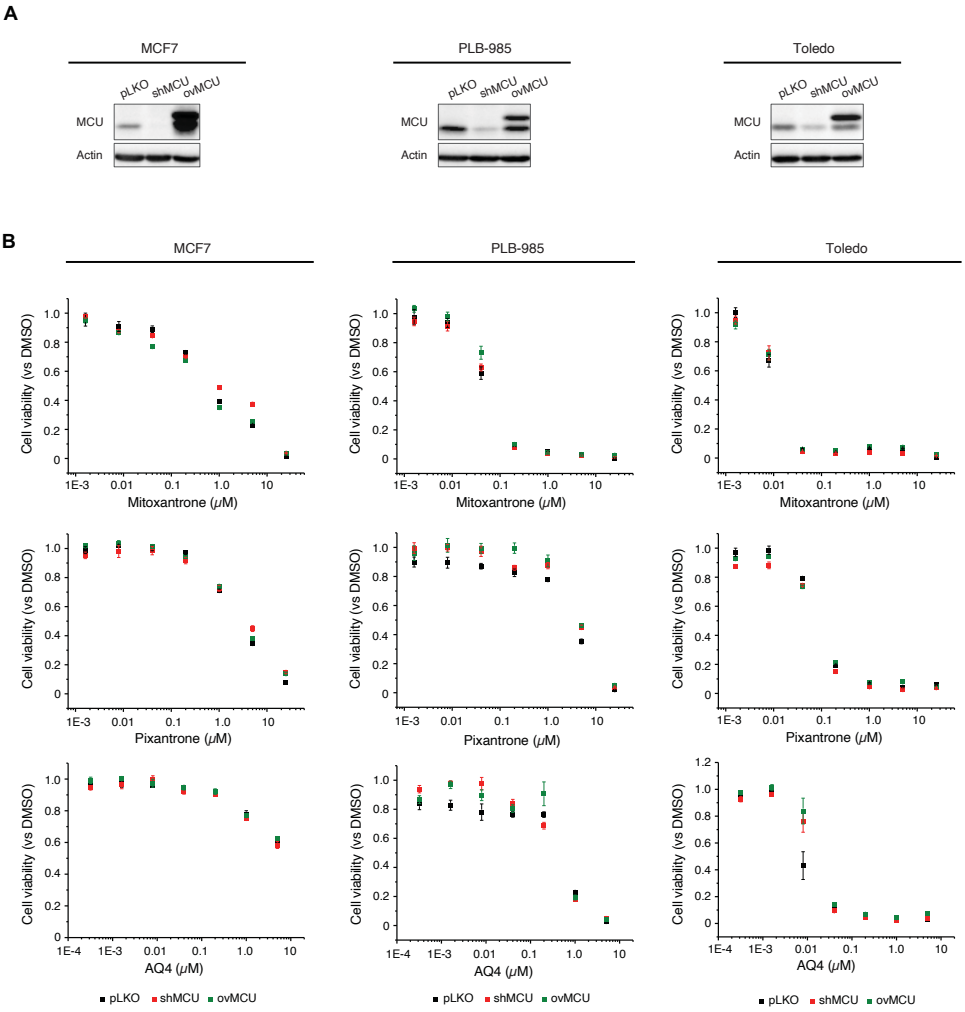
A
MCF7
PLB-985
Toledo
pLKO
shMCU
ovMCU
MCU
Actin
B
MCF7
PLB-985
Toledo
Cell viability (vs DMSO)
Mitoxantrone (μM)
Pixantrone (μM)
AQ4 (μM)
pLKO
shMCU
ovMCU

Figure S6

Figure S6, Related to Figure 6. Effect of mitoxantrone and its analogs on the viability of cancer cell lines expressing different levels of MCU

(**A**) Immunoblot analysis of whole-cell lysate from human breast adenocarcinoma (MCF-7), human peripheral blood acute myeloid leukemia (PLB-985) and non-Hodgkin's B cell lymphoma (Toledo) cells expressing empty vector (pLKO), shRNA against MCU (shMCU; TRCN0000133861, 5'-GCAAGGAGTTTCTTTCTCTTT-3') or V5-tagged wild type human MCU (ovMCU).

(**B**) Analysis of cell viability in response to 48 h drug treatment. Mean ± SEM; n = 4.

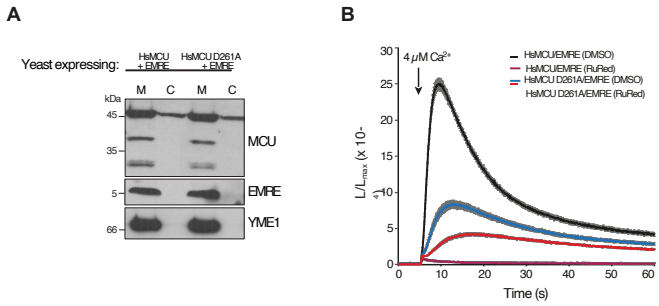

Figure S7

Figure S7, Related to Figure 7. Functional reconstitution of yeast mitochondria with wild type human EMRE and either wild type or mutated human MCU (D261A)

(**A**) Immunoblot analysis of mitochondrial (M) and cytosolic (C) fractions isolated from yeast cells co-expressing wild type human EMRE and either wild type or mutated human MCU (D261A). YME1 (mitochondrial i-AAA protease).

(**B**) Normalized AEQ-based light kinetics in yeast mitochondria after treatment with 0.2% DMSO or 5 μM RuRed. Mean ± SEM; n = 4.

2.2 MICU1 Confers Protection from MCU-Dependent Manganese Toxicity

Declaration of contribution

Jennifer Wettmarshausen*, Valerie Goh*, Kai-Ting Huang, Daniela M Arduino , Utkarsh Tripathi, Anja Leimpek, Yiming Cheng, Alexandros A Pittis, Toni Gabaldón, Dejana Mokranjac, György Hajnóczky, Fabiana Perocchi

MICU1 Confers Protection from MCU-Dependent Manganese Toxicity.

Cell Reports 2018; 25(6):1425-35.e7

*equal author contributions

All experiments were designed in collaboration with Valerie Goh and Dr. Fabiana Perocchi.
I designed and cloned all plasmids and created the MCU-knock-down mtAEQ HeLa cell lines stably expressing Hs-MCU, Af-MCU, ^{HsMTS}Af-MCU, Nc-MCU, and ^{HsMTS}Nc-MCU. The HEK MICU1 KO cell line was a gift from the Vamsi K. Mootha Laboratory. I generated the respective MICU1 WT and EF-mutant rescue cell lines with the technical support of Anja Leimpek (Figure S4 C-D). I generated the yeast strains expressing Dd-MCU, Af-MCU and Nc-MCU. I established the yeast growth assays and performed the experiments included in Figure 1, Figure S1, Figure 2, and Figure S2. Data analysis and visualisation for Figure 1A was performed with the computational help of Dr. Yiming Cheng. Data presented in Figure 1C and 2E have been performed in collaboration with Valerie Goh, whereas I generated the data included in Figure 3A-C. The manuscript was written in with Valerie Goh and Dr. Fabiana Perocchi.

Report

Cell Reports

MICU1 Confers Protection from MCU-Dependent Manganese Toxicity

Graphical Abstract

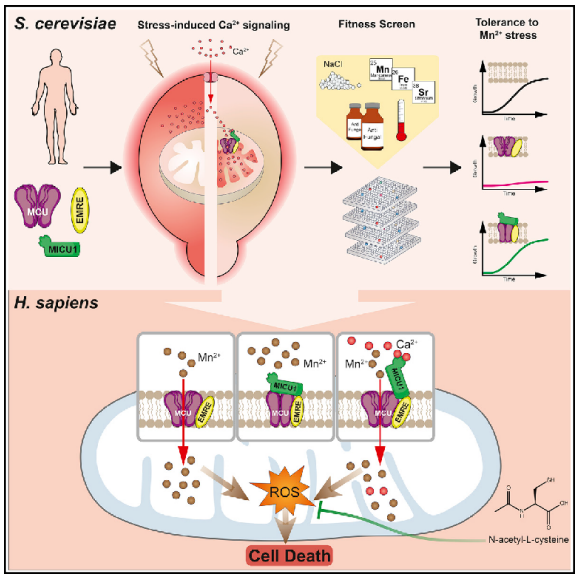

Highlights

- MCU and MICU1 constitute the conserved unit of a eukaryotic uniporter
- Reconstitution of MCU-mediated Ca^{2+} uptake impairs yeast tolerance to Mn^{2+} stress
- MICU1 and MCU functional interaction confers a selective fitness advantage
- Loss of MICU1 hypersensitizes human cells to Mn^{2+}-dependent cell death

Authors

Jennifer Wettmarshausen, Valerie Goh, Kai-Ting Huang, ..., Dejana Mokranjac, György Hajnóczky, Fabiana Perocchi

Correspondence

fabiana.perocchi@helmholtz-muenchen.de

In Brief

Wettmarshausen et al. develop a synthetic biology approach for *in vivo* dissection of functional interconnections between components of the mitochondrial calcium uniporter channel. They demonstrate an essential role of MICU1 in regulating MCU ion selectivity, finding that MICU1 prevents MCU-mediated Mn^{2+} overload and protects from Mn^{2+}-induced cell death.

Wettmarshausen et al., 2018, Cell Reports *25*, 1425–1435
November 6, 2018 [a]
https://doi.org/10.1016/j.celrep.2018.10.037

CellPress

Cell Reports
Report

OPEN ACCESS
CellPress

MICU1 Confers Protection from MCU-Dependent Manganese Toxicity

Jennifer Wettmarshausen,[1,2,9] Valerie Goh,[1,2,9] Kai-Ting Huang,[3] Daniela M. Arduino,[1,2] Utkarsh Tripathi,[2] Anja Leimpek,[1,2] Yiming Cheng,[1,2] Alexandros A. Pittis,[4,5] Toni Gabaldo´n,[4,5,6] Dejana Mokranjac,[7] Gyo¨rgy Hajno´czky,[3] and Fabiana Perocchi[1,2,8,10,*]

[1]Institute for Diabetes and Obesity, Helmholtz Diabetes Center (HDC), Helmholtz Zentrum Mu€nchen, 85764 Neuherberg, Germany
[2]Department of Biochemistry, Gene Center Munich, Ludwig-Maximilians Universita¨t Mu€nchen, 81377 Munich, Germany
[3]Department of Pathology, Anatomy, and Cell Biology, MitoCare Center, Thomas Jefferson University, Philadelphia, PA 19107, USA
[4]Bioinformatics and Genomics Programme, Centre for Genomic Regulation (CRG), 08003 Barcelona, Spain
[5]Departament of Cie`ncies Experimentals I de La Salut, Universitat Pompeu Fabra (UPF), 08003 Barcelona, Spain
[6]Institucio´ Catalana de Recerca i Estudis Avanc¸ats (ICREA), 08010 Barcelona, Spain
[7]Biomedical Center Munich - Physiological Chemistry, Ludwig-Maximilians Universita¨t Mu€nchen, 82152 Martinsried, Germany
[8]Munich Cluster for Systems Neurology, 81377 Munich, Germany
[9]These authors contributed equally
[10]Lead Contact
*Correspondence: fabiana.perocchi@helmholtz-muenchen.de
https://doi.org/10.1016/j.celrep.2018.10.037

SUMMARY

The mitochondrial calcium uniporter is a highly selective ion channel composed of species- and tissue-specific subunits. However, the functional role of each component still remains unclear. Here, we establish a synthetic biology approach to dissect the interdependence between the pore-forming subunit MCU and the calcium-sensing regulator MICU1. Correlated evolutionary patterns across 247 eukaryotes indicate that their co-occurrence may have conferred a positive fitness advantage. We find that, while the heterologous reconstitution of MCU and EMRE *in vivo* in yeast enhances manganese stress, this is prevented by co-expression of MICU1. Accordingly, MICU1 deletion sensitizes human cells to manganese-dependent cell death by disinhibiting MCU-mediated manganese uptake. As a result, manganese overload increases oxidative stress, which can be effectively prevented by NAC treatment. Our study identifies a critical contribution of MICU1 to the uniporter selectivity, with important implications for patients with MICU1 deficiency, as well as neurological disorders arising upon chronic manganese exposure.

INTRODUCTION

Mitochondria from several organisms are able to regulate intracellular calcium (Ca^{2+}) dynamics due to their ability to rapidly and transiently uptake Ca^{2+}. This occurs through an electrophoretic uniporter mechanism that makes use of the steep electrochemical gradient generated by the respiratory chain (Carafoli and Lehninger, 1971; Deluca and Engstrom, 1961; Vasington and Murphy, 1962) and is mediated by a highly selective Ca^{2+} channel located at the inner mitochondrial membrane (Kirichok et al., 2004). However, the molecular identity of the mitochondrial Ca^{2+} uniporter has remained a mystery for decades. Recently, a functional genomics approach has allowed the discovery of the first peripheral Ca^{2+}-dependent regulator (MICU1) (Perocchi et al., 2010) and the transmembrane pore-forming subunit of the uniporter (MCU) (Baughman et al., 2011; De Stefani et al., 2011), paving the way for the identification of several other inhibitory and enhancing effectors of mitochondrial Ca^{2+} (mt-Ca^{2+}) uptake such as MCUb, MICU2, MICU3, and EMRE (De Stefani et al., 2016).

Overall, the complex molecular nature of the mammalian uniporter highlights the physiological relevance of achieving great plasticity and selectivity in mt-Ca^{2+} uptake. Due to the presence of a very large driving force for cation influx, the uniporter must at the same time limit mt-Ca^{2+} accumulation when the cell is at rest to prevent vicious Ca^{2+} cycling and rapidly transmit a cytosolic Ca^{2+} (cyt-Ca^{2+}) signal to the mitochondrial matrix during signaling. The highly selective permeability of the uniporter for Ca^{2+} is thought to derive from the high-affinity binding of the ion to the DXXE motif at the MCU pore (Arduino et al., 2017; Baughman et al., 2011; Cao et al., 2017; Chaudhuri et al., 2013; Oxenoid et al., 2016), whereas both gating and cooperative activation of the uniporter have been attributed to its interaction with hetero-oligomers of MICU1 and MICU2 or MICU3 (Csordás et al., 2013; Kamer et al., 2017; Mallilankaraman et al., 2012; Patron et al., 2014, 2018). However, the respective functional and mechanistic roles of those subunits in regulating uniporter activity have been thus far investigated in mammalian systems, in which the interpretation of results is hampered by differences in the degree of gene silencing, tissue-specific protein composition (Murgia and Rizzuto, 2015; Vecellio Reane et al., 2016), stoichiometry, and compensatory remodeling (Liu et al., 2016; Paillard et al., 2017) of the channel.

The budding yeast *Saccharomyces cerevisiae* represents an ideal testbed for dissecting the functional contribution of each

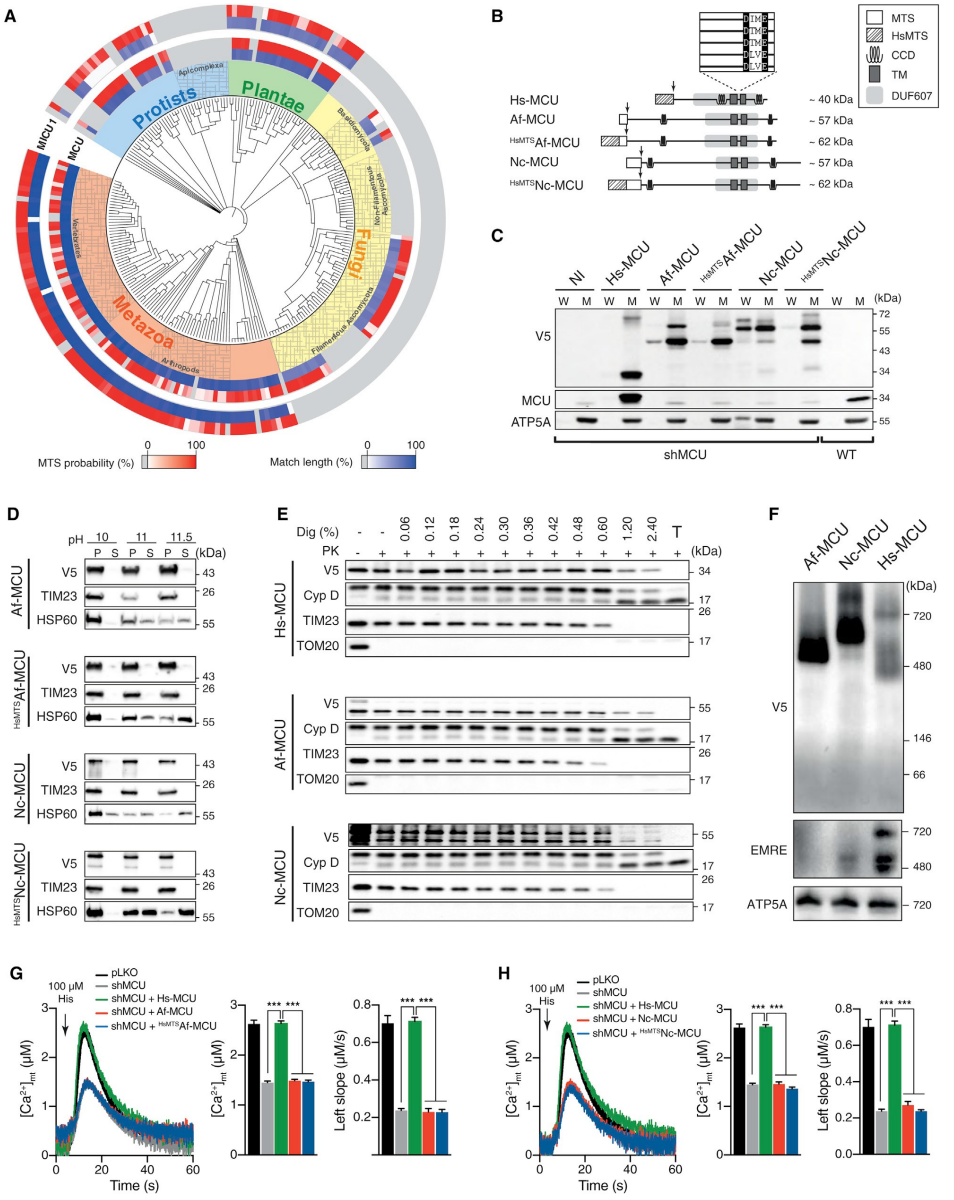

(legend on next page)

component of the human uniporter, given that it completely lacks any detectable MCU homolog (Bick et al., 2012; Cheng and Perocchi, 2015) and endogenous mt-Ca^{2+} transport activity (Arduino et al., 2017; Carafoli and Lehninger, 1971; Kovács-Bogdán et al., 2014; Yamamoto et al., 2016), while enabling the facile expression and targeting of human mitochondrial proteins. Moreover, we and others have shown that mt-Ca^{2+} uptake can be readily reconstituted *in vitro* in isolated yeast mitochondria by co-expressing the human MCU and EMRE subunits (Arduino et al., 2017; Kovacs-Bogdan et al., 2014; Yamamoto et al., 2016). Here, we establish a yeast-based heterologous system to investigate the functional interconnection between MCU and MICU1 *in vivo*. By screening for stress conditions whereby the expression of MICU1 in an MCU-reconstituted yeast strain would confer a fitness advantage, we identify a protective role of MICU1 against MCU-dependent manganese (Mn^{2+}) toxicity. Consistent with these findings, human HEK293 cells lacking MICU1 become permeable to Mn^{2+}, whose uptake is genetically and chemically prevented by the re-introduction of wild-type (WT) MICU1 and by ruthenium red (RuRed), respectively. As a consequence, MICU1 knockout (KO) cells are greatly sensitized to Mn^{2+}-induced cell death that is triggered by an increase in oxidative stress and prevented by *N*-acetyl-L-cysteine (NAC) treatment. Our findings highlight a previously unknown role of MICU1 in regulating the selectivity of the uniporter, with potential implications for both MICU1 and Mn^{2+}-related human disorders.

RESULTS

Phylogenetic Profiling of MCU and MICU1 across 247 Eukaryotes

We examined the co-evolution and predicted mitochondrial co-localization of MCU and MICU1 across 247 fully sequenced eukaryotic species (Figure 1A) from multiple taxonomic levels at different evolutionary distances to maximize the resolution of coupled evolutionary patterns (see also https://itol.embl.de/tree/7747551764250215265034446) (Cheng and Perocchi, 2015). We found that MCU homologs were widely distributed in all of the major eukaryotic groups, present in nearly all Metazoa and Plantae, but only in some Protozoa (e.g., *Trypanosoma cruzi*, *Leishmania major*) and few Fungi. Instead, they apparently had been lost in all Apicomplexa (e.g., *Plasmodium falciparum*), mitochondrial-devoid, single-cell eukaryotes (e.g., *Entamoeba histolytica*, *Giardia lambia*, *E. cuniculi*), and Saccharomycota (e.g., *S. cerevisiae, Schizosaccharomyces pombe, Candida glabrata*). We observed a largely overlapping distribution of MICU1 and MCU homologs, pointing to a strong functional association between the two proteins, which we now know to be part of the same complex. Only a few species within Basidiomycota and Ascomycota fungal clades, such as *Neurospora crassa* and *Aspergillus fumigatus*, contained MCU-like proteins without any detectable MICU1 orthologs.

Given that Fungi also lack EMRE (Sancak et al., 2013), we reasoned that fungal MCU homologs should be self-sufficient to drive mt-Ca^{2+} uptake, similarly to the MCU ortholog from *Dictostillium discoideum* (Dd-MCU) (Arduino et al., 2017; Kovacs-Bogdan et al., 2014). Therefore, we analyzed their ability to complement MCU loss of function in human cells. We expressed *A. fumigatus* (Af-MCU), *N. crassa* (Nc-MCU), or human MCU (Hs-MCU) with a C-terminal V5 tag in MCU knockdown (shMCU) HeLa cells (Figure 1B). To ensure the targeting of fungal MCUs to human mitochondria, we also tested chimera proteins consisting of the Hs-MCU mitochondrial targeting sequence (HsMTS) fused to the full-length form of Nc-MCU (^{HsMTS}Nc-MCU) and Af-MCU (^{HsMTS}Af-MCU). We showed that all constructs were properly localized (Figure 1C) and inserted (Figure 1D) into the inner mitochondrial membrane of shMCU HeLa cells, with the C termini facing the matrix side, similar to Hs-MCU (Figure 1E). Furthermore, on a native gel, both Af-MCU and Nc-MCU formed a large protein complex of a size comparable to that of cells expressing Hs-MCU (Figure 1F). Next, we quantified mt-Ca^{2+} uptake transients in intact (Figures 1G and 1H) and digitonin-permeabilized (Figure S1) shMCU HeLa cells expressing Hs-MCU, Af-MCU, or Nc-MCU, together with a mitochondrial matrix-targeted WT aequorin (mt-AEQ) as a Ca^{2+} sensor. Although the expression of Hs-MCU fully rescued mt-Ca^{2+} uptake, neither Af-MCU nor Nc-MCU, with and without HsMTS, were able to functionally complement Hs-MCU loss of function.

The strong co-evolution of MCU and MICU1, together with the apparent lack of functional MCU homologs in *A. fumigatus*, *N. crassa*, and several other fungal species (Baradaran et al., 2018) that do not express any MICU1-like component, suggest that MCU and MICU1 constitute the conserved unit of a eukaryotic uniporter, and their functional interaction could be required to provide a fitness advantage.

In Vivo Reconstitution of Mitochondrial Calcium Uptake in Yeast

Yeast uses cyt-Ca^{2+} signaling to activate pro-survival, adaptive responses to diverse environmental stresses (Cyert, 2003). We

Figure 1. Evolutionary Analysis of MCU and MICU1 across 247 Eukaryotes

(A) Phylogenetic distribution of MCU and MICU1 homologs (blue, percentage of amino acids match length). MTS, mitochondrial targeting sequence.

(B) Schematic of ectopically expressed fungal MCU constructs and protein domains. DXXE motif and MTS cleavage site prediction (arrow) are also shown. CCD, coiled-coil domain; TM, transmembrane domain.

(C) Analysis of whole-cell (W) and mitochondrial (M) fractions from pLKO (WT) or shMCU HeLa cells stably expressing human (Hs-MCU), *N. crassa* (Nc-MCU), or *A. fumigatus* (Af-MCU) MCU fused to a C-terminal V5-tag. HsMTS, mitochondrial targeting sequence of human MCU; NI, not infected.

(D) Analysis of mitochondrial soluble (S) and membrane pellet (P) fractions.

(E) Analysis of fungal MCU protein topology by proteinase K (PK) treatment. Dig, digitonin; T, triton (1%).

(F) Macromolecular protein complex analysis of fungal MCU constructs by blue native (BN)-PAGE.

(G and H) Representative traces and quantification of mt-Ca^{2+} transients in pLKO (WT) or shMCU HeLa cells stably expressing MCU from human (Hs-MCU) and *A. fumigatus* (Af-MCU) (G) or *N. crassa* (Nc-MCU) (H) upon histamine (His) stimulation.

All data represent means ± SEMs; n = 6–8; ***p < 0.001, one-way ANOVA with Tukey's multiple comparisons test.

See also Figure S1.

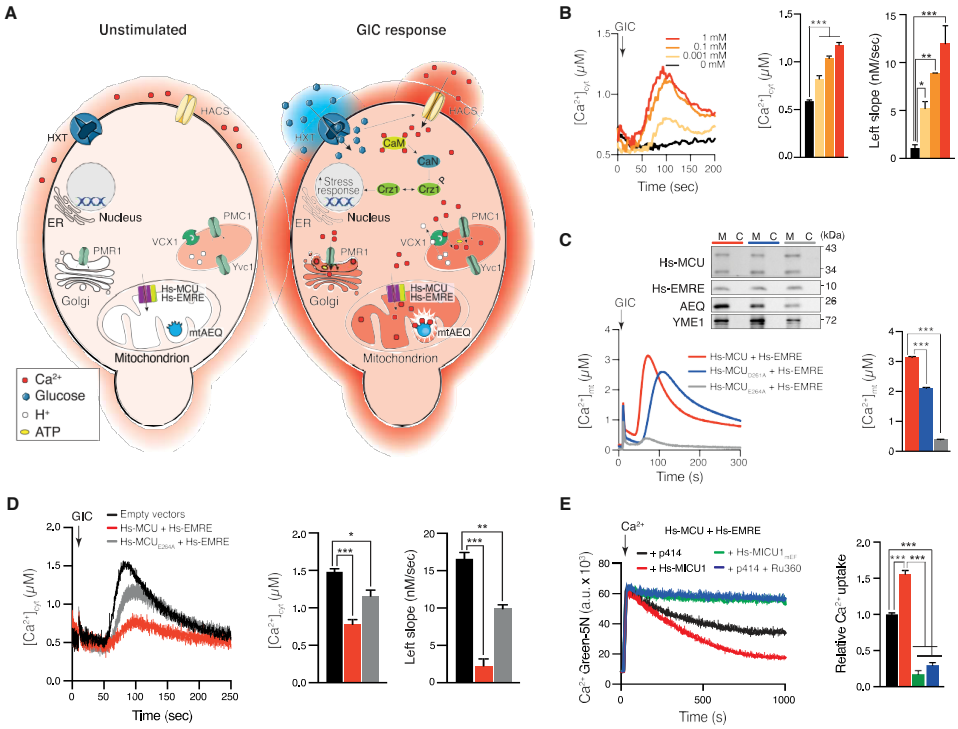

Figure 2. *In vivo* Reconstitution of mt-Ca^{2+} Uptake in Yeast

(A)Schematic of the Ca^{2+} homeostasis system and glucose-induced calcium (GIC) signaling in *S. cerevisiae*. CaM, calmodulin; CaN, calcineurin; Crz1, calcineurin-dependent transcription factor; $Crz1^{P}$, phosphorylated Crz1; ER, endoplasmic reticulum; HACS, high-affinity Ca^{2+} transport system; HXT, hexose transporter; mtAEQ, mitochondria-targeted aequorin; PMC1, vacuolar Ca^{2+}-ATPase; PMR1, ER/Golgi Ca^{2+}-ATPase; VCX1, vacuolar H^{+}/Ca^{2+} exchanger; Yvc1, transient receptor potential cation (TRPC)-type Ca^{2+} channel.

(B)Cyt-Ca^{2+} transients in yeast cells upon GIC stimulation in the presence of different extracellular $CaCl_2$ concentrations (n = 3); *p < 0.05, **p < 0.01, ***p < 0.001; one-way ANOVA with Dunnett's multiple comparisons test.

(C)Mt-Ca^{2+} transients in yeast cells expressing WT mtAEQ, Hs-EMRE, and either WT or mutated Hs-MCU upon GIC stimulation in the presence of 1 mM $CaCl_2$ (n = 3); ***p < 0.0001; one-way ANOVA with Tukey's multiple comparisons test. Inset: immunoblot analysis of cytosolic (C) and mitochondrial (M) fractions.

(D)Cyt-Ca^{2+} transients in yeast cells expressing empty vectors (p425, p423) or Hs-EMRE with either WT or mutant Hs-MCU upon GIC stimulation in the presence of 1 mM $CaCl_2$ (n = 3); *p < 0.05, **p < 0.01, ***p < 0.001; one-way ANOVA with Dunnett's multiple comparisons test.

(E)Extracellular Ca^{2+} clearance by mitochondria isolated from the yeast strains expressing Hs-MCU, Hs-EMRE, and either an empty vector (p414), human WT MICU1 (Hs-MICU1), or EF-hands mutant MICU1 (Hs-MICU1mEF), (n = 3); ***p < 0.001; one-way ANOVA with Tukey's multiple comparisons test.

All data represent means ± SEMs.

See also Figure S2.

therefore asked whether the reconstitution of MCU-mediated mt-Ca^{2+} uptake in yeast would affect the activation of cyt-Ca^{2+} dynamics *in vivo*. As an extracellular stimulus, we chose glucose-induced calcium (GIC) activation, whereby the addition of glucose and extracellular Ca^{2+} to cells starved for >2 hr in hexose-free medium triggers cyt-Ca^{2+} transients (Figures 2A and 2B) (Groppi et al., 2011). Next, we generated yeast strains expressing WT mt-AEQ together with Hs-MCU, Hs-EMRE, or both and confirmed that their co-expression was necessary and sufficient to drive mt-Ca^{2+} uptake *in vivo* (Figure S2A) and to respond to a wide dynamic range of external Ca^{2+} concentrations (Figure S2B). Accordingly, Hs-MCU mutants in highly conserved acidic residues within the DXXE motif (Hs-MCU_{D261A}; Hs-MCU_{E264A}) were either partially functional (Hs-MCU_{D261A}) or almost completely unable (Hs-MCU_{E264A}) to fully transfer GIC-induced cyt-Ca^{2+} signals into the mitochondrial matrix

(Figure 2C). Likewise, yeast strains expressing Af-MCU or Nc-MCU (Figure S2C) were unable to drive Ca^{2+} uptake in the organelle, compared to cells reconstituted with Dd-MCU (Figure S2D). As hypothesized, the *in vivo* reconstitution of MCU-mediated mt-Ca^{2+} uptake resulted in a prompt buffering of GIC-induced cyt-Ca^{2+} elevations (Figure 2D). We then tested whether the expression of WT human MICU1 (Hs-MICU1) (Figure S2E) would be sufficient to reconstitute a Ca^{2+}-regulated uniporter in yeast. Similar to mammalian cells (Csordás et al., 2013; Kamer et al., 2017; Mallilankaraman et al., 2012), the presence of WT but not EF-hands mutant (Hs-MICU1$_{mEF}$) significantly increased the MCU-dependent mt-Ca^{2+} level upon GIC activation in intact cells (Figure S2F) and a bolus of high Ca^{2+} in isolated mitochondria (Figure 2E).

These results validate our *in vivo*, heterologous experimental system for the study of uniporter-mediated Ca^{2+} uptake. They also demonstrate that the expression of Hs-MCU, Hs-EMRE, and Hs-MICU1 in yeast is sufficient to reconstitute Ca^{2+}-regulated uniporter activity in response to physiological stimuli that activate intracellular Ca^{2+} signaling.

MCU Impairs Yeast Tolerance to Metal Stress

We then searched for biological conditions in which the reconstitution of MCU-mediated mt-Ca^{2+} uptake in the absence of the regulatory subunit MICU1 would lead to fitness impairment. We compared the fitness of yeast strains expressing a functional (Hs-MCU/EMRE) or an inactive (Hs-MCU$_{E264A}$/EMRE) uniporter to that of WT cells upon different environmental stresses (Figure 3), including heat shock, fungicide treatment, high salt, and heavy metals. To this end, we used growth rate as a proxy for cell survival and proliferation and ensured their reliance on functional mitochondria by using lactate as a non-fermentable carbon source. Overall, we observed comparable doubling times among the three different strains during normal growth at 30ºC in lactate medium, which was >2-fold higher upon heat shock (37ºC) (Figure 3A). Likewise, treatment with increasing doses of two antifungal drugs, miconazole and amiodarone, either decreased the growth rate of the yeast cultures by >2-fold (miconazole, 100 ng/mL) (Figure 3B) or resulted in a complete cessation of growth (amiodarone, 20 mM) (Figure 3C), regardless of the genetic background. The three strains also showed similar sensitivities to salt stress (NaCl and $CaCl_2$) within the range of the tested concentrations (Figures 3D, 3E, and S3A).

Instead, we observed notable differences among strains in their responses to heavy metals-induced stress (Sr^{2+}, Cu^{2+}, Zn^{2+}, Fe^{2+}, Mn^{2+}) (Figure 3F). Those cations are essential for normal growth and metabolism when present at minimal levels in the medium, but at high concentrations they can induce cytotoxicity (Wysocki and Tamás, 2010). Accordingly, with the exception of Sr^{2+} (Figure S3B), the doubling time of WT yeast cultures was >2-fold higher in the presence of high extracellular concentrations of $CuCl_2$, $FeCl_2$, and $ZnCl_2$ (Figure 3F). While all strains showed a similar tolerance to $CuCl_2$ and $ZnCl_2$, we observed a greater hypersensitivity of the functional MCU-reconstituted strain to both Fe^{2+} and Mn^{2+} toxicity, which manifested as a drastic reduction in cell proliferation at concentrations >10 and 1 mM, respectively (Figure 3F). In addition, expression of Hs-MCU$_{E264A}$ did not impair tolerance to Mn^{2+} stress, whereas the same mutation was not sufficient to prevent Fe^{2+}-induced toxicity, suggesting a potentially different coordination of Fe^{2+} with the DXXE motif.

These observations indicate that in the absence of MICU1, MCU may mediate the cytotoxic accumulation of heavy metals in mitochondria.

MICU1 Protects Human Cells from MCU-Dependent Mn^{2+} Toxicity

We speculate that the co-occurrence of MCU and MICU1 could confer an evolutionary advantage by shielding mitochondria from an unwanted accumulation of heavy metals. Thus, we tested whether the reconstitution of an MICU1-regulated uniporter would be sufficient to protect yeast cells from MCU-dependent Mn^{2+} and Fe^{2+} stresses. We found that the expression of either Hs-MICU1 or Hs-MICU1$_{mEF}$ significantly rescued the hypersensitivity of the MCU-reconstituted strain toward both Fe^{2+} (Figure S4A) and Mn^{2+} (Figure 4A) stresses. This finding indicated that MICU1 interaction with Hs-MCU and Hs-EMRE, rather than functional EF-hands, was required to prevent Fe^{2+} and Mn^{2+} entry into mitochondria, most probably by keeping the channel in a close conformation.

Next, we recapitulated the above findings in mammalian cells. To this end, we compared the viability of WT and MICU1-KO HEK293 cells upon treatment with increasing concentrations of either $FeCl_2$ or $MnCl_2$ for 48 hr. Unlike yeast, neither WT nor MICU1-KO HEK293 cells showed an increased sensitivity to Fe^{2+} treatment (Figure S4B), even at high non-physiological concentrations, indicating major differences in the mechanisms used by fungal and mammalian cells to regulate Fe^{2+} homeostasis and cope with its overload (Philpott, 2012). Instead, we observed a dramatic decrease in cell viability when MICU1-KO cells were treated with concentrations of Mn^{2+} >10 mM, which did not affect WT cells (Figure 4B). As observed in yeast, the protective role of MICU1 toward Mn^{2+} toxicity was not dependent on having functional Ca^{2+}-sensing domains, as a genetic rescue with either Hs-MICU1 or Hs-MICU1$_{mEF}$ resulted in a significantly higher tolerance than MICU1-KO cells to 25 mM Mn^{2+} (Figures S4C and S4D).

These results pointed toward a critical role of MICU1 in inhibiting MCU-dependent Mn^{2+} toxicity, which could be exerted by directly regulating Mn^{2+} entry through the uniporter. We therefore measured mitochondrial Mn^{2+} uptake in WT and MICU1-KO HEK293 cells by monitoring the quenching of the fluorescence signal from mitochondrial compartmentalized Fura-FF upon Mn^{2+} entry in the mitochondrial matrix (Csordás and Hajnóczky, 2003). We confirmed previous findings showing that in the presence of submicromolar cyt-Ca^{2+} levels, mitochondria from WT cells are not permeable to Mn^{2+} (Figure 4C). Instead, in the same conditions, MICU1 KO cells displayed robust mitochondrial Mn^{2+} uptake, as indicated by the time-dependent quenching of the fluorescence signal upon addition of 20 mM Mn^{2+} (Figure 4C). This uptake was completely inhibited by RuRed and fully rescued by the expression of WT MICU1 in the HEK293 KO genetic background (Figure 4D), validating that the observed Mn^{2+} transport was mediated by MCU. Moreover, we showed that the pre-addition of 30 mM Ca^{2+}, a concentration at which the uniporter is disinhibited, resulted in Mn^{2+} entry also

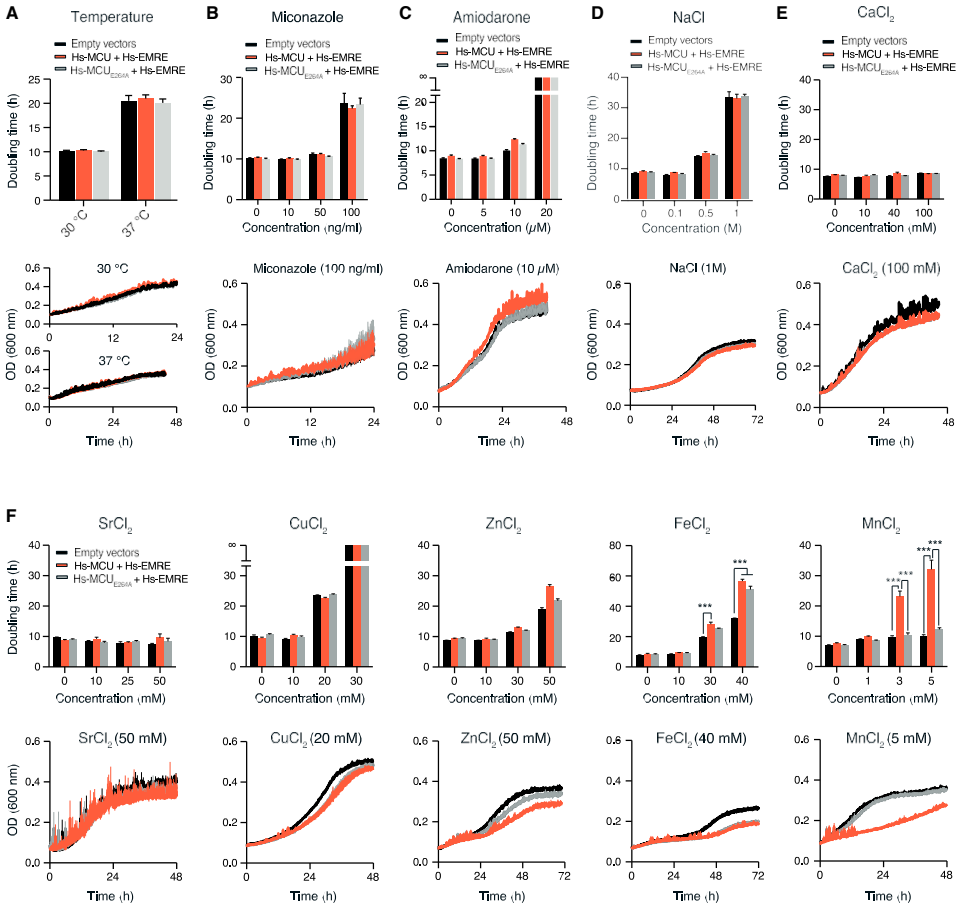

Figure 3. MCU Impairs Yeast Tolerance to Iron and Manganese Stresses

(A–F) Quantification of growth rate and average growth curve of yeast strains expressing empty vectors (p423 and p425) or Hs-EMRE with WT or mutated Hs-MCU at 30°C and 37°C (A), and at increasing concentrations of miconazole (B), amiodarone (C), NaCl (D), $CaCl_2$ (E), or heavy metals (F).

Data represent means ± SEMs; n = 4; ***p < 0.0001; one-way ANOVA with Tukey's multiple comparisons test.

See also Figure S3.

in HEK293 WT cells (Figure 4E), which is consistent with previous results in rat basophilic leukemia (RBL)-2H3 mast cells (Csordás and Hajnóczky, 2003).

Although the mechanism of mitochondrial Mn^{2+} toxicity is not entirely understood, it is believed that increased oxidative stress triggered by Mn^{2+} overload plays a role in the induction of cell death (Smith et al., 2017). Thus, we measured reactive oxygen species (ROS) production in MICU1-KO cells exposed to high extracellular Mn^{2+} concentrations. As shown in Figure 4F, MICU1-KO cells exhibited a significant increase in intracellular ROS production upon 25 mM Mn^{2+} treatment, which is comparable to the level induced by treatment with H_2O_2. We then searched for strategies that could prevent Mn^{2+}-induced toxicity. Fe^{2+} supplementation has already been proposed as a therapeutic strategy to treat or prevent neurological disorders due to a chronic increase of Mn^{2+} level in the blood (O'Neal and Zheng, 2015; Tai et al., 2016), as both cations compete for the same plasma membrane divalent metal transporter.

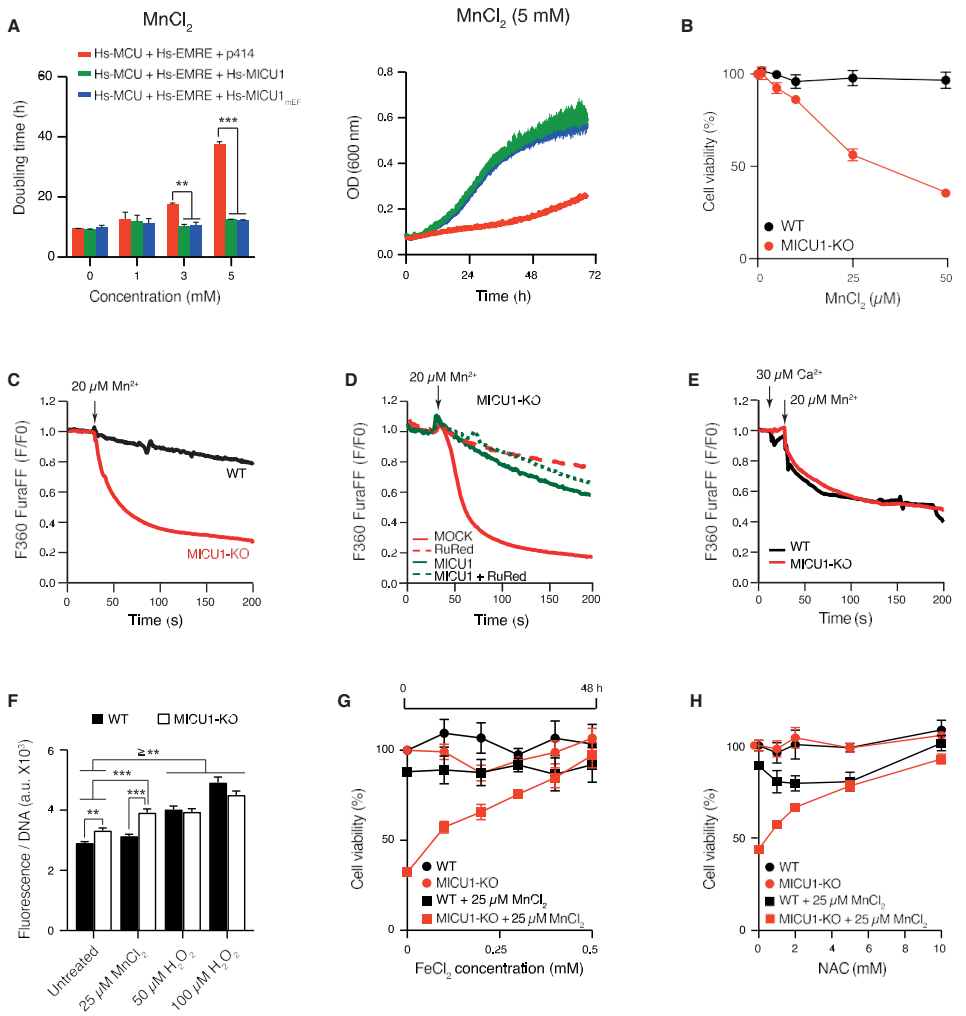

Figure 4. MICU1 Protects from Manganese-Induced Cell Death

(A) Quantification of growth rate and average growth curve of yeast strains treated with $MnCl_2$; n = 4; **p < 0.01; ***p < 0.001; one-way ANOVA with Tukey's multiple comparisons test.

(B) Cell viability of wild-type (WT) and MICU1 knockout (MICU1-KO) HEK293 cells treated for 48 hr with $MnCl_2$; n = 4.

(C–E) Detection of mitochondrial Mn^{2+} uptake through the quench of compartmentalized Fura-FF in permeabilized single WT and MICU1-KO cells in the absence (C) or presence (D) of $CaCl_2$ and upon transfection with MICU1 or pcDNA in the absence and presence of 3 mM RuRed (E). Each trace represents the mean of 40–50 cells from one of three different cell cultures.

(F) Measurements of ROS by 5-(and-6)-chloromethyl-2′, 7′-dichlorodihydrofluorescein diacetate (CM-H_2DCFDA) in WT and MICU1-KO cells treated for 48 hr with vehicle, $MnCl_2$, or H_2O_2. Data represent means ± SEMs; n = 8; **p < 0.01, ***p < 0.001; one-way ANOVA with Tukey's multiple comparisons test.

(legend continued on next page)

Treatment of MICU1-KO cells with 25 mM Mn^{2+} in the presence of 0.5 mM $FeCl_2$ (Figure 4G) consistently resulted in cell survival, whereas $FeCl_2$ pre-treatment for 24 hr was unable to confer protection to Mn^{2+}-induced stress (Figure S4E). We also tested the effect of several antioxidant compounds on Mn^{2+}-induced oxidative stress (Figure S4F) and found that NAC treatment was able to fully rescue Mn^{2+}-induced cell death in MICU1 KO cells (Figure 4H).

Our findings establish an essential role of MICU1 in regulating the permeability of the uniporter to Mn^{2+}, which is essential for preventing Mn^{2+}-induced cytotoxicity.

DISCUSSION

Our phylogenetic analysis (Figure 1) and a previous comparative genomics study (Bick et al., 2012) highlight a widespread co-occurrence of MCU and MICU1 across Metazoa, Plantae, and Protozoa, with the exception of Fungi. The presence of MCU homologs in several Ascomycota and Basidiomycota fungal clades devoid of any detectable MICU1 has led to the hypothesis that MCU could exist independently of a Ca^{2+}-sensing regulator. This is based on the assumption that fungal MCU homologs are able per se to mediate mt-Ca^{2+} uptake, with properties similar to the mammalian uniporter. Our results from functional complementation analyses in human shMCU cells (Figures 1 and S1) and from *in vivo* reconstitution in yeast (Figure S2) show that MCU orthologs from *N. crassa* and *A. fumigatus* are unable to drive mt-Ca^{2+} uptake, despite proper expression, mitochondrial localization, topology, and assembly. Those findings are consistent with previous observations from Carafoli and Lehninger (1971) and from Gonçalves et al. (2015) that mitochondria of *N. crassa* have a limited ability to accumulate Ca^{2+}, which occurs in the range of hours, are only partially inhibited by Ru360, and are not driven by membrane potential. Recently, it was reported that a putative MCU ortholog could mediate Ca^{2+} transport into *A. fumigatus* mitochondria (Song et al., 2016) and the structures of MCU orthologs from several Fungi (Baradaran et al., 2018; Fan et al., 2018; Nguyen et al., 2018), including *N. crassa* (Yoo et al., 2018), have been characterized. However, Af-MCU-KO elicited only a 50% decrease in Ca^{2+} uptake into *A. fumigatus* mitochondria. Moreover, there is currently no direct evidence that MCU orthologs from *Nassarius fischeri* (Nguyen et al., 2018), *Fusarium graminearum*, and *Metarhizium acridum* (Fan et al., 2018) mediate mt-Ca^{2+} uptake in those organisms, neither that other fungal MCUs can reconstitute mt-Ca^{2+} uptake when expressed in yeast or mammalian cells (Baradaran et al., 2018). These results would lead to conjecture that either the MCU-like sequences found in some Fungi encode for proteins that have lost Ca^{2+} uptake ability or they could be involved in Ca^{2+} transport through mechanisms that are different from the mammalian uniporter. Further experiments will be necessary to uncover the function of those MCU-like proteins in Fungi and to resolve the paradox of species with MCU-like sequences without MICU1 orthologs.

To investigate the direct contribution of MICU1 to the uniporter activity, we used the yeast *S. cerevisiae* as a model system. Previous results, including ours, have shown that Hs-MCU and Hs-EMRE are sufficient to drive Ca^{2+} uptake *in vitro* into the matrix of isolated mitochondria (Arduino et al., 2017; Kovács-Bogdán et al., 2014; Yamamoto et al., 2016). Here, we show that they can reconstitute mt-Ca^{2+} entry *in vivo* in yeast in response to a physiological increase in cyt-Ca^{2+} (Figure 2). Furthermore, similar to mammalian cells, the expression of Hs-MICU1 in MCU-reconstituted yeast cells exerts a synergistic effect on mt-Ca^{2+} uptake, which is dependent on its Ca^{2+}-sensing domains. Therefore, we searched for biological conditions whereby a positive MCU-MICU1 genetic interaction would provide a selective fitness advantage over a yeast strain reconstituted with MCU without its regulator (Figure 3). We found that MCU-reconstituted yeast cells are more susceptible to the increase of Mn^{2+} levels in the extracellular medium, which is likely due to its permeation across the uniporter (Cao et al., 2017; Csordás and Hajnóczky, 2003; Mela and Chance, 1968; Romslo and Flatmark, 1973; Saris, 2012; Vinogradov and Scarpa, 1973). Co-expression with MICU1 conferred full protection against uniporter-dependent Mn^{2+} toxicity (Figure 4), regardless of functional EF-hand domains. All of these findings were recapitulated in HEK293 cells, where the KO of MICU1 hypersensitized cells to Mn^{2+}-dependent cell death. Thus, unlike Ca^{2+}, the binding of Mn^{2+} to EF-hands (Senguen and Grabarek, 2012; Shirran and Barran, 2009) would be insufficient to trigger in MICU1 the conformational change needed for the opening of the MCU channel, a hypothesis that was recently validated by Kamer et al. (2018).

Our findings are of great relevance for patients with MICU1 loss-of-function mutations (Lewis-Smith et al., 2016; Logan et al., 2014; Musa et al., 2018). So far, the disease phenotypes observed in human patients and recapitulated in MICU1-KO mice (Antony et al., 2016; Liu et al., 2016) were attributed to high basal mt-Ca^{2+} levels, possibly due to the loss of MICU1-dependent gatekeeping of the uniporter. In light of our results, those could also result from Mn^{2+} accumulation in mitochondria, which would have an additive effect: it would increase mt-Ca^{2+} levels by inhibiting both Na^+-dependent and Na^+-independent mt-Ca^{2+} efflux routes (Gavin et al., 1990), and it would increase oxidative stress and trigger cell death (Smith et al., 2017). Accordingly, antioxidant treatment with NAC fully prevented Mn^{2+}-induced cell death in MICU1-KO cells. This result is consistent with previous findings showing that treatment of cells, mice, rats, and nonhuman primates with NAC during exposure to high doses of $MnCl_2$ is protective against Mn^{2+} cytotoxicity (Smith et al., 2017). Finally, our findings also suggest MICU1 as a possible target for neurological diseases related to chronic

(G) Cell viability of WT and MICU1-KO cells treated for 48 hr with $MnCl_2$ in the presence of $FeCl_2$ (n = 3).
(H) Cell viability of WT and MICU1-KO cells treated for 48 hr with $MnCl_2$ in the presence of *N*-acetyl-L-cysteine (NAC) (n = 3).
All data represent means ± SEMs and are reported as the percentage of viable cells in untreated samples.
See also Figure S4.

exposure to environmental sources of Mn^{2+} such as, for example, Mn^{2+}-rich foods, Mn^{2+} aerosols and dusts in mines and smelters, and air pollution from the combustion of gasoline containing methylcyclopentadienyl Mn^{2+} tricarbonyl (O'Neal and Zheng, 2015).

In summary, our study demonstrates the power of combining comparative genomics analyses with the use of yeast as a model system for dissecting the functional and mechanistic role of each component of the mammalian uniporter. The reconstitution of an MICU1-regulated uniporter in yeast offers an incomparable advantage over similar investigations of MICU1 and MCU interdependence in mammalian cells, in which MICU1 KO or knockdown also has confounding effects on the expression of other uniporter subunits, such as MICU2 and MICU3 (Patron et al., 2014, 2018; Plovanich et al., 2013). Importantly, we unraveled a key role of MICU1 in regulating the selectivity of the uniporter towards Ca^{2+} ions, with important implications for patients with MICU1 deficiency.

STAR+METHODS

Detailed methods are provided in the online version of this paper and include the following:

- KEY RESOURCES TABLE
- CONTACT FOR REAGENT AND RESOURCE SHARING
- EXPERIMENTAL MODEL AND SUBJECT DETAILS
  - Cell lines
  - Yeast Strains
- METHOD DETAILS
  - Phylogenetic Profiling of MICU1 and MCU
  - Protein Domains
  - Plasmids and Reagents
  - Isolation of Crude Mitochondria from HeLa Cells
  - Topology Analysis of Mitochondrial Proteins
  - Blue Native – PAGE Analysis
  - Measurements of Mitochondrial Calcium Uptake in Intact HeLa Cells
  - Measurements of Mitochondrial Calcium Uptake in Digitonin-Permeabilized HeLa Cells
  - Subcellular Fractionation of Yeast Cells
  - Measurements of Calcium Transients in Intact Yeast Cells
  - Measurements of Mitochondrial Calcium Uptake in Isolated Yeast Mitochondria
  - Yeast Growth Measurement
  - Cell Viability Analysis
  - Mitochondrial Mn^{2+} Transport Measurement in Human Cells
  - ROS Measurement
- QUANTIFICATION AND STATISTICAL ANALYSIS
  - Quantification of Calcium Transients
  - Data Analysis

SUPPLEMENTAL INFORMATION

Supplemental Information includes four figures and can be found with this article online at https://doi.org/10.1016/j.celrep.2018.10.037.

ACKNOWLEDGMENTS

We acknowledge support from the German Research Foundation (DFG) under the Emmy Noether Programme (PE 2053/1-1 to F.P. and J.W.), the Munich Center for Systems Neurology (SyNergy EXC 1010 to F.P.), the Juniorverbund in der Systemmedizin "mitOmics" (FKZ 01ZX1405B to V.G. and A.L.), The Bert L & N Kuggie Vallee Foundation (to F.P. and D.M.A.), the DFG (MO1944/1-2 to D.M.), the Spanish Ministry of Economy, Industry, and Competitiveness (MEIC; BFU2015-67107), the European Union's Horizon 2020 research and innovation program under grant agreement ERC-2016-724173 (to T.G. and A.A.P.), and the NIH (RO1 GM102724 to G.H.).

AUTHOR CONTRIBUTIONS

Conceptualization, F.P.; Methodology, F.P., V.G., J.W., K.-T.H., D.M., T.G., and G.H.; Validation, V.G., J.W., K.-T.H., U.T., and A.L.; Formal Analysis, V.G., J.W., K.-T.H., A.A.P., D.M.A., and Y.C.; Investigation, V.G., J.W., and K.-T.H.; Resources, F.P., D.M., G.H., and T.G.; Writing - Original Draft, F.P., V.G., and J.W.; Writing - Review & Editing, F.P., T.G., D.M., G.H., and D.M.A.; Visualization, F.P., V.G., J.W., K.-T.H., and G.H.; Supervision, F.P., G.H, and T.G.; Funding Acquisition, F.P., D.M., T.G, and G.H.

DECLARATION OF INTERESTS

The authors declare no competing interests.

Received: June 30, 2018
Revised: August 9, 2018
Accepted: October 8, 2018
Published: November 6, 2018

REFERENCES

Antony, A.N., Paillard, M., Moffat, C., Juskeviciute, E., Correnti, J., Bolon, B., Rubin, E., Csorda´ s, G., Seifert, E.L., Hoek, J.B., and Hajno´ czky, G. (2016). MICU1 regulation of mitochondrial Ca(2+) uptake dictates survival and tissue regeneration. Nat. Commun. *7*, 10955.

Arduino, D.M., Wettmarshausen, J., Vais, H., Navas-Navarro, P., Cheng, Y., Leimpek, A., Ma, Z., Delrio-Lorenzo, A., Giordano, A., Garcia-Perez, C., et al. (2017). Systematic identification of MCU modulators by orthogonal interspecies chemical screening. Mol. Cell *67*, 711–723.e7.

Baradaran, R., Wang, C., Siliciano, A.F., and Long, S.B. (2018). Cryo-EM structures of fungal and metazoan mitochondrial calcium uniporters. Nature *559*, 580–584.

Baughman, J.M., Perocchi, F., Girgis, H.S., Plovanich, M., Belcher-Timme, C.A., Sancak, Y., Bao, X.R., Strittmatter, L., Goldberger, O., Bogorad, R.L., et al. (2011). Integrative genomics identifies MCU as an essential component of the mitochondrial calcium uniporter. Nature *476*, 341–345.

Bick, A.G., Calvo, S.E., and Mootha, V.K. (2012). Evolutionary diversity of the mitochondrial calcium uniporter. Science *336*, 886.

Bonora, M., Giorgi, C., Bononi, A., Marchi, S., Patergnani, S., Rimessi, A., Rizzuto, R., and Pinton, P. (2013). Subcellular calcium measurements in mammalian cells using jellyfish photoprotein aequorin-based probes. Nat. Protoc. *8*, 2105–2118.

Cao, C., Wang, S., Cui, T., Su, X.-C., and Chou, J.J. (2017). Ion and inhibitor binding of the double-ring ion selectivity filter of the mitochondrial calcium uniporter. Proc. Natl. Acad. Sci. USA *114*, E2846–E2851.

Carafoli, E., and Lehninger, A.L. (1971). A survey of the interaction of calcium ions with mitochondria from different tissues and species. Biochem. J. *122*, 681–690.

Chaudhuri, D., Sancak, Y., Mootha, V.K., and Clapham, D.E. (2013). MCU encodes the pore conducting mitochondrial calcium currents. eLife *2*, e00704.

Cheng, Y., and Perocchi, F. (2015). ProtPhylo: identification of protein-phenotype and protein-protein functional associations via phylogenetic profiling. Nucleic Acids Res. *43*, W160–W168.

Csordás, G., and Hajnóczky, G. (2003). Plasticity of mitochondrial calcium signaling. J. Biol. Chem. *278*, 42273–42282.

Csordás, G., Golenár, T., Seifert, E.L., Kamer, K.J., Sancak, Y., Perocchi, F., Moffat, C., Weaver, D., de la Fuente Perez, S., Bogorad, R., et al. (2013). MICU1 controls both the threshold and cooperative activation of the mitochondrial Ca^{2+} uniporter. Cell Metab. *17*, 976–987.

Cyert, M.S. (2003). Calcineurin signaling in Saccharomyces cerevisiae: how yeast go crazy in response to stress. Biochem. Biophys. Res. Commun. *311*, 1143–1150.

De Stefani, D., Raffaello, A., Teardo, E., Szabó, I., and Rizzuto, R. (2011). A forty-kilodalton protein of the inner membrane is the mitochondrial calcium uniporter. Nature *476*, 336–340.

De Stefani, D., Rizzuto, R., and Pozzan, T. (2016). Enjoy the trip: calcium in mitochondria back and forth. Annu. Rev. Biochem. *85*, 161–192.

Deluca, H.F., and Engstrom, G.W. (1961). Calcium uptake by rat kidney mitochondria. Proc. Natl. Acad. Sci. USA *47*, 1744–1750.

Fan, C., Fan, M., Orlando, B.J., Fastman, N.M., Zhang, J., Xu, Y., Chambers, M.G., Xu, X., Perry, K., Liao, M., and Feng, L. (2018). X-ray and cryo-EM structures of the mitochondrial calcium uniporter. Nature *559*, 575–579.

Gavin, C.E., Gunter, K.K., and Gunter, T.E. (1990). Manganese and calcium efflux kinetics in brain mitochondria. Relevance to manganese toxicity. Biochem. J. *266*, 329–334.

Gonçalves, A.P., Cordeiro, J.M., Monteiro, J., Lucchi, C., Correia-de-Sá, P., and Videira, A. (2015). Involvement of mitochondrial proteins in calcium signaling and cell death induced by staurosporine in Neurospora crassa. Biochim. Biophys. Acta *1847*, 1064–1074.

Groppi, S., Belotti, F., Brandão, R.L., Martegani, E., and Tisi, R. (2011). Glucose-induced calcium influx in budding yeast involves a novel calcium transport system and can activate calcineurin. Cell Calcium *49*, 376–386.

Kamer, K.J., and Mootha, V.K. (2014). MICU1 and MICU2 play non redundant roles in the regulation of the mitochondrial calcium uniporter. EMBO Rep *15*, 299–307.

Kamer, K.J., Grabarek, Z., and Mootha, V.K. (2017). High-affinity cooperative Ca^{2+} binding by MICU1-MICU2 serves as an on-off switch for the uniporter. EMBO Rep. *18*, 1397–1411.

Kamer, K.J., Sancak, Y., Fomina, Y., Meisel, J.D., Chaudhuri, D., Grabarek, Z., and Mootha, V.K. (2018). MICU1 imparts the mitochondrial uniporter with the ability to discriminate between Ca^{2+} and Mn^{2+}. Proc. Natl. Acad. Sci. USA *115*, E7960–E7969.

Kirichok, Y., Krapivinsky, G., and Clapham, D.E. (2004). The mitochondrial calcium uniporter is a highly selective ion channel. Nature *427*, 360–364.

Kovács-Bogdán, E., Sancak, Y., Kamer, K.J., Plovanich, M., Jambhekar, A., Huber, R.J., Myre, M.A., Blower, M.D., and Mootha, V.K. (2014). Reconstitution of the mitochondrial calcium uniporter in yeast. Proc. Natl. Acad. Sci. USA *111*, 8985–8990.

Lewis-Smith, D., Kamer, K.J., Griffin, H., Childs, A.M., Pysden, K., Titov, D., Duff, J., Pyle, A., Taylor, R.W., Yu-Wai-Man, P., et al. (2016). Homozygous deletion in MICU1 presenting with fatigue and lethargy in childhood. Neurol. Genet. *2*, e59.

Liu, J.C., Liu, J., Holmström, K.M., Menazza, S., Parks, R.J., Fergusson, M.M., Yu, Z.X., Springer, D.A., Halsey, C., Liu, C., et al. (2016). MICU1 serves as a molecular gatekeeper to prevent in vivo mitochondrial calcium overload. Cell Rep. *16*, 1561–1573.

Logan, C.V., Szabadkai, G., Sharpe, J.A., Parry, D.A., Torelli, S., Childs, A.M., Kriek, M., Phadke, R., Johnson, C.A., Roberts, N.Y., et al.; UK10K Consortium (2014). Loss-of-function mutations in MICU1 cause a brain and muscle disorder linked to primary alterations in mitochondrial calcium signaling. Nat. Genet. *46*, 188–193.

Mallilankaraman, K., Doonan, P., Cárdenas, C., Chandramoorthy, H.C., Müller, M., Miller, R., Hoffman, N.E., Gandhirajan, R.K., Molgó, J., Birnbaum, M.J., et al. (2012). MICU1 is an essential gatekeeper for MCU-mediated mitochondrial Ca(2+) uptake that regulates cell survival. Cell *151*, 630–644.

Mela, L., and Chance, B. (1968). Spectrophotometric measurements of the kinetics of Ca2+ and Mn2+ accumulation in mitochondria. Biochemistry *7*, 4059–4063.

Mumberg, D., Müller, R., and Funk, M. (1995). Yeast vectors for the controlled expression of heterologous proteins in different genetic backgrounds. Gene *156*, 119–122.

Murgia, M., and Rizzuto, R. (2015). Molecular diversity and pleiotropic role of the mitochondrial calcium uniporter. Cell Calcium *58*, 11–17.

Musa, S., Eyaid, W., Kamer, K., Ali, R., Al-Mureikhi, M., Shahbeck, N., Al Mesaifri, F., Makhseed, N., Mohamed, Z., AlShehhi, W.A., et al. (2018). A Middle Eastern founder mutation expands the genotypic and phenotypic spectrum of mitochondrial MICU1 deficiency: a report of 13 patients. JIMD Rep. Published online May 3, 2018. https://doi.org/10.1007/8904_2018_107.

Nguyen, N.X., Armache, J.P., Lee, C., Yang, Y., Zeng, W., Mootha, V.K., Cheng, Y., Bai, X.C., and Jiang, Y. (2018). Cryo-EM structure of a fungal mitochondrial calcium uniporter. Nature *559*, 570–574.

O'Neal, S.L., and Zheng, W. (2015). Manganese toxicity upon overexposure: a decade in review. Curr. Environ. Health Rep. *2*, 315–328.

Oxenoid, K., Dong, Y., Cao, C., Cui, T., Sancak, Y., Markhard, A.L., Grabarek, Z., Kong, L., Liu, Z., Ouyang, B., et al. (2016). Architecture of the mitochondrial calcium uniporter. Nature *533*, 269–273.

Paillard, M., Csordás, G., Szanda, G., Golenár, T., Debattisti, V., Bartok, A., Wang, N., Moffat, C., Seifert, E.L., Spät, A., and Hajnóczky, G. (2017). Tissue-specific mitochondrial decoding of cytoplasmic Ca^{2+} signals is controlled by the stoichiometry of MICU1/2 and MCU. Cell Rep. *18*, 2291–2300.

Patron, M., Checchetto, V., Raffaello, A., Teardo, E., Vecellio Reane, D., Mantoan, M., Granatiero, V., Szabó, I., De Stefani, D., and Rizzuto, R. (2014). MICU1 and MICU2 finely tune the mitochondrial Ca2+ uniporter by exerting opposite effects on MCU activity. Mol. Cell *53*, 726–737.

Patron, M., Granatiero, V., Espino, J., Rizzuto, R., and De Stefani, D. (2018). MICU3 is a tissue-specific enhancer of mitochondrial calcium uptake. Cell Death Differ. Published online May 3, 2018. https://doi.org/10.1038/s41418-018-0113-8.

Perocchi, F., Gohil, V.M., Girgis, H.S., Bao, X.R., McCombs, J.E., Palmer, A.E., and Mootha, V.K. (2010). MICU1 encodes a mitochondrial EF hand protein required for Ca(2+) uptake. Nature *467*, 291–296.

Philpott, C.C. (2012). Coming into view: eukaryotic iron chaperones and intracellular iron delivery. J. Biol. Chem. *287*, 13518–13523.

Plovanich, M., Bogorad, R.L., Sancak, Y., Kamer, K.J., Strittmatter, L., Li, A.A., Girgis, H.S., Kuchimanchi, S., De Groot, J., Speciner, L., et al. (2013). MICU2, a paralog of MICU1, resides within the mitochondrial uniporter complex to regulate calcium handling. PLoS One *8*, e55785.

Romslo, I., and Flatmark, T. (1973). Energy-dependent accumulation of iron by isolated rat liver mitochondria. II. Relationship to the active transport of Ca2+. Biochim. Biophys. Acta *325*, 38–46.

Sancak, Y., Markhard, A.L., Kitami, T., Kovács-Bogdán, E., Kamer, K.J., Udeshi, N.D., Carr, S.A., Chaudhuri, D., Clapham, D.E., Li, A.A., et al. (2013). EMRE is an essential component of the mitochondrial calcium uniporter complex. Science *342*, 1379–1382.

Saris, N.-El. (2012). Mitochondrial uptake of Ca2+ and other bivalent cations. Biochem. Anal. Biochem. *1*, 112.

Schreiner, B., Westerburg, H., Forne, I., Imhof, A., Neupert, W., and Mokranjac, D. (2012). Role of the AAA protease Yme1 in folding of proteins in the intermembrane space of mitochondria. Mol. Biol. Cell *23*, 4335–4346.

Senguen, F.T., and Grabarek, Z. (2012). X-ray structures of magnesium and manganese complexes with the N-terminal domain of calmodulin: insights into the mechanism and specificity of metal ion binding to an EF-hand. Biochemistry *51*, 6182–6194.

Shirran, S.L., and Barran, P.E. (2009). The use of ESI-MS to probe the binding of divalent cations to calmodulin. J. Am. Soc. Mass Spectrom. *20*, 1159–1171.

Sikorski, R.S., and Hieter, P. (1989). A system of shuttle vectors and yeast host strains designed for efficient manipulation of DNA in Saccharomyces cerevisiae. Genetics *122*, 19–27.

OPEN ACCESS CellPress

STAR+METHODS

KEY RESOURCES TABLE

REAGENT or RESOURCE	SOURCE	IDENTIFIER
Antibodies		
Rabbit polyclonal anti-MCU	Sigma-Aldrich	Cat#HPA016480; Lot#C0114358; RRID: AB_2071893
Rabbit polyclonal anti-EMRE - C22orf32 (clone C-12)	Santa Cruz Biotechnology	Cat#sc-86337; Lot#K0215; RRID: AB_2250685
Mouse monoclonal anti-Aequorin (clone 6E3.2)	Merck/Millipore	Cat#MAB4405; RRID: AB_94900; RRID: AB_94900
Rabbit polyclonal anti-MICU1	Sigma-Aldrich	Cat#HPA037480; Lot#N107141; RRID: AB_10696934
Anti-Sc-Yme1 produced in rabbit	Schreiner et al., 2012	N/A
Mouse monoclonal anti-TIM23	BD Bioscience	Cat#611222; Lot#3067849; RRID: AB_398754
Rabbit polyclonal anti-MICU1	Atlas Antibody	Cat#HPA037479; Lot#R34024; RRID: AB_2675495
Mouse monoclonal anti-Cyclophilin D [E11AE12BD4]	Abcam	Cat#ab110324; Lot#GR134866-15; RRID: AB_10864110
Mouse monoclonal anti-ATP5A	Invitrogen	Cat#43-9800; Lot#TA2516391; RRID: AB_2533548
Mouse monoclonal anti-V5	Life Technologies	Cat#R96025; Lot#1792242; RRID: AB_2556564
Mouse monoclonal anti-HSP60	R&D System	Cat#MAB1800; Lot#UNG02; RRID: AB_11212084
Mouse monoclonal anti-TOMM20	Abcam	Cat#Ab56783; Lot#GR3188177-1; RRID: AB_945896
Mouse monoclonal anti-b-Actin	Sigma-Aldrich	Cat#A2228; Lot#085M4754V; RRID: AB_476697
Chemicals, Peptides, and Recombinant Proteins		
Amiodarone hydrochloride	Sigma-Aldrich	Cat#A8423; CAS: 19774-82-4
Antioxidant Supplement (1000 3)	Sigma-Aldrich	Cat#A1345
Calcium chloride dihydrate	Merck/Millipore	Cat#208290; CAS: 10035-04-8
Calcium Green-5N, Hexapotassium Salt, cell impermeant	Thermo Fisher Scientific	Cat#C3737; CAS: 153130-66-6
CM-H2DCFDA (General Oxidative Stress Indicator)	Thermo Fisher Scientific	Cat#C6827
Coelenterazine, native	Abcam	Cat#ab145165; CAS: 55779-48-1
Copper(II) chloride	Sigma-Aldrich	Cat#751944; CAS: 7447-39-4
Digitonin	Sigma-Aldrich	Cat#D141; CAS: 11024-24-1
Hydrogen peroxide 30% (w/w) solution	Sigma-Aldrich	Cat#H1009; CAS: 7722-84-1
Idebenone	Santhera Pharmaceuticals	CAS: 58186-27-9; Lot#99826G001B
Iron(II) chloride tetrahydrate	Merck/Millipore	Cat#1038610250; CAS: 13478-10-9
L-Glutathione reduced	Sigma-Aldrich	Cat#G6013; CAS: 70-18-8
Mn^{2+}(II) chloride tetrahydrate	Merck/Millipore	Cat#1059271000; CAS: 13446-34-9
Miconazole nitrate salt	Sigma-Aldrich	Cat#M3512; CAS: 22832-87-7
N-Acetyl-L-cysteine	Sigma-Aldrich	Cat#A9165; CAS: 616-91-1
Native Mark Unstained Protein Standard-5	Life Technologies	Cat#LC0725
Native PAGE 20x Cathode Buffer	Life Technologies	Cat#BN2002
Native PAGE Novex 3-12%, Bis-Tris Protein, 10well	Life Technologies	Cat#BN1001
Native PAGE Running Buffer (20x)	Life Technologies	Cat#BN2001
NativePAGE 5% G-250 Sample Additive	Life Technologies	Cat#BN2004
NativePAGE Sample Buffer (4x)	Life Technologies	Cat#BN2003
Ru360	Calbiochem	Cat#557440
Strontium chloride hexahydrate	Merck/Millipore	Cat#1078650250; CAS: 10025-70-4
Thiazolyl Blue Tetrazolium Bromide (MTT)	Sigma-Aldrich	Cat#M5655; CAS: 298-93-1
Zinc chloride	Sigma-Aldrich	Cat#Z0152; CAS: 7646-85-7
Zymolyase 20T from *Arthrobacter luteus*	Amsbio	Cat#120491-1
6-Hydroxy-2,5,7,8-tetramethylchromane-2-carboxylic acid (Trolox)	Sigma-Aldrich	Cat#238813; CAS: 53188-07-1

(*Continued on next page*)

OPEN ACCESS CellPress

Continued

REAGENT or RESOURCE	SOURCE	IDENTIFIER
Ruthenium Red	Sigma	R2751
Fura-2 low affinity (AM)	Teflabs	0-136
Thapsigargin	Enzo Life Sciences	BML-PE180-0005
CGP-37157	Enzo Life Sciences	BML-CM119-0005
Lipofectamine 3000	Life Technologies	L3000008
Critical Commercial Assays		
Pierce BCA Protein Assay Kit	Thermo Fisher Scientific	Cat#23227
CyQUANT Cell Proliferation Assay Kit	Thermo Fisher Scientific	Cat#C7026
Experimental Models: Cell Lines		
HEK293T cells	ATCC	CRL-11268
MICU1-knockout HEK293T cells (MICU1-KO)	Vamsi K. Mootha Laboratory	Kamer and Mootha (2014); Kamer et al. (2017)
MICU1-KO HEK293T cells rescued with WT MICU1	This paper	N/A
MICU1-knockout HEK293T cells rescued with EF-hands mutant MICU1	This paper	N/A
pLKO HeLa cells stably expressing WT mt-AEQ	This paper	N/A
shMCU HeLa cells stably expressing WT mt-AEQ	This paper	N/A
shMCU HeLa cells stably expressing WT mt-AEQ + HsMCU	This paper	N/A
shMCU HeLa cells stably expressing WT mt-AEQ + ^{HsMTS}AfMCU	This paper	N/A
shMCU HeLa cells stably expressing WT mt-AEQ + AfMCU	This paper	N/A
shMCU HeLa cells stably expressing WT mt-AEQ + NcMCU	This paper	N/A
shMCU HeLa cells stably expressing WT mt-AEQ + ^{HsMTS}NcMCU	This paper	N/A
Experimental Models: Organisms/Strains		
S. cerevisiae: Strain background: YPH499 expressing HsMCU + HsEMRE + WT mt-AEQ	Arduino et al., 2017	N/A
S. cerevisiae: Strain background: YPH499 expressing HsMCU$_{E264A}$ + HsEMRE + WT mt-AEQ	This paper	N/A
S. cerevisiae: Strain background: YPH499 expressing HsMCU$_{D261A}$ + HsEMRE + WT mt-AEQ	This paper	N/A
S. cerevisiae: Strain background: YPH499 expressing HsMCU + WT mt-AEQ	This paper	N/A
S. cerevisiae: Strain background: YPH499 expressing DdMCU + WT mt-AEQ	This paper	N/A
S. cerevisiae: Strain background: YPH499 expressing AfMCU + WT mt-AEQ	This paper	N/A
S. cerevisiae: Strain background: YPH499 expressing NcMCU + WT mt-AEQ	This paper	N/A
S. cerevisiae: Strain background: YPH499 expressing HsEMRE + WT mt-AEQ	This paper	N/A
S. cerevisiae: Strain background: YPH499 expressing HsMCU + HsEMRE + HsMICU1 + WT mt-AEQ	This paper	N/A
S. cerevisiae: Strain background: YPH499 expressing HsMCU + HsEMRE + HsMICU1$_{mEF}$ + WT mt-AEQ	This paper	N/A
S. cerevisiae: Strain background: YPH499 + p414GPD expressing HsMCU + HsEMRE + WT mt-AEQ	This paper	N/A

(*Continued on next page*)

OPEN ACCESS CellPress

Continued		
REAGENT or RESOURCE	SOURCE	IDENTIFIER
S. cerevisiae: Strain background: YPH499 +p423GPD + p425GPD expressing WT mt-AEQ	This paper	N/A
S. cerevisiae: Strain background: YPH499 expressing WT mt-AEQ	This paper	N/A
Oligonucleotides		
MCU shRNA targeting sequence: 5′-GCAAGGAGTTTCTTTCTCTTT-3′	RNAi Consortium, Broad Institute	TRCN0000133861
Recombinant DNA		
p316GPD (plasmid)	Arduino et al., 2017	N/A
p423GPD (plasmid)	Mumberg et al., 1995	N/A
p425GPD (plasmid)	Mumberg et al., 1995	N/A
p414GPD (plasmid)	Mumberg et al., 1995	N/A
MCU full-length with V5-tag (pLX304)	Arduino et al., 2017	N/A
AfMCU full-length with V5-tag (pLX304)	This paper	N/A
^{HsMTS}AfMCU full-length with V5-tag (pLX304)	This paper	N/A
^{HsMTS}NcMCU full-length with V5-tag (pLX304)	This paper	N/A
NcMCU full-length with V5-tag (pLX304)	This paper	N/A
DdMCU full-length with V5-tag (pLX304)	This paper	N/A
MCU full-length with V5-tag (p423GPD)	Arduino et al., 2017	N/A
AfMCU full-length with V5-tag (p423GPD)	This paper	N/A
NcMCU full-length with V5-tag (p423GPD)	This paper	N/A
DdMCU full-length with V5-tag (p423GPD)	This paper	N/A
pcDNA-dest40-MICU1-HA	(Kamer et al., 2017)	N/A
Software and Algorithms		
GraphPad Prism 5.0 or newer	GraphPad Software	N/A
MATLAB R2014b	MathWorks	N/A
ProtPhylo	Cheng and Perocchi, 2015	www.protphylo.org
Phylogenetic tree generator	N/A	https://phylot.biobyte.de/
iTOL	N/A	https://itol.embl.de/
Canvas X	N/A	N/A
SigmaPlot 12.5	N/A	N/A

CONTACT FOR REAGENT AND RESOURCE SHARING

Further information and requests for resources and reagents should be directed to and will be fulfilled by the Lead Contact, Fabiana Perocchi (fabiana.perocchi@helmholtz-muenchen.de).

EXPERIMENTAL MODEL AND SUBJECT DETAILS

Cell lines

All mammalian cells were grown in high-glucose Dulbecco's modified Eagle's medium (DMEM) (Sigma-Aldrich; D6429) supplemented with 10% FBS (Sigma-Aldrich, F7524) at 37°C and 5% CO_2. HeLa cells stably expressing a WT mitochondrial matrix-targeted GFP-aequorin (mt-AEQ HeLa) were generated as previously described (Arduino et al., 2017) and selected with 100 mg/ml geneticin (Thermo Fisher Scientific, 10131027). Mt-AEQ HeLa cells stably expressing either an empty vector (pLKO; Addgene, 8453) or a pLKO vector expressing a shRNA targeting Hs-MCU (shMCU; Sigma Aldrich, TRCN0000133861) were generated as previously described (Baughman et al., 2011) and selected with 2 mg/mL puromycin (Life Technologies, A11138) and 100 mg/ml geneticin. MCU-knockdown mtAEQ HeLa cells stably expressing Hs-MCU, Nc-MCU, Af-MCU, ^{HsMTS}Af-MCU and ^{HsMTS}Nc-MCU from the pLX304 lentiviral vector were generated by transduction. Lentivirus production and infection were performed according to guidelines from the Broad RNAi Consortium and infected cell lines were selected 48 hr post-transduction with the respective selection markers. MICU1- knockout HEK293 cells were kindly provided by Prof. Vamsi Mootha (Howard Hughes Medical Institute). MICU1-knockout

HEK293 cells stably expressing either wild-type (Hs-MICU1) or mutant Hs-MICU1 (Hs-MICU1$_{mEF}$) from the pLX304 vector were generated by transduction and selected with 10 mg/mL blasticidin.

Yeast Strains

Yeast strains expressing mt-AEQ or cyt-AEQ were generated by transforming the wild-type yeast strain YPH499 and selecting transformants in glucose medium lacking uracil (Sikorski and Hieter, 1989). Yeast strains expressing Dd-MCU, Af-MCU, Nc-MCU, Hs-EMRE, Hs-MCU, Hs-MICU1 and their mutants were generated by transforming the YPH499 strain with the respective plasmids and by selecting transformants on glucose medium lacking uracil (empty vector p316GPD or mt-AEQ and cyt-AEQ), histidine (empty vector p423GPD or Hs-MCU, Hs-MCU$_{D261A}$, Hs-MCU$_{E264A}$, Dd-MCU, Af-MCU, and Nc-MCU), leucine (empty vector p425GPD or Hs-EMRE), and tryptophan (empty vector p414GPD or Hs-MICU1, Hs-MICU1$_{mEF}$) as selection markers.

METHOD DETAILS

Phylogenetic Profiling of MICU1 and MCU

Homologs of human MCU and MICU1 across 247 eukaryotes were retrieved from ProtPhylo (www.protphylo.org) (Cheng and Perocchi, 2015) using OrthoMCL with more than 0% match length and inflation index of 1.1 for orthology assignment. The percentage of amino acids match length was determined based on BLASTp-NIH. The phylogenetic tree of 247 eukaryotes was reconstructed using the phylogenetic tree generator (https://phylot.biobyte.de/) and visualized using iTOL (https://itol.embl.de/). The mitochondrial-targeting sequence (MTS) probability was determined with MitoProt (https://ihg.gsf.de/ihg/mitoprot.html).

Protein Domains

Protein sequences of *Homo sapiens* MCU (Hs-MCU, NP_612366.1) *Neurospora crassa* MCU (Nc-MCU, XP_959658.1), and *Aspergillus fumigatus* MCU (Af-MCU, XP_751795.1) were analyzed to predict MTS, DUF607 motif, coiled coil domains (CCD) (https://embnet.vital-it.ch/software/COILS_form.html), and transmembrane domains (TM) (TMHMM 2.0). Clustal Omega was used for proteins alignment and sequence similarities above 80% were color-coded with the Sequence Manipulation Suite tool.

Plasmids and Reagents

The lentiviral vector pLX304 was obtained from the Broad Institute's RNAi Consortium and used for expressing V5- tagged cDNAs. Full-length, human wild-type EMRE (Hs-EMRE), MCU (Hs-MCU), MICU1 (Hs-MICU1) and their mutants (Hs-MCU$_{D261A}$, Hs-MCU$_{E264A}$, and Hs-MICU1$_{mEF}$) cDNAs without a stop codon were obtained from Addgene. Hs-MICU1$_{mEF}$ contains two point mutations in both first (D231A, E242K) and second (D421A, E432K) EF-hand domains as described in (Perocchi et al., 2010).

Dd-MCU, Af-MCU and Nc-MCU with (^{HsMTS}Af-MCU and ^{HsMTS}Nc-MCU) and without the N-terminal MTS of Hs-MCU (aminoacids 1-56) and without a stop codon were codon optimized for human expression, synthesized *de novo* in the PuC57 vector (GenScript) and amplified with flanked *att*B1 and *att*B2 sites by PCR using the following primers: fw-DdMCU (5^0-GGG GAC AAG TTT GTA CAA AAA AGC AGG CTT AGC CAC CAT GAA CTC CTT TGT CAT CAG-3^0); rv-DdMCU (5^0-GGG GAC AAG TTT GTA CAA AAA AGC AGG CTT AGC CAC CAT GAA TTG CGT GAG AAT GAG ACT C-3^0); fw-NcMCU (5^0-GGG GAC AGG TTT GTA CAA AAA AGC AGG CTT AGC CAC CAT GAA TTG CGT GAG AAT GAG ACT C-3^0); rv-NcMCU (5^0-GGG GAC CAC TTT GTA CAA GAA AGC TGG GTT ACT GTC TCC GCT GGT CTC TTT-3^0), fw-AfMCU (5^0-GGG GAC AAG TTT GTA CAA AAA AGC AGG CTT AGC CAC CAT GGT CCT GTC TTG TGA TAC TAG A-3^0); rv-AfMCU (5^0-GGG GAC CAC TTT GTA CAA GAA AGC TGG GTT GTC GTC ATC TCG GTC ATC GTT-3^0); fw-HsMTS (5^0-GGG GAC AAG TTT GTA CAA AAA AGC AGG CTT AGC CAC CAT GGC GGC CGC CGC AGG TAG A-3^0). PCR products were integrated into the pDONR221 vector using a site-specific recombination system (GATEWAY cloning technology) according to manufacturer's instructions (Life Technologies). For the expression in mammalian cells, cDNAs were integrated from the pDONR221 Gateway vector (Thermo Fisher Scientific, 1253607), by site-specific recombination, into the pLX304 vector according to manufacturer's instructions (Life Technologies).

Cytosolic aequorin (cyt-AEQ) plasmid was kindly provided by Prof. Teresa Alonso (University Valladolid) and a mitochondria-targeted GFP-aequorin (mt-AEQ) plasmid was generated as previously described in (Arduino et al., 2017). cDNAs of Dd-MCU, Af-MCU, Nc-MCU, Hs-EMRE, Hs-MCU, Hs-MICU1 and their mutants were amplified by PCR using the following primers: fw-DdMCU (5^0-CCC TCT AGA ATG AAC TCC TTT GTC ATC AG-3^0); fw-AfMCU (5^0-CCC TCT AGA ATG GTC CTG TCT TGT GAT AC-3^0); fw-NcMCU (5^0-CCC TCT AGA ATG AAT TGC GTG AGA ATG AG-3^0); rv-V5 (5^0-GGG CTC GAG CTA CGT AGA ATC GAG ACC GAG-3^0); fw-HsEMRE (5^0-CCC GGA TCC ATG GCG TCC GGA GCG GCT CGC-3^0); rv-HsEMRE (5^0-GGG CTC GAG TTA GTC ATC ATC ATC ATC ATC CTC-3^0); fw-HsMCU (5^0-CCC TCT AGA ATG GCG GCC GCC GCA GGT AG-3^0); rv-HsMCU (5^0-GGG CTC GAG TTA ATC TTT TTC ACC AAT TTG TCG-3^0); fw-HsMICU1 (5^0-CCC GGA TCC ATG TTT CGT CTG AAC TCA CTT TC-3^0); rv-HsMICU1 (5^0-GGG CTC GAG TTA CTG TTT GGG TAA AGC GAA G-3^0), and cloned into the yeast expression plasmids p423GPD (Dd-MCU, Af-MCU, Nc-MCU, Hs-MCU, Hs-MCU$_{D261A}$, Hs-MCU$_{E264A}$), p414GPD (Hs-MICU1, Hs-MICU1$_{mEF}$) and p425GPD (Hs-EMRE) as in (Mumberg et al., 1995).

Isolation of Crude Mitochondria from HeLa Cells

Crude mitochondria were prepared from cultured HeLa cells as previously described (Wettmarshausen and Perocchi, 2017). Briefly, HeLa cells were grown to confluency in 245 3 245 3 20 mm cell culture plates. Culture medium was removed and cells were rinsed

with 30 mL PBS, scraped down and resuspended in 5 mL PBS. After 5 minutes of centrifugation at 600 x g, 4ºC, the cell pellet was resuspended in ~15 mL of ice cold isolation buffer (IB; 220 mM mannitol, 70 mM sucrose, 5 mM HEPES-KOH pH 7.4, 1 mM EGTA-KOH pH 7.4), with one protease inhibitor tablet added per 50 mL of buffer. Cell suspension was immediately subjected to nitrogen cavitation at 600 psi for 10 minutes at 4ºC. Nuclei and intact cells were pelleted by centrifugation at 600 x g for 10 minutes at 4ºC. Supernatants were transferred into new tubes and centrifuged at 8000 x g for 10 minutes at 4ºC. The resulting pellet containing crude mitochondria was resuspended in 50-200 mIB for further analyses.

Topology Analysis of Mitochondrial Proteins

Alkaline carbonate extraction from crude mitochondria was performed as described previously (Baughman et al., 2011). Briefly, 100 mg of mitochondria were pelleted by centrifugation at 8000 x g for 10 minutes at 4º C. Pellets were resuspended in 0.1 M Na_2CO_3 at pH 10, pH 11 or pH 12 and incubated for 30 minutes on ice. Samples were then centrifuged at 45,000 x g for 10 minutes at 4ºC. Pellets were resuspended in 100 ml of 2 x Laemmli buffer, boiled at 98ºC for 5 minutes and stored at -80ºC until further use (pellet sample). Supernatants were mixed with 40 ml of 100% TCA and incubated overnight at -20ºC. On the following day, supernatants were centrifuged at 16,000 x g for 25 min at 4ºC. Pellets were then washed twice with cold acetone, air-dried for 20-30 minutes at room temperature, resuspended in 100 ml of 2 x Laemmli buffer and heated up to 98ºC for 5 minutes (supernatant sample). 25 ml of supernatant and pellet samples were analyzed by SDS-PAGE. TIM23 and HSP60, integral inner membrane and soluble matrix targeted proteins, respectively, are used as controls.

Proteinase K protection assay was performed by incubating 30 mg of mitochondria in 30 ml of isolation buffer with increasing concentrations of digitonin or 1% Triton X-100 in the presence of 100 mg/ml proteinase K to sequentially permeabilize outer and inner membranes. The reaction was carried out at room temperature for 15 minutes and was stopped by the addition of 5 mM PMSF, followed by incubation on ice for 10 minutes. Samples were mixed with 10 ml of 4 X Laemmli buffer containing 10% 2-mercaptoethanol and boiled for 5 minutes at 98ºC. Samples were then loaded at 10 ml per lane and were analyzed by SDS-PAGE. TOM20 and cyclophilin D (Cyp D), an integral outer membrane and a soluble matrix protein, respectively, were used as controls.

Blue Native – PAGE Analysis

Samples for BN-PAGE analysis were prepared by incubating 10 mg of crude mitochondria on ice for 10 minutes in 9.5 ml of Invitrogen 1X NativePAGE™ sample buffer containing 1% digitonin. Samples were centrifuged at 20,000 x g for 30 minutes at 4ºC. Supernatants were transferred into new tubes and 0.5 ml of NativePAGE™ 5% G-250 Sample Additive was added to a final concentration of 0.25%. Anode and cathode buffers for gel electrophoresis were prepared according to the manufacturer's protocol for the Invitrogen NativePAGE™ Novex Bis-Tris Gel System and were cooled to 4ºC before use. Electrophoresis was performed at 4ºC and gels were performed at 40 V for 1 hour. The voltage was then increased to 60 V for 30 minutes and subsequently to 100 V until the dye front had traveled through 1/3 of the gel, at which point the Dark Blue Cathode Buffer was replaced with Light Blue Cathode Buffer. Electrophoresis was continued at 100 V for 30 minutes and then increased to 150 V until completed. Proteins were transferred onto PVDF membranes by electrophoretic wet transfer overnight at 40 V, 4ºC. After transfer, proteins were fixed on the membrane by incubating in 8% acetic acid for 15 minutes at room temperature on a shaker. Immunoblot analyses were performed with the following antibodies: anti-MCU (Sigma Aldrich, HPA01648), anti-V5 (Life Technologies, R96025), and anti-ATP5A (Abcam, MS507), anti-TIM23 (BD Bioscience, 611222), and anti-HSP60 (R&D System, MAB1800), anti-TOM20 (Abcam, ab56783), and anti-Cyclophilin D (Abcam, ab110324).

Measurements of Mitochondrial Calcium Uptake in Intact HeLa Cells

Mitochondrial Ca^{2+} uptake was measured in mt-AEQ HeLa cells as previously described (Arduino et al., 2017). Briefly, HeLa cells stably expressing mt-AEQ were seeded in white 96-well plates at 25,000 cells/well in growth medium. After 24 hours, mt-AEQ was reconstituted with 2 mM native coelenterazine (Abcam, ab145165) for 2 hours at 37ºC. Mt-AEQ-based measurements of Ca^{2+}-dependent light kinetics were performed upon 100 mM histamine stimulation. Light emission was measured in a luminescence counter (MicroBeta2 LumiJET Microplate Counter, PerkinElmer) at 469 nm every 0.1 s. At the end of each experiment, cells were lysed with a solution containing 0.5% Triton X-100 and 10 mM $CaCl_2$ to release all the residual aequorin counts.

Measurements of Mitochondrial Calcium Uptake in Digitonin-Permeabilized HeLa Cells

HeLa cells stably expressing mt-AEQ were harvested at a density of 500,000 cells/mL in growth medium supplemented with 20 mM HEPES (pH 7.4/NaOH) and the photoprotein aequorin was reconstituted by incubation with 3 mM native coelenterazine for 2.5 hours at room temperature. Cells were then centrifuged at 300 *g* for 3 minutes and the pellet was re-suspended in an extracellular-like buffer containing 145 mM NaCl, 5 mM KCl, 1 mM $MgCl_2$, 10 mM glucose, 10 mM HEPES and 500 mM EGTA (pH 7.4/NaOH), supplemented with 200 nM thapsigargin. After 20 minutes at room temperature, cells were collected by centrifugation at 300 *g* for 3 minutes and the pellet was resuspended in an intracellular-like buffer containing 140 mM KCl, 1 mM KH_2PO_4/K_2HPO_4, 1 mM $MgCl_2$, 20 mM HEPES, 100 mM EGTA (pH 7.2/KOH), supplemented with 1 mM Na^+-pyruvate, 1 mM ATP/$MgCl_2$ and 2 mM Na^+-succinate. Cells were per- meabilized with 60 mM digitonin for 5 minutes, collected by centrifugation at 300 *g* for 3 minutes and resuspended in intracellular-like buffer at a density of ~900 cells/mL. Then, 90 mL of cell suspension was dispensed into a white 96-well plate (PerkinElmer). Cells were incubated for 5 minutes at room temperature and Ca^{2+}-stimulated light signal was recorded at 469 nm every 0.1 s using a lumines- cence counter (MicroBeta2 LumiJET Microplate Counter, PerkinElmer). Ru360 (10 mM) was used as a positive control.

Subcellular Fractionation of Yeast Cells

To test the expression and subcellular localization of heterologous proteins, yeast cells were grown at 30ºC in a selective lactate medium (S-LAC) containing 8.5 g/L yeast nitrogen base, 25 g/L ammonium sulfate, 2% (v/v) lactic acid (90%), 0.1% glucose (pH 5.5/KOH), supplemented with the respective selection markers. At an OD ~0.8, cells were harvested at 1000 g for 5 minutes at room temperature. The cell pellet was re-suspended in SHK buffer (0.6 M sorbitol, 20 mM HEPES/KOH pH 7.2, 80 mM KCl, and 1 mM PMSF) and vortexed five times for 30 s with glass beads (425-600 mm diameter), with a 30 s cooling interval in between. This sample was then centrifuged at 1000 *g* for 5 minutes at 4ºC and the supernatant was further centrifuged at 20,000 *g* for 10 minutes at 4ºC to obtain the mitochondrial fraction (pellet). The resulting supernatant (cytosolic fraction) was precipitated with trichloroacetic acid at -20°C for 1 hour, washed once with cold acetone and centrifuged at 20,000 g for 10 minutes at 4ºC to obtain the cytosolic fraction (pellet). Both cytosolic and mitochondrial fractions were directly resuspended in Laemmli buffer and separated under reducing conditions in 12 or 14% SDS-PAGE gels. Immunoblotting was performed according to the standard procedures using the following antibodies: anti-MCU (Sigma-Aldrich, HPA016480); anti-EMRE (Santa Cruz Biotechnology, sc- 86337); anti-MICU1 (Sigma Aldrich, HPA037480); anti-YME1 (Thermofisher/Novex, 459250); anti-AEQ (Merck/Millipore, MAB4405).

Measurements of Calcium Transients in Intact Yeast Cells

In vivo analyses of cytosolic and mitochondrial Ca^{2+} dynamics in yeast cells were performed as described by (Groppi et al., 2011) with some modifications. Yeast were grown in S-LAC at 30ºC overnight to an OD ~0.8, (~24x10^6 cells/mL), and cells were harvested by centrifugation at 3,500 *g* for 5 minutes at room temperature. Yeast cell pellet was washed three times with milliQ water and resuspended in a nutrient-free buffer (NFB; 100 mM Tris, pH 6.5) at a density of 1x10^8 cells/mL. Cells were incubated for 1.5 hours at room temperature (starvation), collected by centrifugation at 3,500 rpm for 5 minutes and concentrated in the same buffer to a density of 25x10^8 cells/mL. The photoprotein aequorin was then reconstituted with 50 mM native coelenterazine in the dark for 30 minutes at room temperature. Excess of coelenterazine was washed thrice with NFB and the cell pellet was resuspended to a final density of 5x10^8 cells/mL. Then, a suspension of 0.5x10^8 cells/well were plated into a white 96-well plate and Ca^{2+}-dependent aequorin light signal was recorded upon stimulation with containing 1 mM $CaCl_2$ and 100 mM glucose, at 0.5 s interval in a MicroBeta2 LumiJET Microplate Counter. At the end of each experiment, a lysis solution containing 5 mM digitonin, 450 mM EGTA, 100 mM Tris (pH 6.5/KOH) was added at a ratio of 1:5 for 5 minutes at 37ºC and light response was measured upon the addition of $CaCl_2$ to a final concentration of 140 mM to release all the residual aequorin counts.

Measurements of Mitochondrial Calcium Uptake in Isolated Yeast Mitochondria

Crude mitochondria were isolated from yeast strains as described previously (Arduino et al., 2017). Mitochondria were then resuspended in a buffer containing 0.6 M sorbitol, 20 mM HEPES, 2 mM $MgCl_2$, 10 mM KH_2PO_4, 3 mM glutamate, 3 mM malate, 3 mM succinate, 50 mM EDTA, and 0.1 mM Calcium Green-5N (Life technologies, C3737) and seeded into a black 96-well plate at 150 mg/100 mL. Calcium Green-5N fluorescence (excitation 506 nm, emission 531 nm) was monitored every 2 s at room temperature using a CLARIOstar microplate reader (BMG Labtech Perkin-Elmer Envision) after injection of $CaCl_2$ (100 mM final concentration). The MCU inhibitor Ru360 (10 mM) was used as a positive control.

Yeast Growth Measurement

For growth assays in liquid media, overnight yeast cultures grown at 30ºC in S-LAC were diluted to an OD of 0.1 (3x10^6 cells/mL) and then 0.3x10^6 cells/well were seeded in a black, gas-permeable Lumox 96-well plate. Absorbance measurements of yeast suspension light scattering were performed at I_{max} = 600 nm and intervals of 340 s using a CLARIOstar microplate reader (BMG Labtech) for 48-72 hours with shaking at 30ºC, 37ºC, or in the presence of sterile solutions of sodium chloride (NaCl, 0.1-1 M), calcium chloride ($CaCl_2$, 10-100 mM), copper (II) chloride ($CuCl_2$, 10-30 mM), iron (II) chloride ($FeCl_2$, 10-40 mM), Mn^{2+} (II) chloride ($MnCl_2$, 1-5 mM), strontium (II) chloride ($SrCl_2$, 10-50 mM), zinc (II) chloride ($ZnCl_2$, 10-50 mM), or antifungal drugs (miconazole, 10-100 ng/ml; amoidarone, 5-20 mM). The average time taken by the yeast culture to double in the log-growth phase (doubling time) was calculated using the following equation:

$$Doubling\ time = \frac{\delta Tf - Ti\flat * \log\delta 2\flat}{\log\delta Nf\flat - \log\delta Ni\flat}$$

where T is the time between the log-growth phase from Ti to Tf and N the number of cells measured as an optical density at I_{max} = 600 nm at the time point Ti (Ni) and Tf (Nf).

For spot assays, yeast cultures grown at 30ºC in S-LAC were harvested at an OD of 1.0 (30x10^6 cells/mL) at 3200 g for 5 minutes at room temperature. The cell pellet was re-suspended in sterile water to 30x10^6 cells/mL and diluted in a 10-fold series. Aliquots of 5 mL from each dilution were spotted onto a S-LAC plate with or without the respective treatment ($CaCl_2$, 100-600 mM; $SrCl_2$, 50-500 mM). Plates were then incubated at 30ºC for 72 h.

Cell Viability Analysis

A colorimetric 3-(4,5-dimethylthiazol-2-yl)-2,5-diphenyltetrazolium bromide (MTT) metabolic activity assay was used to determine cell viability. HEK293 cells were seeded at 50,000 cells/well in 1 mL of DMEM with high glucose and 10% FBS in a transparent

OPEN ACCESS
CellPress

24-well plate at 37°C and 5% CO_2. After 24 hours, cells were incubated in the presence or absence of metal ions ($FeCl_2$, 0.1-1 mM; $MnCl_2$, 5-50 mM) or antioxidants (N-acetyl-L-cysteine, NAC, 1-10 mM; L-glutathione, GSH, 1-20 mM; antioxidant supplement, 1-20X concentration according to manufacturer's protocol; Trolox, 0.5-5 mM; Idebenone, 0.1 mM), together with 10-50 mM of $MnCl_2$, for further 48 hours. Afterward, 500 mL of medium was replaced, 50 mL of MTT solution (Sigma Aldrich, M5655; 5 mg/ml in PBS) was added, and cells were incubated for 3 hours at 37°C. Finally, cells were lysed with 500 mL of solubilization solution (1% SDS and 0.1 M HCl in isopropanol) for 15 minutes at 37°C and absorbance at l_{max} 570 nm was monitored in a CLARIOstar microplate reader (BMG Labtech).

Mitochondrial Mn^{2+} Transport Measurement in Human Cells

Measurements of Mn^{2+} uptake in mitochondria were performed as previously described (Csordás and Hajnóczky, 2003). Briefly, cells were first loaded with Fura2FF/AM (4 mM for 60 min) and then rinsed with a Ca^{2+}-free extracellular buffer containing 100 mM EGTA. Permeabilization was carried out in 1 mL ICM (120 mM KCl, 10 mM NaCl, 1 mM KH_2PO_4, 20 mM Tris-HEPES, 2 mM MgATP, and 1 mg/ml each of antipain, leupeptin and pepstatin at pH 7.2) supplemented with saponin (20 mg/ml) and 20 mM EGTA/Tris (pH 7.4) in the incubation chamber for 5 min (35°C). Subsequently, fresh ICM supplemented with succinate (2 mM) and CGP (20 mM) to energize mitochondria and to inhibit mitochondrial Ca^{2+} efflux, respectively. Fluorescence imaging of Fura2FF-quenching by Mn^{2+} was carried out using a multiwavelength beamsplitter/emission filter combination and a high quantum-efficiency cooled CCD camera. Fura2FF was excited at 360 nm (Mn^{2+} quench). Image analysis was performed using custom-made software (Spectralyzer). Genetic rescue of MICU1-KO HEK293 cells was performed with either WT MICU1 or pcDNA 48 hr before imaging.

ROS Measurement

HEK293 cells were loaded with 10 mM of 5-(and-6)-chloromethyl-2', 7'-dichlorodihydrofluorescein diacetate (CM-H_2DCFDA) in Krebs buffer (140 mM NaCl, 5 mM KCl, 1 mM $MgCl_2$, 5.6 mM D-glucose, 20 mM HEPES, 1.5 mM $CaCl_2$, 1 mM NaH_2PO_4, pH 7.4) for 30 minutes at 37°C. Cells were washed once with PBS, re-suspended in DMEM (without phenol red, REF, source ID), supplemented with 5 mM glucose, 1 mM pyruvate, 2 mM L-glutamine and 10% FBS, seeded at 20,000 cells/well in a black 96-well plate, and treated with 25 mM of $MnCl_2$ for 48 hours. H_2O_2 (50-100 mM) was used as a positive control. Fluorescence was measured at an excitation and emission wavelength of 485 nm and 520 nm respectively. Data was normalized to cell number quantified using a CyQUANT Cell Proliferation Assay Kit (Thermo Fisher Scientific).

QUANTIFICATION AND STATISTICAL ANALYSIS

Quantification of Calcium Transients

Quantification of mt-Ca_{2+} concentration was performed using a MATLAB software as previously described in (Arduino et al., 2017). The dynamics of mt-Ca^{2+}-dependent luminescence signal was smoothed by the cubic spline function:

$$p \sum_{1}^{n} (y_i - f(x_i))^2 + (1 - p) \int \left(\frac{d^2 f}{dx^2}\right)^2 dx$$

Where, p is a smoothing parameter, controlling the tradeoff between fidelity to the data and roughness of the function estimate, f is the estimated cubic spline function to minimize the above function, and x_i and y_i are the dynamical data points. Here, p is set at 0.5. Parametrization of the Ca^{2+}-dependent luminescence kinetics was performed in order to determine the maximal amplitude of the luminescence signal (peak) and the left slope of the bell-shaped kinetic trace. Aequorin-based luminescence signal calibration into mt-Ca^{2+} concentration was performed using the algorithm reported in (Bonora et al., 2013) for wild-type aequorin and native coelenterazine, with the following formula:

$$Ca^{2+} = \frac{\left(\frac{L}{L_{max}}\right)^{\frac{1}{n}} + \left(\frac{L}{L_{max}}\right)^{\frac{1}{n}} K_{TR} - 1}{K_R - \left(\frac{L}{L_{max}}\right)^{\frac{1}{n}} K_R}$$

Where $l = 1$, $K_R = 7.23 \times 10^6$, $K_{TR} = 120$ and $n = 2.99$ are the calibration values used for WT aequorin and native coelenterazine.

Data Analysis

Data are represented as mean ± SEM and the statistical analysis of each experiment is described in the figure legends including the statistical tests used and the exact value of n. Here n represents the number of biological replicates. For each biological replicate experiment at least 3 technical replicates were used for quantification and data analysis. Normal distribution was tested by Shapiro-Wilk normality test. Differences between two datasets were evaluated by two-tailed unpaired Student's t test. Statistical tests between multiple datasets and conditions were carried out using one-way analysis of variance (ANOVA) followed by Tukey's or Dunnett's Multiple Comparison tests. Statistical analyses were performed using GraphPad Prism (GraphPad Software, version 7).

Cell Reports, Volume 25

Supplemental Information

MICU1 Confers Protection from MCU-Dependent Manganese Toxicity

Jennifer Wettmarshausen, Valerie Goh, Kai-Ting Huang, Daniela M. Arduino, Utkarsh Tripathi, Anja Leimpek, Yiming Cheng, Alexandros A. Pittis, Toni Gabaldón, Dejana Mokranjac, György Hajnóczky, and Fabiana Perocchi

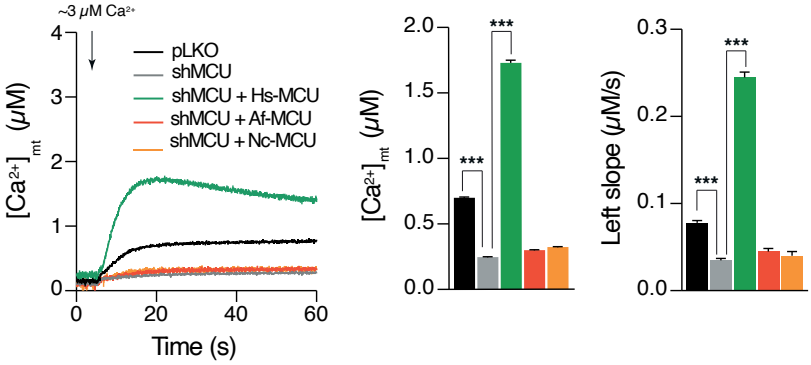

Figure S1. Mt-Ca^{2+} uptake in permeabilized shMCU HeLa cells expressing MCU orthologs from *N. crassa* and *A. fumigatus*. Related to Figure 1. Representative traces and quantification of mt-Ca^{2+} transients in digitonin-permeabilized control (pLKO) and shMCU HeLa cells expressing human and fungal MCU constructs. All data represent mean ± SEM; n=6-12; ***p <0.001, one-way ANOVA with Tukey's Multiple Comparison Test.

Figure S1 Wettmarshausen et *al.*

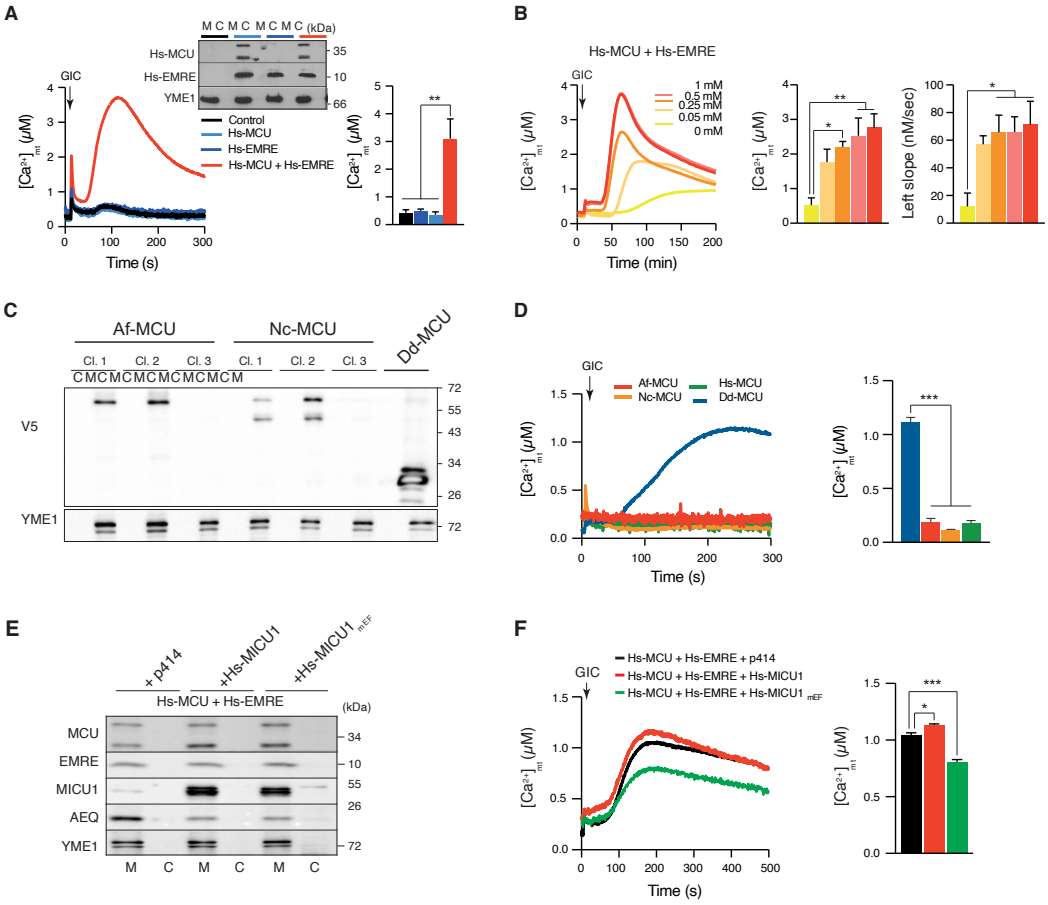

Figure S2. Reconstitution of mt-Ca^{2+} uptake in yeast cells. Related to Figure 2. (**A**) Representative traces and quantification of mt-Ca^{2+} transients in yeast cells expressing WT mtAEQ with either empty vector (control), Hs-EMRE, Hs-MCU, or both upon GIC stimulation in presence of 1 mM $CaCl_2$ (n=3); ***p < 0.001, one-way ANOVA with Tukey's Multiple Comparisons test. Inset, immunoblot analysis of cytosolic (C) and mitochondrial (M) fractions. (**B**) Mt-Ca^{2+} transients in Hs-MCU and Hs-EMRE reconstituted yeast cells upon GIC stimulation in presence of different extracellular $CaCl_2$ concentrations (n=3); *p < 0.05, **p <0.01, one-way ANOVA with Dunnett's Multiple Comparisons Test. (**C**) Analysis of cytosolic (C) and mitochondrial (M) fractions from yeast clones (Cl. 1-3) expressing MCU orthologs from *N. crassa* (Nc-MCU), *A. fumigatus* (Af-MCU) or *D. discoideum* (Dd-MCU) fused to a C-terminal V5-tag. (**D**) Representative traces and quantification of mt-Ca^{2+} transients in yeast cells expressing WT mtAEQ with MCU orthologs from *N. crassa* (Cl. 2), *A. fumigatus* (Cl. 2), or *D. discoideum* upon GIC stimulation in presence of 1 mM $CaCl_2$ (n=4); ***p < 0.001, one-way ANOVA with Tukey's Multiple Comparisons Test. (**E**) Immunoblot analysis of cytosolic (C) and mitochondrial (M) fractions isolated from yeast strains expressing Hs-MCU, Hs-EMRE and either an empty vector (p414), human WT MICU1 (Hs-MICU1), or EF-hands mutant MICU1 (Hs-MICU1$_{mEF}$). (**F**) Mt-Ca^{2+} transients in the yeast strains described in (E) upon GIC stimulation in presence of 1 mM CaCl (n=3); *p < 0.05, ***p < 0.001, one-way ANOVA with Dunnett's Multiple Comparisons Test.

Figure S2 Wettmarshausen *et al.*

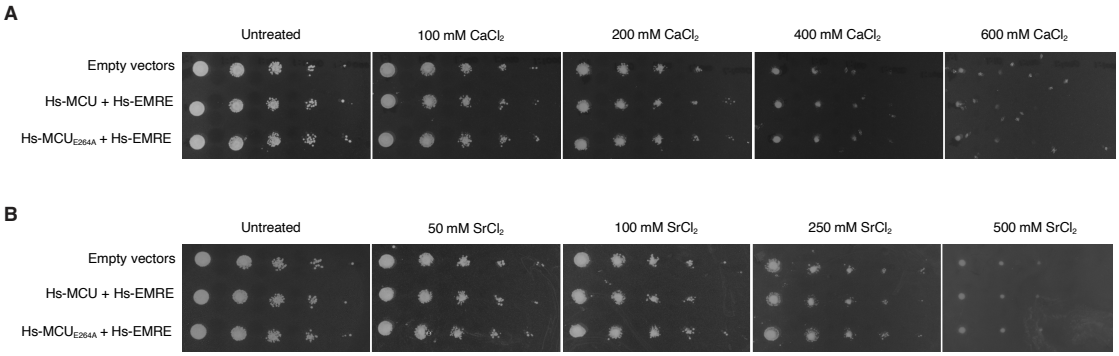

Figure S3. Yeast tolerance to calcium and strontium stress. Related to Figure 3. Growth assay of ten-fold serial dilutions of yeast strains expressing empty vectors (p423 and p425) or Hs-EMRE with WT or mutated Hs-MCU at 30°C on S-LAC plates containing increasing concentrations of $CaCl_2$ (**A**) and $SrCl_2$ (**B**).

Figure S3 Wettmarshausen et *al*.

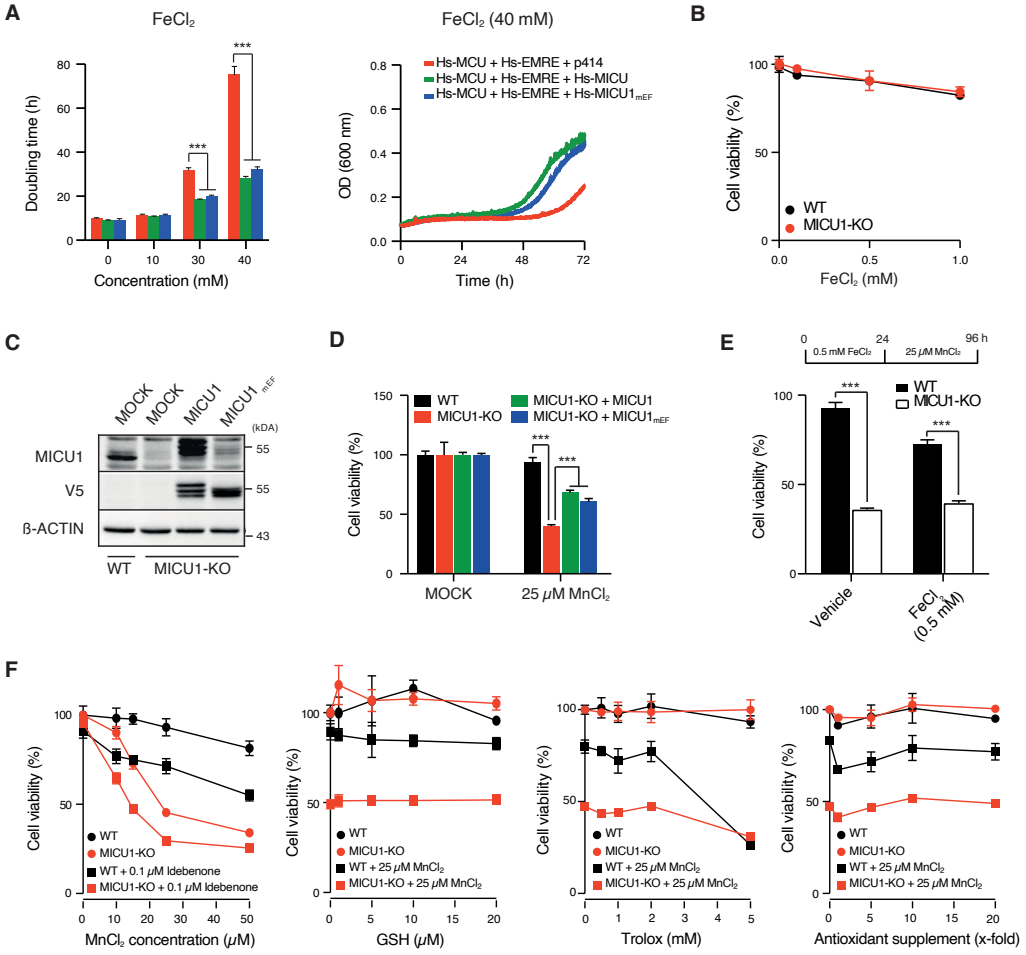

Figure S4. Role of MICU1 in manganese-induced cytotoxicity. Related to Figure 4. (**A**) Quantification of growth rate and average growth curve of yeast strains expressing Hs-MCU, Hs-EMRE and either empty vector (p414), Hs-MICU1 or Hs-MICU1$_{mEF}$ and treated with $FeCl_2$; n=4; ***p < 0.001, one-way ANOVA with Tukey's Multiple Comparisons Test. (**B**) Cell viability assays of wild-type (WT) and MICU1 knockout (MICU1-KO) HEK-293 cells treated for 48 hours with $FeCl_2$; n=4. (**C**) Immunoblot analysis of whole cell lysates from WT and MICU1-KO cells that were either MOCK-treated or rescued by lentiviral expression of Hs-MICU1 or Hs-MICU1$_{mEF}$. (**D**) Cell viability assays of uninfected WT and MICU1-KO cells that were either MOCK-treated or rescued by lentiviral expression of Hs-MICU1 or Hs-MICU1$_{mEF}$ upon $MnCl_2$ treatment for 48 hours; n=4; ***p < 0.001, one-way ANOVA with Tukey's Multiple Comparisons Test. (**E**) Cell viability assays of WT and MICU1-KO HEK-293 cells pre-treated with either $FeCl_2$ or vehicle (water) for 24 hours followed by 48 hours of incubation with $MnCl_2$ (n=3). (**F**) Cell viability assays of WT and MICU1-KO HEK-293 cells treated for 48 hours with $MnCl_2$ in the presence of idebenone, L-glutathione (GSH), trolox, or an antioxidant supplement from Sigma, (n=3). Data are reported as the percentage of viable cells in untreated samples. All data represent mean ± SEM.

Figure S4 Wettmarshausen *et al.*

3 Discussion

Calcium acts as one of the most versatile signalling molecules and is involved in a diversity of physiological function. By shaping cellular Ca^{2+} currents, mitochondria serve as important modulator of Ca^{2+} signalling. Despite mitochondria are present in almost all eukaryotic cells, mt-Ca^{2+} uptake activity is not conserved in the yeast *Saccharomyces cerevisiae*.

The discovery of Ca^{2+} uptake by isolated mammalian mitochondria as a rapid, electrogenic and relatively selective process driven by the negative membrane potential across the IMM has been already made in the 1960s [20, 21]. It took additional 50 years and a smart combination of comparative physiology, organelle proteomics and focused RNAi strategy to identify the first subunits of the MCU macro-molecular complex [31, 32, 37].

This identification of the molecular identity of the mitochondrial Ca^{2+} machinery enabled the possibility to characterize the function of its subunits as well as the development of systematic drug screens to identify novel modulators of MCUC.

The yeast *S. cerevisiae*, which lacks MCU, provides an effective testbed for dissecting human mitochondrial Ca^{2+} signaling : 1) It offers advantages of both eukaryotic protein expression mechanism and bacteria-like growth and handling, which allows reconstitution of mt-Ca^{2+} transients by expressing human MCU and EMRE with or without its regulatory subunits. Yeast cultures can be easily expanded allowing efficient isolation of large quantities of intact and functional mitochondria. Expression of the mitochondrial-targeted, Ca^{2+} sensitive luminescence-based sensor aequorin enables sensitive measurements of mitochondrial matrix Ca^{2+} concentration, in intact as well as in isolated mitochondria. 2) *S. cerevisiae* mitochondria exhibit a simplified OXPHOS system lacking RCCI but including a D-lactate:cytochrome *c* oxidoreductase (DLD), which is sensitive to D-lactate and enables the direct transfer of electrons to cytochrome *c* oxidase (RCCIV). In presence of D-lactate as respiratory substrate, yeast mitochondria employ a bioenergetic shunt pathway that bypasses the majority of the ETC complexes and NADH generating pathways while still producing sufficient energy to build up mt-$\Delta\Psi$ [14, 89]. 3) The selective expression of human MCUC components in a null genetic background such as the yeast *S. cerevisiae* allows mapping direct functional and regulatory interconnections between its subunits. In contrast, in mammalian systems the inter-functional interaction between MICU1 and MCU has been obscured by the contribution of other MCUC subunits, i.e. MICU2 [39, 48, 52]. Finally, heterologous expression of MCU and EMRE in *S. cerevisiae* was used to demonstrate the essential role of EMRE in the mammalian MCUC [56].

The first publication cited in this thesis uses the above outlined advantages of reconstituted yeast mitochondria to develop a powerful semi-high-throughput drug screening strategy to identify specific and direct modulators of MCU activity, by minimizing false discovery rate due to confounding effects of drug-mediated inhibition of mt-$\Delta\Psi$ and bioenergetics, ETC and signalling events upstream of mitochondria. In a screen of approximately 700 FDA-approved drugs, mitoxantrone was identified as cell-permeable, specific inhibitor of MCU [88].

In the second publication, yeast was used to analyse potential fitness advantage conferred by the widespread evolutionary co-occurrence of MCU and MICU1 across 247 eukaryotes. A yeast-based heterologous system was developed by expressing pore forming subunits MCU and EMRE with or without its regulator MICU1. A newly developed assay triggering cytosolic Ca^{2+} currents upon a physiological stimulus showed a successful reconstitution of mt-Ca^{2+} influx also *in vivo* in alignment with previously published *in vitro* results [56, 87, 88]. Similar to its role in mammalian cells, co-expression of MICU1 augmented mitochondrial calcium uptake in yeast *in vivo*. The possibility to perform systematic growth assays of yeast were further exploited to screen for synthetic interactions that would provide a fitness advantage when MCU and MICU1 where part of the same complex. Mn^{2+} was found to be lethal to yeast lacking MICU1 but expressing MCU and EMRE. Permeability of the MCU uniporter to Mn^{2+} has been reported previously [90-93] and an independent study demonstrated the high affinity binding of Mn^{2+} to the DXXE domain of MCU [79].

Contrary, heterologous co-expression of MICU1, independent of functional EF-hand -domains, protect yeast cells with reconstituted mt-Ca^{2+} update from Mn^{2+} toxicity. This indicates that MICU1 inhibits Mn^{2+} influx, acting as a selectivity lid, only allowing the entry of Ca^{2+} and Mn^{2+} ions through the uniporter upon binding of Ca^{2+} to its EF-hands domains. This occurs independently of the other gating subunits MICU2 and MICU3. These findings were confirmed in human HEK293 cells lacking MICU1, which showed a decreased cell viability in presence of high level of Mn^{2+}. The latter could be rescued by re-expressing MICU1 independently of functional EF-hand domains. Thus, unlike Ca^{2+}, the binding of Mn^{2+} to EF-hands [94, 95] would be insufficient to trigger a conformation change of MICU1 required for the opening of MCU channel, a hypothesis that was recently validated [96]. The results obtained in our study could be of relevance for patients with MICU1 loss-of-function mutations [70, 71, 97] whereby disease phenotypes were mainly attributed to high basal mt-Ca^{2+} concentrations. In light of the results presented in this thesis, these patient could suffer from altered mitochondrial Mn^{2+} homeostasis, which would have an additive effect: Mn^{2+} would further increase mt-Ca^{2+} levels by inhibiting Na^{+}-dependent and Na^{+}-independent mt-Ca^{2+} efflux routes [98] and further increase oxidative stress and cell death. In alignment with this hypothesis, treatment with antioxidant NAC was able to fully prevent Mn^{2+}-induced cell death in MICU1 knockout HEK293 cells.

Overall, purification techniques of intact and respiratory-competent mitochondrial organelles allowed downstream analyses like calcium and bioenergetics measurements, and biochemical analysis, e.g. protein topology and fraction analysis of mitochondrial proteins, native-page macromolecular protein complex analysis. Isolation protocols for mitochondrial from cultured cells and mouse tissues have been successfully established in the lab and published in Wettmarshausen and Perocchi (2017) [99] and Wettmarshausen and Perocchi 2019 [100].

In summary, both publications of this thesis demonstrate the power of combining comparative genomics analysis with synthetic biology approaches to selectively reconstitute components and function of the mammalian MCUC and to screen for direct chemical modulators.

4 Appendix

4.1 Index of abbreviations

Abbreviation	Full written
ADP	Adenosine diphosphate
ATP	Adenosine triphosphate
BN-PAGE	Blue native page
Ca^{2+}	Calcium
CCCP	Carbonylcyanid-*m*-chlorphenylhydrazon
CCDC90b	coiled-coiled domain containing protein 90b
Conc.	concentration
CypD	Cyclophilin D
DMSO	Dimethylsulphoxid
DNA	Deoxyribonucleic acid
E. coli	*Escherichia coli*
EDTA	Ethylenediaminetetraacetic acid
EGTA	ethylene glycol-bis(β-aminoethyl ether)-N,N,N',N'-tetraacetic acid
EMRE	essential MCU regulator
ER	Endoplasmatic reticulum
FBS	Fetal Bovine Serum
GOI	Gene of interest
GSH	L-glutathione
IMM	Inner Mitochondrial Membrane
KO	Knockout
LB Medium	Luria Bertani medium
LC-MS/MS	Liquid-Chromatography-Massenspectometry/ Massenspectometry)
MCU	mitochondrial calcium uniporter
MCUC	Mitochondrial Calcium Unitporter Complex
$MgCl_2$	Magnesium chloride
$MgSO_4$	Magnesium sufate
MICU1	mitochondrial calcium uptake 1
MICU2	mitochondrial calcium uptake 2
MICU3	mitochondrial calcium uptake 3
Min / mins	Minute / minutes
Mn^{2+}	Manganese
Mt-AEQ	Mitochondrial aequorin
Mt-Ca^{2+}	Mitochondrial calcium
Na^{+}	Sodium
NAC	N-acetyl-L-cysteine
NaCl	Sodium chloride
NADH	Adenine dinucleotide
NaOH	Sodium hydroxide
OCR	Oxygen consumption rate
OXPHOS	Oxidative phosphorylation
PBS	Phosphate buffered saline
PCR	Polymerase chain reaction
PEG	polyethylene glycol
PI	Proteinase inhibitor
PK	Proteinase K
RIPA	Radioimmunoprecipitation assay
RNA	Ribonucleic Acid
ROS	Reactive oxygen species
rpm	Rounds per minute
RuRed	Ruthenium red
SDS-PAGE	sodium dodecyl sulfate polyacrylamide gel electrophoresi

Sec / secs	Second / seconds
WT	Wild-type

4.2 Index of figures

Figure 1: Mitochondrial Calcium Transporters 12

Figure 2: Pathophysiology of imbalanced mt-Ca^{2+} homeostasis 15

4.3 References

1. Dyall, S.D., M.T. Brown, and P.J. Johnson, *Ancient invasions: from endosymbionts to organelles.* Science, 2004. **304**(5668): p. 253-7.
2. Gould, S.B., R.F. Waller, and G.I. McFadden, *Plastid evolution.* Annu Rev Plant Biol, 2008. **59**: p. 491-517.
3. Kleine, T., U.G. Maier, and D. Leister, *DNA transfer from organelles to the nucleus: the idiosyncratic genetics of endosymbiosis.* Annu Rev Plant Biol, 2009. **60**: p. 115-38.
4. Colombini, M., *A candidate for the permeability pathway of the outer mitochondrial membrane.* Nature, 1979. **279**: p. 643.
5. Siekvitz, P., *Powerhouse of the cell.* Sci. Am. 197, 131–144. doi: 10.1038/scientificamerican0757-131, 1957.
6. Nicholls, D.G. and S.J. Ferguson, *5 - Respiratory Chains*, in *Bioenergetics (Fourth Edition)*. 2013, Academic Press: Boston. p. 91-157.
7. Hirst, J., et al., *The nuclear encoded subunits of complex I from bovine heart mitochondria.* Biochimica et Biophysica Acta (BBA) - Bioenergetics, 2003. **1604**(3): p. 135-150.
8. Carroll, J., et al., *Bovine complex I is a complex of 45 different subunits.* J Biol Chem, 2006. **281**(43): p. 32724-7.
9. Grivennikova, V.G., A.N. Kapustin, and A.D. Vinogradov, *Catalytic activity of NADH-ubiquinone oxidoreductase (complex I) in intact mitochondria. evidence for the slow active/inactive transition.* J Biol Chem, 2001. **276**(12): p. 9038-44.
10. Kovářová, N., et al., *High Molecular Weight Forms of Mammalian Respiratory Chain Complex II.* PLoS ONE, 2013. **8**(8): p. e71869.
11. Anderson, S., et al., *Sequence and organization of the human mitochondrial genome.* Nature, 1981. **290**: p. 457.
12. Ludwig, B., et al., *Cytochrome C oxidase and the regulation of oxidative phosphorylation.* Chembiochem, 2001. **2**(6): p. 392-403.
13. Jonckheere, A.I., J.A.M. Smeitink, and R.J.T. Rodenburg, *Mitochondrial ATP synthase: architecture, function and pathology.* Journal of Inherited Metabolic Disease, 2012. **35**(2): p. 211-225.
14. Pajot, P. and M.L. Claisse, *Utilization by yeast of D-lactate and L-lactate as sources of energy in the presence of antimycin A.* Eur J Biochem, 1974. **49**(1): p. 275-85.
15. Canto, C., K.J. Menzies, and J. Auwerx, *NAD(+) Metabolism and the Control of Energy Homeostasis: A Balancing Act between Mitochondria and the Nucleus.* Cell Metab, 2015. **22**(1): p. 31-53.
16. Frezza, C., *Mitochondrial metabolites: undercover signalling molecules.* Interface Focus, 2017. **7**(2): p. 20160100.
17. Shadel, G.S. and T.L. Horvath, *Mitochondrial ROS signaling in organismal homeostasis.* Cell, 2015. **163**(3): p. 560-9.
18. Couvillion, M.T., et al., *Synchronized mitochondrial and cytosolic translation programs.* Nature, 2016. **533**(7604): p. 499-503.
19. Tait, S.W. and D.R. Green, *Mitochondria and cell death: outer membrane permeabilization and beyond.* Nat Rev Mol Cell Biol, 2010. **11**(9): p. 621-32.
20. Deluca, H.F. and G.W. Engstrom, *Calcium uptake by rat kidney mitochondria.* Proc Natl Acad Sci U S A, 1961. **47**: p. 1744-50.
21. Vasington, F.D. and J.V. Murphy, *Ca ion uptake by rat kidney mitochondria and its dependence on respiration and phosphorylation.* J Biol Chem, 1962. **237**: p. 2670-7.
22. Carafoli, E. and A.L. Lehninger, *A survey of the interaction of calcium ions with mitochondria from different tissues and species.* Biochem J, 1971. **122**(5): p. 681-90.
23. Raffaello, A., et al., *Calcium at the Center of Cell Signaling: Interplay between Endoplasmic Reticulum, Mitochondria, and Lysosomes.* Trends in Biochemical Sciences. **41**(12): p. 1035-1049.
24. Berridge, M.J., P. Lipp, and M.D. Bootman, *The versatility and universality of calcium signalling.* Nat Rev Mol Cell Biol, 2000. **1**(1): p. 11-21.
25. De Stefani, D., et al., *VDAC1 selectively transfers apoptotic Ca2+ signals to mitochondria.* Cell Death And Differentiation, 2011. **19**: p. 267.

26. Rapizzi, E., et al., *Recombinant expression of the voltage-dependent anion channel enhances the transfer of Ca2+ microdomains to mitochondria.* J Cell Biol, 2002. **159**(4): p. 613-24.
27. Brand, M.D., *The stoichiometry of the exchange catalysed by the mitochondrial calcium/sodium antiporter.* Biochem J, 1985. **229**(1): p. 161-6.
28. Carafoli, E., et al., *The release of calcium from heart mitochondria by sodium.* J Mol Cell Cardiol, 1974. **6**(4): p. 361-71.
29. Kirichok, Y., G. Krapivinsky, and D.E. Clapham, *The mitochondrial calcium uniporter is a highly selective ion channel.* Nature, 2004. **427**(6972): p. 360-4.
30. Jiang, D., L. Zhao, and D.E. Clapham, *Genome-wide RNAi screen identifies Letm1 as a mitochondrial Ca2+/H+ antiporter.* Science, 2009. **326**(5949): p. 144-7.
31. Perocchi, F., et al., *MICU1 encodes a mitochondrial EF hand protein required for Ca(2+) uptake.* Nature, 2010. **467**(7313): p. 291-6.
32. Baughman, J.M., et al., *Integrative genomics identifies MCU as an essential component of the mitochondrial calcium uniporter.* Nature, 2011. **476**(7360): p. 341-5.
33. Balcavage, W.X., et al., *Cation movements and respiratory response in yeast mitochondria treated with high Ca2+ concentrations.* Biochim Biophys Acta, 1973. **305**(1): p. 41-51.
34. Docampo, R. and A.E. Vercesi, *Ca2+ transport by coupled Trypanosoma cruzi mitochondria in situ.* J Biol Chem, 1989. **264**(1): p. 108-11.
35. Uribe, S., P. Rangel, and J.P. Pardo, *Interactions of calcium with yeast mitochondria.* Cell Calcium, 1992. **13**(4): p. 211-7.
36. Vercesi, A.E. and R. Docampo, *Ca2+ transport by digitonin-permeabilized Leishmania donovani. Effects of Ca2+, pentamidine and WR-6026 on mitochondrial membrane potential in situ.* Biochem J, 1992. **284 (Pt 2)**: p. 463-7.
37. De Stefani, D., et al., *A forty-kilodalton protein of the inner membrane is the mitochondrial calcium uniporter.* Nature, 2011. **476**(7360): p. 336-40.
38. Sancak, Y., et al., *EMRE is an essential component of the mitochondrial calcium uniporter complex.* Science, 2013. **342**(6164): p. 1379-82.
39. Plovanich, M., et al., *MICU2, a paralog of MICU1, resides within the mitochondrial uniporter complex to regulate calcium handling.* PLoS One, 2013. **8**(2): p. e55785.
40. Raffaello, A., et al., *The mitochondrial calcium uniporter is a multimer that can include a dominant-negative pore-forming subunit.* Embo j, 2013. **32**(17): p. 2362-76.
41. Mallilankaraman, K., et al., *MCUR1 is an essential component of mitochondrial Ca2+ uptake that regulates cellular metabolism.* Nat Cell Biol, 2012. **14**(12): p. 1336-43.
42. Chaudhuri, D., et al., *MCU encodes the pore conducting mitochondrial calcium currents.* Elife, 2013. **2**: p. e00704.
43. Murphy, E., et al., *Unresolved questions from the analysis of mice lacking MCU expression.* Biochemical and Biophysical Research Communications, 2014. **449**(4): p. 384-385.
44. Lee, Y., et al., *Structure and function of the N-terminal domain of the human mitochondrial calcium uniporter.* EMBO Rep, 2015. **16**(10): p. 1318-33.
45. Lee, S.K., et al., *Structural Insights into Mitochondrial Calcium Uniporter Regulation by Divalent Cations.* Cell Chem Biol, 2016.
46. Joiner, M.-l.A., et al., *CaMKII determines mitochondrial stress responses in heart.* Nature, 2012. **491**: p. 269.
47. Dong, Z., et al., *Mitochondrial Ca2+ Uniporter Is a Mitochondrial Luminal Redox Sensor that Augments MCU Channel Activity.* Mol Cell, 2017. **65**(6): p. 1014-1028.e7.
48. Patron, M., et al., *MICU1 and MICU2 finely tune the mitochondrial Ca2+ uniporter by exerting opposite effects on MCU activity.* Mol Cell, 2014. **53**(5): p. 726-37.
49. Kretsinger, R.H., et al., *The structure of a calcium-binding protein from carp muscle.* Cold Spring Harb Symp Quant Biol, 1972. **36**: p. 217-20.
50. Carafoli, E., et al., *Generation, control, and processing of cellular calcium signals.* Crit Rev Biochem Mol Biol, 2001. **36**(2): p. 107-260.
51. Kamer, K.J. and V.K. Mootha, *MICU1 and MICU2 play nonredundant roles in the regulation of the mitochondrial calcium uniporter.* EMBO Rep, 2014. **15**(3): p. 299-307.
52. Kamer, K.J., Z. Grabarek, and V.K. Mootha, *High-affinity cooperative Ca2+ binding by MICU1-MICU2 serves as an on-off switch for the uniporter.* EMBO Rep, 2017. **18**(8): p. 1397-1411.
53. Csordas, G., et al., *MICU1 controls both the threshold and cooperative activation of the mitochondrial Ca(2)(+) uniporter.* Cell Metab, 2013. **17**(6): p. 976-87.
54. Patron, M., et al., *MICU3 is a tissue-specific enhancer of mitochondrial calcium uptake.* Cell Death Differ, 2018.
55. Tsai, M.F., et al., *Dual functions of a small regulatory subunit in the mitochondrial calcium uniporter complex.* Elife, 2016. **5**.
56. Kovacs-Bogdan, E., et al., *Reconstitution of the mitochondrial calcium uniporter in yeast.* Proc Natl Acad Sci U S A, 2014. **111**(24): p. 8985-90.
57. Tsai, C.W., et al., *Proteolytic control of the mitochondrial calcium uniporter complex.* Proc Natl Acad Sci U S A, 2017. **114**(17): p. 4388-4393.

58. Konig, T., et al., *The m-AAA Protease Associated with Neurodegeneration Limits MCU Activity in Mitochondria.* Mol Cell, 2016. **64**(1): p. 148-162.
59. Tomar, D., et al., *MCUR1 Is a Scaffold Factor for the MCU Complex Function and Promotes Mitochondrial Bioenergetics.* Cell Rep, 2016. **15**(8): p. 1673-85.
60. Vais, H., et al., *MCUR1, CCDC90A, Is a Regulator of the Mitochondrial Calcium Uniporter.* Cell Metab, 2015. **22**(4): p. 533-5.
61. Paupe, V., et al., *CCDC90A (MCUR1) is a cytochrome c oxidase assembly factor and not a regulator of the mitochondrial calcium uniporter.* Cell Metab, 2015. **21**(1): p. 109-16.
62. Chaudhuri, D., et al., *Mitochondrial calcium uniporter regulator 1 (MCUR1) regulates the calcium threshold for the mitochondrial permeability transition.* Proc Natl Acad Sci U S A, 2016. **113**(13): p. E1872-80.
63. Pan, X., et al., *The physiological role of mitochondrial calcium revealed by mice lacking the mitochondrial calcium uniporter.* Nat Cell Biol, 2013. **15**(12): p. 1464-72.
64. Luongo, T.S., et al., *The Mitochondrial Calcium Uniporter Matches Energetic Supply with Cardiac Workload during Stress and Modulates Permeability Transition.* Cell Rep, 2015. **12**(1): p. 23-34.
65. Kwong, J.Q., et al., *The Mitochondrial Calcium Uniporter Selectively Matches Metabolic Output to Acute Contractile Stress in the Heart.* Cell Rep, 2015. **12**(1): p. 15-22.
66. Rasmussen, T.P., et al., *Inhibition of MCU forces extramitochondrial adaptations governing physiological and pathological stress responses in heart.* Proceedings of the National Academy of Sciences, 2015: p. 201504705.
67. Wu, Y., et al., *The mitochondrial uniporter controls fight or flight heart rate increases.* Nat Commun, 2015. **6**: p. 6081.
68. Holmström, K.M., et al., *Assessment of cardiac function in mice lacking the mitochondrial calcium uniporter.* Journal of Molecular and Cellular Cardiology, 2015. **85**: p. 178-182.
69. Mammucari, C., et al., *The mitochondrial calcium uniporter controls skeletal muscle trophism in vivo.* Cell Rep, 2015. **10**(8): p. 1269-79.
70. Lewis-Smith, D., et al., *Homozygous deletion in MICU1 presenting with fatigue and lethargy in childhood.* Neurol Genet, 2016. **2**(2): p. e59.
71. Logan, C.V., et al., *Loss-of-function mutations in MICU1 cause a brain and muscle disorder linked to primary alterations in mitochondrial calcium signaling.* Nat Genet, 2014. **46**(2): p. 188-93.
72. Shamseldin, H.E., et al., *A null mutation in MICU2 causes abnormal mitochondrial calcium homeostasis and a severe neurodevelopmental disorder.* Brain, 2017. **140**(11): p. 2806-2813.
73. Giorgi, C., et al., *Mitochondrial calcium homeostasis as potential target for mitochondrial medicine.* Mitochondrion, 2012. **12**(1): p. 77-85.
74. Moore, C.L., *Specific inhibition of mitochondrial Ca++ transport by ruthenium red.* Biochem Biophys Res Commun, 1971. **42**(2): p. 298-305.
75. Nathan, S.R., et al., *Synthetic Methods for the Preparation of a Functional Analogue of Ru360, a Potent Inhibitor of Mitochondrial Calcium Uptake.* Inorg Chem, 2017. **56**(6): p. 3123-3126.
76. Ying, W.L., et al., *Inhibition of mitochondrial calcium ion transport by an oxo-bridged dinuclear ruthenium ammine complex.* Biochemistry, 1991. **30**(20): p. 4949-52.
77. Walters, W.P. and M. Namchuk, *Designing screens: how to make your hits a hit.* Nat Rev Drug Discov, 2003. **2**(4): p. 259-66.
78. Gunter, K.K. and T.E. Gunter, *Transport of calcium by mitochondria.* J Bioenerg Biomembr, 1994. **26**(5): p. 471-85.
79. Cao, C., et al., *Ion and inhibitor binding of the double-ring ion selectivity filter of the mitochondrial calcium uniporter.* Proc Natl Acad Sci U S A, 2017. **114**(14): p. E2846-e2851.
80. Oxenoid, K., et al., *Architecture of the mitochondrial calcium uniporter.* Nature, 2016. **533**(7602): p. 269-73.
81. Murgia, M. and R. Rizzuto, *Molecular diversity and pleiotropic role of the mitochondrial calcium uniporter.* Cell Calcium, 2015. **58**(1): p. 11-7.
82. Vecellio Reane, D., et al., *A MICU1 Splice Variant Confers High Sensitivity to the Mitochondrial Ca2+ Uptake Machinery of Skeletal Muscle.* Mol Cell, 2016. **64**(4): p. 760-773.
83. Liu, J.C., et al., *MICU1 Serves as a Molecular Gatekeeper to Prevent In Vivo Mitochondrial Calcium Overload.* Cell Rep, 2016. **16**(6): p. 1561-73.
84. Paillard, M., et al., *Tissue-Specific Mitochondrial Decoding of Cytoplasmic Ca2+ Signals Is Controlled by the Stoichiometry of MICU1/2 and MCU.* Cell Rep, 2017. **18**(10): p. 2291-2300.
85. Bick, A.G., S.E. Calvo, and V.K. Mootha, *Evolutionary Diversity of the Mitochondrial Calcium Uniporter.* Science (New York, N.Y.), 2012. **336**(6083): p. 886-886.
86. Cheng, Y. and F. Perocchi, *ProtPhylo: identification of protein-phenotype and protein-protein functional associations via phylogenetic profiling.* Nucleic Acids Res, 2015. **43**(W1): p. W160-8.
87. Yamamoto, T., et al., *Analysis of the structure and function of EMRE in a yeast expression system.* Biochim Biophys Acta, 2016. **1857**(6): p. 831-9.
88. Arduino, D.M., et al., *Systematic Identification of MCU Modulators by Orthogonal Interspecies Chemical Screening.* Mol Cell, 2017. **67**(4): p. 711-723.e7.
89. Gregolin, C. and A. D'Alberton, *On the properties of a D(-)lactic oxidase system in respiratory particles of yeast.* Biochem Biophys Res Commun, 1964. **14**: p. 103-8.

90. Mela, L., *Interactions of La3+ and local anesthetic drugs with mitochondrial Ca++ and Mn++ uptake.* Arch Biochem Biophys, 1968. **123**(2): p. 286-93.
91. Vinogradov, A. and A. Scarpa, *The initial velocities of calcium uptake by rat liver mitochondria.* J Biol Chem, 1973. **248**(15): p. 5527-31.
92. Romslo, I. and T. Flatmark, *Energy-dependent accumulation of iron by isolated rat liver mitochondria. II. Relationship to the active transport of Ca2+.* Biochimica et Biophysica Acta (BBA) - Bioenergetics, 1973. **325**(1): p. 38-46.
93. Csordas, G. and G. Hajnoczky, *Plasticity of mitochondrial calcium signaling.* J Biol Chem, 2003. **278**(43): p. 42273-82.
94. Shirran, S.L. and P.E. Barran, *The use of ESI-MS to probe the binding of divalent cations to calmodulin.* J Am Soc Mass Spectrom, 2009. **20**(6): p. 1159-71.
95. Senguen, F.T. and Z. Grabarek, *X-ray structures of magnesium and manganese complexes with the N-terminal domain of calmodulin: insights into the mechanism and specificity of metal ion binding to an EF-hand.* Biochemistry, 2012. **51**(31): p. 6182-94.
96. Kamer, K.J., et al., *MICU1 imparts the mitochondrial uniporter with the ability to discriminate between Ca(2+) and Mn(2+).* Proceedings of the National Academy of Sciences of the United States of America, 2018. **115**(34): p. E7960-E7969.
97. Musa, S., et al., *A Middle Eastern Founder Mutation Expands the Genotypic and Phenotypic Spectrum of Mitochondrial MICU1 Deficiency: A Report of 13 Patients.* JIMD Rep, 2018.
98. Gavin, C.E., K.K. Gunter, and T.E. Gunter, *Manganese and calcium efflux kinetics in brain mitochondria. Relevance to manganese toxicity.* The Biochemical journal, 1990. **266**(2): p. 329-334.
99. Wettmarshausen, J. and F. Perocchi, *Isolation of Functional Mitochondria from Cultured Cells and Mouse Tissues.* Methods Mol Biol, 2017. **1567**: p. 15-32.
100. Wettmarshausen, J. and F. Perocchi, *Assessing Calcium-Stimulated Mitochondrial Bioenergetics Using the Seahorse XF96 Analyzer.* Methods Mol Biol, 2019. **1925**: p. 197-222.
101 Zulkifli, M., Neff, J.K., Timbalia, S.A. *et al.* Yeast homologs of human MCUR1 regulate mitochondrial proline metabolism. *Nat Commun* **11,** 4866 (2020). https://doi.org/10.1038/s41467-020-18704-1

5 Acknowledgement

I would like to share my sincere gratitude to my supervisor Dr. Fabiana Perocchi for her invaluable guidance, fruitful discussions, contagious enthusiasm on science, and support throughout these PhD years. Thank you for the many great opportunities and challenges you provided to me during this time supporting my personal and professional development.

I would also like to thank Prof. Dr. Förstemann for agreeing to be the 2nd referee for my defence.

A big thank you to PD Dr. Dejana Mokranjac for her help and guidance during experiments and scientific discussions. Thank you to Dr. T. M. Alonso for providing the HeLa mt-AEQ cell line and mt-AEQ construct.

To all the members of AG Perocchi, thank you for all your collaboration and scientific discussion as well as fun, laughter, and friendship over the years. I would like to specially thank Anja, Valerie, Daniela, Li, Yiming for the collaboration on joined projects. Thank you to Anja, for jumping in wherever required, keeping the lab organized, stocks full, and being a scientific and mental support over the whole time. It was fantastic journey and pleasure to setup the lab together with you and Fabiana!

To my dearest family, thank you for all the love and support throughout these years. Thank you to my Mom and Dad for all the support, efforts and dependability, which enable me following my dreams. Thank you to my brother Thomas for always being ready for a joke to cheer me up and keep me going. Thank you to my dear grandma for teaching me to be brave, independent and reminding me that I can ask for more. You will be forever missed.

Last but not least, greatest thank you to Henrik. Thank you for being on my side throughout all these years Thank you for being an endless resource of support and energy during this journey. Thank you for all the joined adventures I would have missed without you and the new once to come.